

AD-A241 321



NAVAL POSTGRADUATE SCHOOL

Monterey, California



DTIC
SELECTE
OCT. 10 1991
S B D

THESIS

EVALUATION OF THE SSM/I RAIN ANALYSES
FOR
SELECTIVE STORMS IN THE ERICA PROJECT

by

Edmund F. Cataldo III

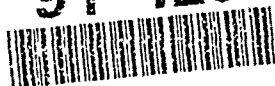
September 1990

Thesis Advisor

Carlyle H. Wash

Approved for public release; distribution is unlimited.

91-12680



91-12680-016

Unclassified

security classification of this page

REPORT DOCUMENTATION PAGE

1a Report Security Classification Unclassified			1b Restrictive Markings		
2a Security Classification Authority			3 Distribution/Availability of Report		
2b Declassification Downgrading Schedule			Approved for public release; distribution is unlimited.		
4 Performing Organization Report Number(s)			5 Monitoring Organization Report Number(s)		
6a Name of Performing Organization Naval Postgraduate School		6b Office Symbol (if applicable) 35	7a Name of Monitoring Organization Naval Postgraduate School		
6c Address (city, state, and ZIP code) Monterey, CA 93943-5000			7b Address (city, state, and ZIP code) Monterey, CA 93943-5000		
8a Name of Funding/Sponsoring Organization		8b Office Symbol (if applicable)	9 Procurement Instrument Identification Number		
8c Address (city, state, and ZIP code)			10 Source of Funding Numbers		
			Program Element No	Project No	Task No
			Work Unit Accession No		
11 Title (include security classification) EVALUATION OF THE SSM/I RAIN ANALYSES FOR SELECTIVE STORMS IN THE ERICA PROJECT					
12 Personal Author(s) Edmund F. Cataldo III					
13a Type of Report Master's Thesis		13b Time Covered From To		14 Date of Report (year, month, day) September 1990	15 Page Count 94
16 Supplementary Notation The views expressed in this thesis are those of the author and do not reflect the official policy or position of the Department of Defense or the U.S. Government.					
17 Cosati Codes			18 Subject Terms (continue on reverse if necessary and identify by block number)		
Field	Group	Subgroup	Microwave, ERICA, SSM/I, Precipitation forecasting, Rain		
19 Abstract (continue on reverse if necessary and identify by block number)					
<p>Evaluation of the SSM/I HAC precipitation algorithm is presented. SSM/I rainrate data from five passes during ERICA IOP 2 and 3 were compared to all available ship observations, dropwindsonde soundings and coastal radar. Four different techniques were applied to the seven SSM/I channels to analyze rain rate. They are. SSM/I HAC algorithm, the $T_b(19H)$ GHz channel with a threshold of $160^\circ K$, the $T_b(37H)$ GHz channel with a threshold of $190^\circ K$, and the $T_b(37V-37H)$ image with a threshold of less than a $30^\circ K$ difference. For the two IOP 2 passes the Spencer et al (1989) Polarized Correction Temperature (PCT) algorithm using the two 85 GHz channels was also studied.</p> <p>There is considerable uncertainty in the interpretation of the SSM/I HAC rain rate algorithm. Specifically large areas of out-of-limit values are present in the vicinity of mid-latitude winter cyclones. Study of the SSM/I HAC rain rate has indicated the out-of-limit areas occur when the rain flag is triggered, but the calculated rain rate from the HAC algorithm is less than zero.</p> <p>From this study it is obvious that the four channel SSM/I HAC regression algorithm, in its current form, can not satisfactorily analyze the precipitation. Further study is needed to determine if a regression equation can be used to estimate precipitation areas, particularly those with light precipitation. Treating the out-of-limits values as light precipitation would dramatically improve the quality of the SSM/I HAC analysis. However, if a regression equation can not be used to estimate precipitation, using the $T_b(37H)$ channel for a better overall analysis of light precipitation and showers and the $T_b(19H)$ channel for a better analysis of the moderate to heavy precipitation is a viable solution.</p>					
20 Distribution/Availability of Abstract			21 Abstract Security Classification		
<input checked="" type="checkbox"/> unclassified unlimited <input type="checkbox"/> same as report <input type="checkbox"/> DTIC users			Unclassified		
22a Name of Responsible Individual Carlisle H. Wash			22b Telephone (include Area code) (408) 646-2295	22c Office Symbol 63WX	

DD FORM 1473,84 MAR

83 APR edition may be used until exhausted
All other editions are obsolete

security classification of this page

Unclassified

Approved for public release; distribution is unlimited.

Evaluation of the SSM/I Rain Analyses for
Selective Storms in the ERICA Project

by

Edmund F. Cataldo III
Lieutenant, United States Navy
B.S., United States Naval Academy, 1982

Submitted in partial fulfillment of the
requirements for the degree of

MASTER OF SCIENCE IN METEOROLOGY AND PHYSICAL
OCEANOGRAPHY

from the

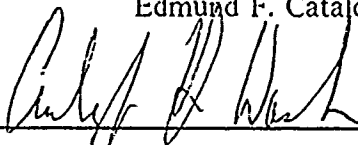
NAVAL POSTGRADUATE SCHOOL
September 1990

Author:

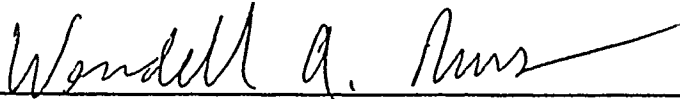


Edmund F. Cataldo III

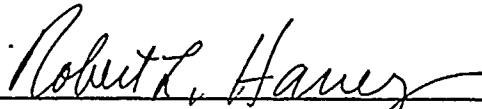
Approved by:



Carlyle H. Wash, Thesis Advisor



Wendell A. Nuss, Second Reader



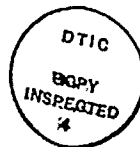
Robert L. Haney, Chairman,
Department of Meteorology

ABSTRACT

Evaluation of the SSM/I HAC precipitation algorithm is presented. SSM/I rainrate data from five passes during ERICA IOP 2 and 3 were compared to all available ship observations, dropwinsonde soundings and coastal radar. Four different techniques were applied to the seven SSM/I channels to analyze rain rate. They are: SSM/I HAC algorithm, the $T_b(19H)$ GHz channel with a threshold of $160^\circ K$, the $T_b(37H)$ GHz channel with a threshold of $190^\circ K$, and the $T_b(37V-37H)$ image with a threshold of less than a $30^\circ K$ difference. For the two IOP 2 passes the Spencer et al (1989) Polarized Correction Temperature (PCT) algorithm using the two 85 GHz channels was also studied.

There is considerable uncertainty in the interpretation of the SSM/I HAC rain rate algorithm. Specifically large areas of out-of-limit values are present in the vicinity of mid-latitude winter cyclones. Study of the SSM/I HAC rain rate has indicated the out-of-limit areas occur when the rain flag is triggered, but the calculated rain rate from the HAC algorithm is less than zero.

From this study it is obvious that the four channel SSM/I HAC regression algorithm, in its current form, can not satisfactorily analyze the precipitation. Further study is needed to determine if a regression equation can be used to estimate precipitation areas, particularly those with light precipitation. Treating the out-of-limits values as light precipitation would dramatically improve the quality of the SSM/I HAC analysis. However, if a regression equation can not be used to estimate precipitation, using the $T_b(37H)$ channel for a better overall analysis of light precipitation and showers and the $T_b(19H)$ channel for a better analysis of the moderate to heavy precipitation is a viable solution.



Accession For	
NTIS GRA&I	<input checked="checked" type="checkbox"/>
DTIC TAB	<input type="checkbox"/>
Unannounced	<input type="checkbox"/>
Justification _____	
By _____	
Distribution/	
Availability Codes	
Dist	Avail and/or Special
A-1	

TABLE OF CONTENTS

I. INTRODUCTION	1
II. SATELLITE PRECIPITATION ESTIMATION	3
A. VISUAL AND INFRARED DATA	3
B. LIFE HISTORY METHOD	4
C. MICROWAVE TECHNIQUES	5
III. CURRENT MICROWAVE PRECIPITATION TECHNIQUES	7
A. HUGHES AIRCRAFT COMPANY ALGORITHM	7
B. OTHER MICROWAVE PRECIPITATION ALGORITHMS	8
IV. ERICA IOP 2 AND 3 PRECIPITATION ANALYSES	12
1. 12/2303 DECEMBER 1988	12
a. SSM/I Data for 12/2303 December 1988	15
b. Ship and Radar Reports for 12/2303 December 1988	17
2. 13/2257 DECEMBER 1988	20
a. SSM/I Data for 13/2257 December 1988	20
b. Ship and Radar Reports for 14/0000 December 1988	22
3. 16/2220 December 1988	24
a. SSM/I Data for 16/2220 December 1988	25
b. Ship Reports for 17/0000 December 1988	27
4. 17/2208 December 1988	28
a. SSM/I Data for 17/2208 December 1988	28
b. Ship Reports for 18/0000 December 1988	29
5. 18/0941 December 1988	31
a. SSM/I Data for 18/0941 December 1988	32
b. Ship Reports for 18/1200 December 1988	32
V. SUMMARY AND CONCLUSIONS	36
APPENDIX A. SATELLITE PRECIPITATION ESTIMATION FIGURES ...	41

APPENDIX B. CASE STUDY OF IOP 2	48
APPENDIX C. CASE STUDY OF IOP 3	62
APPENDIX D. WMO WEATHER CODE TABLE	80
LIST OF REFERENCES	81
INITIAL DISTRIBUTION LIST	83

LIST OF TABLES

Table 1.	ERICA CYCLONES STUDIED	2
Table 2.	PRECIPITATION OVER OCEAN COEFFICIENTS FOR THE HAC ALGORITHM	7
Table 3.	RAIN CRITERIA FOR THE HAC ALGORITHM	9
Table 4.	DEFINITION OF HAC CLIMATE CODES	10
Table 5.	SSM/I HAC PRECIPITATION ALGORITHM IMAGE COLOR CODE TABLE.	13
Table 6.	PCT PRECIPITATION IMAGE COLOR CODE TABLE	13
Table 7.	19H GHZ BRIGHTNESS TEMPERATURE COLOR CODE TABLE. .	14
Table 8.	37H GHZ BRIGHTNESS TEMPERATURE COLOR CODE TABLE. .	15
Table 9.	37V - 37H GHZ BRIGHTNESS TEMPERATURE COLOR CODE TA- BLE.	15
Table 10.	COMPARISON OF BRIGHTNESS TEMPERATURES AND RAIN RATES AT 13/0000 DECEMBER 1988	18
Table 11.	COMPARISON OF BRIGHTNESS TEMPERATURES AND RAIN RATES AT 14/0000 DECEMBER 1988	23
Table 12.	COMPARISON OF BRIGHTNESS TEMPERATURES AND RAIN RATES AT 17/0000 DECEMBER 1988	26
Table 13.	COMPARISON OF BRIGHTNESS TEMPERATURES AND RAIN RATES AT 18/0000 DECEMBER 1988	30
Table 14.	COMPARISON OF BRIGHTNESS TEMPERATURES AND RAIN RATES AT 18/1200 UTC DECEMBER 88	33
Table 15.	RAIN/NO RAIN STATISTICS FOR THE SSM/I HAC IMAGE	37
Table 16.	RAIN/NO RAIN STATISTICS FOR THE SSM/I HAC IMAGE	38
Table 17.	RAIN/NO RAIN STATISTICS FOR THE	39
Table 18.	RAIN/NO RAIN STATISTICS FOR THE	39
Table 19.	RAIN/NO RAIN STATISTICS FOR THE	39

LIST OF FIGURES

Fig. 1.	Two dimensional precipitation histogram	41
Fig. 2.	Satellite rain rate versus radar rain rate.	42
Fig. 3.	Mie volume scattering coefficients	43
Fig. 4.	Volume absorption coefficients	44
Fig. 5.	Single scattering albedos	45
Fig. 6.	Brightness temperature versus rain rate.	46
Fig. 7.	Mid-latitude ocean brightness temperature versus rain rate at 19 and 37 GHz.	47
Fig. 8.	GOES infrared east coast U.S. sector imagery for 12/2301 December 1988.	48
Fig. 9.	SSM/I HAC precipitation image at 12/2303 December 1988.	49
Fig. 10.	SSM/I 19H GHz brightness temperature image at 12/2303 December 1988.	50
Fig. 11.	SSM/I 37H GHz brightness temperature image at 12/2303 Decce: 1988.	51
Fig. 12.	SSM/I 37V - 37H GHz brightness tempèrature image at 12/2303 December 1988.	52
Fig. 13.	PCT brightness temperature image at 12/2303 December 1988.	53
Fig. 14.	Weather rain map for 13/0000 December 1988.	54
Fig. 15.	GOES infrared east coast U.S. sector imagery for 13/2301 UTC December 1988.	55
Fig. 16.	SSM/I HAC precipitation image at 13/2257 December 1988.	56
Fig. 17.	SSM/I 19H GHz brightness temperature image at 13/2257 December 1988.	57
Fig. 18.	SSM/I 37H GHz brightness temperature image at 13/2257 December 1988.	58
Fig. 19.	SSM/I 37V - 37H GHz brightness temperature image at 13/2257 December 1988.	59
Fig. 20.	PCT brightness temperature image at 13/2257 December 1988.	60
Fig. 21.	Weather rain map for 14/0000 December 1988.	61
Fig. 22.	GOES infrared east coast U.S. sector imagery for 16/2231 December 1988.	62
Fig. 23.	SSM/I HAC precipitation image at 16/2220 December 1988.	63
Fig. 24.	SSM/I 19H GHz brightness temperature image at 16,2220 December 1988.	64
Fig. 25.	SSM/I 37V - 37H GHz brightness temperature image at 16/2220 December 1988.	65
Fig. 26.	SSM/I 37H GHz brightness temperature image at 16,2220 December 1988.	66

Fig. 27. Weather rain map for 17/0000 December 1988.	67
Fig. 28. GOES infrared east coast U.S. sector imagery for 17/2231 UTC December 1988.	68
Fig. 29. SSM/I HAC precipitation image at 17/2208 December 1988.	69
Fig. 30. SSM/I 19H GHz brightness temperature image at 17/2208 December 1988.	70
Fig. 31. SSM/I 37H GHz brightness temperature image at 17/2208 December 1988.	71
Fig. 32. SSM/I 37V - 37H GHz brightness temperature image at 17/2208 December 1988.	72
Fig. 33. Weather rain map for 18/0000 December 1988.	73
Fig. 34. GOES infrared east coast U.S. sector imagery for 18/0901 UTC December 1988.	74
Fig. 35. SSM/I HAC precipitation image at 18/0941 December 1988.	75
Fig. 36. SSM/I 19H GHz brightness temperature image at 18/0941 December 1988.	76
Fig. 37. SSM/I 37H GHz brightness temperature image at 18/0941 December 1988.	77
Fig. 38. SSM/I 37V - 37H GHz brightness temperature image at 18/0941 December 1988.	78
Fig. 39. Weather rain map for 18/1200 December 1988.	79
Fig. 40. The Standard WMO Codes	80

ACKNOWLEDGEMENTS

I would like to thank my advisor, Dr. Carlyle Wash, for the assistance and strong support he gave me while guiding me throughout this project. I would like to acknowledge Dr. Wendall Nuss for his helpful suggestions and direction as my second reader. I also wish to acknowledge Dr. Andy Goroch of the Naval Oceanography and Atmospheric Research Laboratory for suppling me with SSM/I data for IOP 2, and Donna Burch for spending hours in reprogramming the SSM,I data input program to run on the Idea Lab computers. Finally, I wish to thank my wife Donna for her love and understanding during my tour at the Naval Postgraduate School.

I. INTRODUCTION

Satellite imagery has become an essential tool for the analysis of significant mesoscale and subsynoptic weather phenomena. Of these phenomena, precipitation-producing systems are of critical importance to the operational forecaster. Accurately analyzing precipitation, which has small spatial and temporal scales, is difficult. Visual and infrared satellite imagery are the only data with enough spatial (to 1 km) and temporal (to 30 minutes) resolution to resolve precipitation systems over a large region. However, interpretation of satellite imagery is very subjective and time consuming. So, while satellite imagery is being used extensively, the true potential of satellite data, in digital form, has not been fully utilized operationally to estimate precipitation amounts (Sheridan 1988).

Recently, numerous studies have been conducted using the Scanning Multichannel Microwave Radiometer (SMMR) images aboard Seasat and Nimbus-7 satellites and the Special Sensor Microwave Imager (SSM/I) data aboard the Defense Meteorological Satellite Program (DMSP) satellite to estimate precipitation amounts. These studies test a variety of algorithms using the brightness temperatures from different channels to determine a threshold for rain, no rain. However, according to Katsaros et al. (1989), a definite algorithm has not yet been developed because of the complex and variable microphysical and mesoscale structure of precipitation, combined with the rather coarse spatial resolution of current sensors. Therefore, continued research into estimation of precipitation using satellite data, especially over the data sparse oceans, is needed.

The Experiment on Rapidly Intensifying Cyclones over the Atlantic (ERICA), conducted from 01 December 1988 to 26 February 1989, was designed to seek new scientific understanding of the rapid intensification of storms at sea (Hadlock and Kreitzberg 1988). ERICA had three main objectives: (1) to understand the fundamental physical processes occurring in the atmosphere during rapid intensification of winter cyclones at sea, (2) determine those physical processes that need to be incorporated into dynamical prediction models through efficient parameterizations if necessary, and 3) identify measurable precursors of rapid development that must be incorporated into the initial analysis for accurate and detailed operational model predictions. The combination of additional surface, upper air and aircraft data over the western North Atlantic Ocean makes the ERICA systems desirable for the validation of oceanic precipitation analysis.

To be considered an ERICA-type storm a system had to have a deepening rate of at least 10mb/6h for at least 6 hours. During the experiment the observed ERICA-type storms occurred mainly between 35N and 45N in close association with the path of the Gulf Stream. There were eight Intensive Observation Periods (IOP) and data describing two major cyclones of the experiment (IOP 2 and 3) will be used in this study (Table 1).

Table 1. ERICA CYCLONES STUDIED

IOP	Start Time	End Time
2	1500 UTC 12 December 1988	0000 UTC 15 December 1988
3	0000 UTC 17 December 1988	0000 UTC 19 December 1988

The main goal of this thesis is to study the Hughes Aircraft Company (HAC) SSM/I rain algorithm, (Hollinger et al 1987), for selective storms in the ERICA project, then compare these results with the 85.5 GHz polarization corrected brightness temperature ($PCT_{85.5}$) from Spencer et al. (1989) and other microwave precipitation methods. Based upon the results, modifications that will improve the use of microwave data for precipitation will be suggested.

Chapter II discusses the three main methods currently employed to estimate precipitation using satellite images. Chapter III will discuss the microwave precipitation techniques presently used to remotely determine rainfall amount. Chapter IV will compare all available ERICA ground truth data, such surface based radars, ship and land observations with the precipitation estimates from the two algorithms associated with the SSM/I image and analyze the results. Conclusions and recommendations are given in chapter V.

II. SATELLITE PRECIPITATION ESTIMATION

The three main methods currently used for estimating precipitation using satellite imagery are: (1) satellite visual reflectance and cloud top temperature thresholds (Fig. 1), (2) the cloud life history method and, (3) multichannel microwave brightness temperature algorithms. Although this thesis primarily uses microwave data, other methods will be briefly discussed.

A. VISUAL AND INFRARED DATA

Muench and Keegan (1979), Liljas (1982) and others have related cloud reflectivity to rainfall rate. In addition precipitating clouds generally have high cloud tops and resultant cold cloud top temperatures which indicates a relationship between rainfall and cloud top temperature. Using these two observations, cloud top temperature and visual reflectance can be used together to estimate precipitation amount.

To quantify the satellite data, the visual data counts are converted to albedos using a brightness normalization scheme such as Muench and Keegan (1979), and the infrared data counts are converted to temperatures using the appropriate satellite calibration. Then, using thresholds established for a particular geographic area, the amount of precipitation is estimated. An example of this application for GOES data is given by a NPS model described by Wash et al (1985) and Sheridan (1988). If the cloud top temperature is less than -15°C and visual albedos greater than 60% the NPS cloud and precipitation model assumes that the cloud is a rain cloud, such as cumulonimbus or nimbostratus. It then estimates precipitation for that location. The lower the temperature and higher the albedo the greater the amount of precipitation.

The advantage of this method is high time resolution available with the GOES data. GOES images and associated precipitation analyses currently are possible every 30 minutes. An additional advantage of GOES data is the coverage of large areas. For example the current United States GOES covers all of North, Central and South America and adjacent waters.

The major disadvantage with visual and infrared precipitation thresholds is that the satellite data is still measuring cloud features, not the actual precipitation. Other problems include: (1) underestimation of rainfall amounts from stratiform type clouds with warm tops, (2) incorrect classification of cirrus anvils that extends some distance from rain producing thunderstorms and (3) the difficulty of distinguishing between thick cold

clouds which are vertically developed and precipitating versus those which are confined to the middle and/or upper troposphere.

B. LIFE HISTORY METHOD

Life history methods are based on the fact that most precipitation in the tropics comes from convective clouds and that these types of clouds are easily identifiable on satellite pictures. One of the earliest schemes conceived was that of Stout et al (1977). This scheme measures the rainfall produced by a cumulonimbus cloud or a group of cumulus clouds using the following formula:

$$R_v = a_0 A_c + a_1 \frac{dA_c}{dt} \quad (2.1)$$

where R_v is the volumetric rain rate for each cloud, A_c is the area of the cloud at time t , $\frac{dA_c}{dt}$ is cloud area change and a_0 and a_1 are empirical coefficients. The cloud areas determined by satellite, and volumetric rain rate of individual cumulonimbus clouds determined by radar, were measured throughout the cloud lifetimes. The coefficients a_0 and a_1 were then calculated from the combined measurements by least squares regression.

To make precipitation estimates using this scheme a sequence of geostationary satellite images is required. All cumulus and cumulonimbus clouds are measured by area and location then tracked throughout the sequence until each system or cloud has dissipated. Volumetric rain rate is calculated for each cloud and is then summed or mapped to get the amount and distribution of rainfall. This scheme has been validated against calibrated radars with a correlation of 84% Stout et al 1979, (Fig. 2). However, there are two inherent problems with this type of scheme: (1) it can not locate warm cloud precipitation, or precipitating clouds of type other than cumulonimbus, and (2) each cloud of the same size and growth rate is calculated to have the same volumetric rain rate regardless of other synoptic conditions. For clouds associated with an average volumetric rain rate this method is satisfactory, but for the clouds at either end of the spectrum the estimation will be much less accurate (Barrett and Martin 1981). Also, this method requires large amounts of man-computer interaction and, therefore, is not timely enough to be of use to the operational forecaster.

Two other life-history methods are those of (1) Griffith et al. (1976 and 1978) and Woodley et al. (1980), and (2) Scofield and Oliver (1977). The first was intended to provide estimates of convective rainfall beyond the range of calibrated radars, while the second offers forecasters a way to measure convective rainfall using the enhanced infra-

red SMS/GOES satellite pictures. The scheme of Griffith and Woodley is functionally the same as Stout et al. except Griffith and Woodley use cloud echo area vice just cloud area in their expression of change for the area of the cloud. The method of Scofield and Oliver makes a rainfall analysis for the active part of a cold convective cloud. The assignment of particular rainfall rates to categories of cloud top temperature, growth, position, texture and relationship with other convective systems is based on standard gauge measurements of convective rainfall over one summer season in the central United States, modified by physical reasoning and experience (Barrett and Martin 1981).

C. MICROWAVE TECHNIQUES

The last method uses passive microwave data such as the SSM/I imagery from the DMSP satellite. Precipitation is estimated by microwave radiation using either absorption or scattering approaches. The three primary microwave frequencies used to measure precipitation are 19.35, 37, and 85.5 GHz. Looking at Figs. 3 and 4 it can be seen that (1) ice essentially does not absorb microwave radiation (scattering dominates), and (2) absorption dominates over scattering for liquid drops. Figure 5 illustrates that both scattering and absorption increase with frequency and rain rate, however, scattering by ice increases much more rapidly with frequency than scattering by the liquid drops.

Below approximately 32 GHz, absorption is the primary mechanism affecting the transfer of microwave radiation through the atmosphere. The scattering that occurs is of secondary importance. Above 60 GHz scattering processes dominates absorption. At lower frequencies, such as 19.35 GHz, rain is highly absorptive and results in an apparent warm brightness temperature over a cold background such as the ocean. With increasing rain rate, the difference in brightness temperature between the two polarizations at a given frequency such as 37 GHz tend to decrease (Fig. 7). However, above 60 GHz, ice scattering is the dominant process, therefore, microwave energy sees only the ice and masks the rain below. Cloud droplets, water vapor and oxygen absorb, but do not scatter microwave radiation and affect the precipitation measurements based solely on absorption.

Using the absorption approach, rainfall is measured through the emission of thermal energy. Since liquid raindrops are the main source of this emission, they provide a direct relationship to the microwave radiance (Sheridan 1988). The technique used by Wilheit et al (1977) and others rely on the increase of brightness temperature with rain rate over the ocean. They cannot determine rain rate greater than a saturation rain rate, which decreases with increasing frequency (Fig. 6). Therefore, lower frequencies are preferred

for oceanic precipitation estimates. The Nimbus-7 satellite launched in November of 1978 carried the Scanning Multichannel Microwave Radiometer (SMMR), a five channel microwave dual polarized instrument used to measure precipitation with a 30-97 km resolution.

The two main problems associated with the absorption scheme used to estimate rain rate using passive microwave radiometry were: (1) cloud and rain water are difficult to separate, especially using a single wavelength and, (2) the beam-filling and nonlinearity problem due to large fields-of-view (FOV). Space constraints aboard satellites have resulted in small antenna size, therefore, the measured wavelengths are long. This forces microwave radiometers to have large (225 km^2 - 3025 km^2) footprints. The radiometer averages brightness temperature over the entire footprint. These footprints are too large to have a uniform rain rate associated with the whole area, thereby causing errors in precipitation estimates. But since brightness temperature is highly nonlinear in rain rate (Fig. 6), it also does not provide a good estimate of rain rate for clouds that do not fill the field-of-view (Kidder and Vonder Harr 1990).

For the scattering approach, rainfall is measured by estimating the scattering within the cloud. Scattering has the potential to be a better means of measuring precipitation than absorption since precipitation (liquid water and ice) is the only constituent that scatters microwave radiation. All others absorb it. Therefore, the more accurate the scattering can be measured the greater the confidence in the precipitation measurement. Currently, scattering measurement techniques are too new to accurately estimate their ability, therefore, absorption is presently the more credible of the two. The best results in microwave imaging are obtained over a relatively cold background, like the ocean. However, the ocean has few in situ measurements so validation of the results becomes difficult.

The advantage of microwave measurement is the direct influence of precipitation on the microwave radiance. Currently the major disadvantage is that the passive microwave measurements are made from a polar orbiting satellite, so coverage is only available twice a day at each location. Other limitations are related to the reduced spatial resolution of existing radiometers compared to visual and infrared data. The SSM/I resolutions are only 15 km at 85.5 GHz, 32 km at 37 GHz, 48 km at 22.2 GHz, and 55 km at 19.3 GHz. Another problem is variable effective height of the rainfall because microwave measurements record all liquid raindrops detected within the cloud layer, independent of whether the drops actually fall to the ground. Therefore, if the liquid drops are not striking the ground, erroneous results will be obtained.

III. CURRENT MICROWAVE PRECIPITATION TECHNIQUES

Making atmospheric analyses over a data sparse area such as the oceans is a formidable task. Measuring precipitation which has small spatial and temporal scales is even more difficult. The goal of the next two chapters is to evaluate the accuracy of the SSM/I HAC rain algorithm over the ocean areas during certain IOP's of the ERICA study. In this chapter additional details of the HAC and other microwave precipitation algorithms are presented.

A. HUGHES AIRCRAFT COMPANY ALGORITHM

The method currently used to determine precipitation using only SSM/I data is the HAC algorithm introduced earlier. This algorithm uses brightness temperatures as independent variables in a linear regression equation. The regression coefficients, which reside in a data file as part of the software system, are determined using geophysical models, radiative transfer models, an inversion algorithm and climatology. Regression coefficients (Table 2) and threshold values (Table 3) have been prepared for 11 climate zones (Table 4).

The criteria used for mid-latitude winter ocean cases include the critical temperature of the 19.35 GHz brightness temperature for the 'maybe rain' case, CMRO (160 K), and the critical brightness temperature difference between the two 37 GHz channels for 'maybe rain', CMRDO (30 K) given in Table 3. When either of the two criteria is met, the algorithm assumes that there is rain. The criterion for 'heavy rain' over the ocean is also based upon the difference between the brightness temperatures of the two 37 GHz channels. When $T_b(37V) - T_b(37H)$ is less than CHRDO (20 K), the 'heavy rain' condition is assumed. When the algorithm has determined that a criterion for rain has been met it calculates rain rate (RR) using the following algorithm (Hollinger et al 1987):

$$RR = C_0 + C_1(T_b19H) + C_2(T_b22V) + C_3(T_b37V) + C_4(T_b37H) \quad (3.1)$$

The coefficients used in equation 3.1 are taken from Table 2 and are based upon the climate code determined in Table 4. For the ERICA cases climate code 7, mid-latitude winter, applies.

Table 2. PRECIPITATION OVER OCEAN COEFFICIENTS FOR THE HAC ALGORITHM: [After Hollinger et al (1987).]

CLIMATE CODE	C_0	C_1	C_2	C_3	C_4
1	210.2800	.1217	-.7829	-.1830	.0998
2	215.1800	.1026	-.8059	-.1944	.1354
3	173.0400	.1938	-.6500	-.2291	.0808
4	169.2900	.1523	-.6065	-.3531	.2162
5	123.4000	.2019	-.4070	-.5117	.2969
6	135.8000	.2659	-.5170	-.2751	.0618
7	114.5500	.2708	-.6228	-.2836	.2521
8	9.5432	.1796	-.2109	.1214	-.0753
9	24.1020	.0825	.1367	-.3411	.0843
10	9.5432	.1796	-.2109	.1214	-.0753
11	24.1020	.0825	.1367	-.3411	.0843

B. OTHER MICROWAVE PRECIPITATION ALGORITHMS

To validate the SSM/I precipitation amounts determined by the HAC algorithm an 85.5 GHz Polarization Corrected Temperature (PCT) approach, formulated by Spencer et al (1989) will be studied for IOP 2 passes only. The SSM/I's polarization differences can help alleviate the ambiguity between low brightness temperatures due to surface water bodies versus those due to precipitation. The polarization correction temperature is defined as:

$$PCT = (\beta T_{Bh} - T_{Bv}) / (\beta - 1) \quad (3.2)$$

where

$$\beta = (T_{Bvc} - T_{Bvo}) / (T_{Bhc} - T_{Bho}) \quad (3.3)$$

Table 3. RAIN CRITERIA FOR THE HAC ALGORITHM: [After Hollinger et al (1987).]

Climate Code	CMRO	CMRDO	CHRDO	CFGL	CHRL	CHRDl	CMRL	CMRDL
1	190	25	10	150	273	10	263	5
2	190	25	10	150	273	10	263	5
3	190	25	10	150	273	10	263	5
4	190	25	10	150	273	10	263	5
5	170	25	20	240	270	10	240	--
6	190	25	15	150	270	10	263	5
7	160	30	20	240	270	10	240	--
8	150	35	20	240	270	10	240	--
9	140	35	20	270	270	--	270	--
10	150	35	20	240	270	10	240	--
11	140	35	20	270	270	--	270	--
CMRO = Criterion for maybe rain over ocean for $T_h(19H)$								
CMRDO = Criterion for maybe rain over ocean for $T_b(37V) - T_b(37H)$								
CHRDO = Criterion for heavy rain over ocean for $T_b(37V) - T_h(37H)$								
CFGL = Criterion for frozen ground for $T_b(37V)$								
CHRL = Criterion for heavy rain over land for $T_h(37V)$								
CHRDl = Criterion for heavy rain over land for $T_b(37V) - T_h(37H)$								
CMRL = Criterion for maybe rain over land for $T_h(37V)$								
CMRDL = Criterion for maybe rain over land for $T_b(37V) - T_h(37H)$								

and where T_{Bhc} and T_{Bvc} refer to the horizontally and vertically polarized cloud free ocean brightness temperatures, respectively, and T_{Bh} and T_{Bv} are the horizontally and vertically polarized brightness temperatures that are at least partially affected by any combination of clouds and precipitation. T_{Bvo} and T_{Blo} are the vertically and horizontally polarized brightness temperatures, respectively, of the ocean with no overlying atmosphere. Model calculations, run by Spencer et al (1989), for a standard tropical airmass over an ocean with a 302 K surface temperature yields $\beta = 0.38$ and a PCT of 288 K. When the PCT is compared with SSM/I measured brightness temperatures of dry high latitude oceanic airmass (with $\beta = 0.38$), the PCT's are consistently 10 to 15 degrees lower than the model calculations.

Therefore, an empirically modified value for β is used. With β equal to 0.45, this leads to a PCT in the desired range of 275K to 290K and equation 3.2 becomes:

$$PCT_{85.5} = 1.818(T_{Bv}) - 0.818(T_{Bh}) \quad (3.4)$$

Table 4. DEFINITION OF HAC CLIMATE CODES: [After Hollinger et al (1987).]

CLIMATE CODE No.	DEFINITION
1	Tropical-warm
2	Tropical-cool
3	Lower Latitude Transition-warm
4	Lower Latitude Transition-cool
5	Mid. Lat.-Spring/Fall
6	Mid. Lat.-Summer
7	Mid. Lat.-Winter
8	Upper Lat. Transition-cool
9	Upper Lat. Transition-cold
10	Polar-cool
11	Polar-cold

where T_{Bv} is the vertical 85.5 GHz brightness temperature and T_{Bh} is the horizontal 85.5 GHz brightness temperature (Spencer et al, 1989).

Another recently developed microwave technique for estimating precipitation occurrence comes from Katsaros et al (1989). The 37 GHz horizontal channel from the SSM/I flags the location of frontal rain by applying a simple threshold to the 37 GHz horizontally polarized brightness temperature. Following Wilheit and Chang (1980) $T_b(37H)$ greater than 190 K is used to identify rain. Katsaros et al (1989) show that the rain flag captures the activity near the apex between warm and cold fronts and often accurately analyzes warm and cold frontal precipitation. This technique will be compared with the above methods in analyzing oceanic rain rate for ERICA IOP's 2 and 3.

Verifying satellite derived oceanic rain rate is a difficult problem given the large areas of the satellite pass and the sparsity of in situ data. The data analysis section of this study will examine the SSM/I IAC rain rate algorithm for five orbits during the two ERICA IOP's. HAC rain estimates will be compared with the Polarization Corrected Temperature (PCT) from Spencer et al (1989), and with certain threshold values for the,

T_b (19H) GHz, the T_b (37V) GHz, and the difference between the 37V and 37H GHz brightness temperature channels. All available ship, dropwinsonde, and coastal radar data, collected during the experiment, will then be used to evaluate the HAC analysis and the other microwave rain signatures.

IV. ERICA IOP 2 AND 3 PRECIPITATION ANALYSES

The ERICA IOP 2 event was characterized by the rapid development of several surface cyclone centers. Around 0000 UTC 13 December 1988 (hereafter UTC date/time will be referred to as day, time, i.e. 13,0000), the first of two upper-air troughs during this IOP began moving offshore along the Georgia-South Carolina Coast. A surface cyclone developed with this system and moved eastward along 30°N. A second and stronger region of upper-air forcing moved offshore near Virginia and North Carolina about 13,1200. It was associated with an upper-level jet streak and an amplifying upper-air short wave trough. Surface pressures began to fall significantly over a large area of the western North Atlantic Ocean and a surface trough developed northward from the Gulf Stream east of Cape Hatteras toward Long Island and southern New England (Chalfant 1989). A surface system emerged east of Hatteras then rapidly intensified on 14 December as its central pressure dropped from 991 mb to 963 mb. Satellite precipitation analyses for two key time periods during this IOP now will be studied.

1. 12/2303 DECEMBER 1988

The first SSM/I pass during IOP 2 occurred at 12,2303 December 1988. This pass is actually just before the official start of IOP 2 on 13,0000. In the hours before the pass, a cold front had passed through the Carolina coastal waters and cold air was now spreading eastward over the western North Atlantic Ocean as evident in the GOES imagery for 12,2301 (Fig. 8). This frontal cloud band extends from 30°N 60°W westward to the tip of Florida. Also shown is a cloud shield associated with the first IOP 2 cyclone, a 1010 mb low centered near the Georgia coast at 28°N 77°W. To the north and east, the GOES imagery shows a large outbreak of cellular clouds associated with the movement of cold air driven seaward by the circulation of a 1039 mb high located over Long Island.

Table 5. SSM/I HAC PRECIPITATION ALGORITHM IMAGE COLOR CODE TABLE. Out of limits values are those that have passed through the screening logic of the algorithm but the value returned from the equation is unrealizable. Indeterminate values are those values that do not even pass the screening logic, usually over land, or missing or bad data.

PRECIPITATION AMOUNT (mm/h)	COLOR CODE
0	black
1 - 3	yellow
4 - 8	orange
9 - 15	aqua
16 - 30	green
31 - 45	blue
46 - 61	purple
out of limits	red
indeterminate	white

The SSM/I brightness temperatures and the HAC rain rate images for the 12,2301 pass were earth-located and remapped to a mercator projection with a resolution of 32.2 km. The HAC algorithm rain rate image was color coded in mm/h according to the scale given in Table 5. Recall the HAC rain rate algorithm uses SSM/I channels 19H, 22V, 37V, and 37H. To explore the 85 GHz data, a PCT image was constructed by combining the two 85.5 GHz channels using the Spencer et al (1989) algorithm discussed previously and color coded according to Table 6.

Table 6. PCT PRECIPITATION IMAGE COLOR CODE TABLE

PRECIPITATION AMOUNT (mm/h)	COLOR CODE
no data	black
> 10	red
7 - 10	orange
4 - 6	blue
1 - 3	yellow
no rain	green
out of range	white

To further interpret the rain rate results, remapped brightness temperatures for key SSM/I channels are presented. The $T_b(37V)$ and $T_b(37V-37H)$ channel difference data will be used to understand the rain rate algorithm and the ability of the SSM/I to analyze ocean rainfall. Enhancements of important brightness temperature thresholds will be applied to these channels in their interpretation. For the 19H GHz brightness temperature image a threshold of 160 K was chosen as a rain/no rain flag for two reasons: (1) the HAC algorithm for "may be rain" over the ocean uses 160 K as its rain/no rain threshold (Table 3), and (2) simulations of the 19H GHz channel response to rain (Fig. 7) shows 160 K indicates a steady rain rate of 1.25 mm/h. To distinguish the different brightness temperature ranges easily, the $T_b(19H)$ image temperatures from 160 K to 180 K were color coded yellow, 181 to 200 K, color coded blue, and brightness temperatures greater than 200 K color coded red (Table 7). Temperatures less than 160 K are not enhanced. The $T_b(19H)$ data was mapped with a resolution of 55 km. Recall that warmer T_b indicates higher rain rate, so the blue and red area indicate moderate (4-8 mm/h) and heavy rain rates (> 8 mm/h).

Table 7. 19H GHZ BRIGHTNESS TEMPERATURE COLOR CODE TABLE.

BRIGHTNESS TEMPERATURE	COLOR CODE
< 160	grey shades
160 - 180	yellow
181 - 200	blue
201 - 255	red

For the 37H GHz channel a brightness temperature less than 190 K corresponds to a rain rate of less than 1 mm/h and was chosen as the rain/no rain threshold for this channel. This also follows the work of Katsaros et al (1989). The color enhancements for Table 8 was constructed similar to Table 7 with brightness temperature less than 190 K not enhanced, 190-205 K color coded as yellow, 206-220 K as blue and, greater than 220 K as red. The $T_b(37H)$ data was mapped with a resolution of 32 km. Note that the 37H GHz is more sensitive to rain rate (Fig. 7) and the yellow and red areas correspond to smaller rain rates than similar areas for the 19H channel.

Table 8. 37H GHZ BRIGHTNESS TEMPERATURE COLOR CODE TABLE.

BRIGHTNESS TEMPERATURE	COLOR CODE
< 190	grey shades
190 - 205	yellow
206 - 220	blue
221 - 255	red

The difference between the two 37 GHz channels is also sensitive to rain rate. Since the radiance from the ocean is polarized, a large difference between the 37V and 37H channels indicates no rain. As the difference between the channels decreases, the probability of emission from unpolarized rain increases. The HAC algorithm uses a 30 K difference as a rain flag. When the difference is 20 K, the HAC algorithm designates the pixel as having a heavy rain rate of 10 mm/h. The $T_b(37V-37H)$ brightness temperature differences of 30K, 20K, and 10K are enhanced according to Table 9.

Table 9. 37V - 37H GHZ BRIGHTNESS TEMPERATURE COLOR CODE TABLE.

BRIGHTNESS TEMPERATURE	COLOR CODE
0	black
1 - 9	red
10 - 20	blue
21 - 30	yellow
> 30	no change

a. SSM/I Data for 12/2303 December 1988

The SSM/I pass for 12/2301 covered the coastal North Atlantic Ocean waters from Cuba northward to New England including the incipient cyclone system indicated by the canopy of cold clouds in the GOES infrared image (Fig. 8). The SSM/I HAC rain rate image (Fig. 9) shows two different rain features. A large area of rain rate "out-of-limits" is analyzed along 30°N from the Florida coast eastward to the eastern edge of the pass (66°W). This area is located along the old frontal zone and is related to a variety of overcast clouds on the GOES image (Fig. 8). The visual and infrared satellite

data and synoptic situation would suggest light precipitation in this area and the reason for the "out-of-limit" category is not known. A second much smaller rain area is analyzed near the center of the incipient cyclone (33N 77W). Rain rates are analyzed to be 1-3 mm/h with a maximum of 4-8 mm/h. There is a gap of no rain analyzed between the coastal rain area and the large out-of-limits area. The curved southern edge of the out-of-limits area is due to a 1° band of missing data.

Since the HAC rain rate has large out-of-limits areas, the brightness temperatures for the 19 and 37 GHz channels will aid our analysis. The 19H, 37H, and the $T_b(37V-37H)$ brightness temperature images, Figs. 10, 11 and 12 respectively, describe a large area of precipitation just off the South Carolina and Georgia coast associated with the developing cyclone. There is good agreement between these images as to the extent of the precipitation. Using $T_b(19H)$ greater than 160 degrees or $T_b(37H)$ greater than 190 degrees gives a similar rain, no rain boundary. Using the $T_b(37V-37H)$ brightness temperature difference, rain area is analyzed to be somewhat smaller and centered on the incipient cyclone center. The $T_b(19H)$ and $T_b(37H)$ images also suggest light rain with the old frontal band as outlined in the GOES data. In particular, precipitation is analyzed from 28N 70W westward to south of the tip of Florida. The $T_b(37V-37H)$ analysis indicates only some rain areas on the front. The $T_b(19H)$ image has two large well defined cells of heavy precipitation embedded within the moderate rain area centered around this center. Around the incipient cyclone center the 37H channel shows a large analyzed area of heavy precipitation and no moderate to light rain along its southern and western edge. The sensitivity of the 37H channel to higher rain rates is illustrated by the large heavy precipitation in Fig. 11. While the $T_b(37V-37H)$ channel also shows its heaviest precipitation around the cyclone center, it also analyzes a few scattered smaller cells within the larger region.

Precipitation signatures in the 85 GHz data are investigated using a PCT image (equation 3.2) following the Spencer algorithm. The horizontal and vertical 85 GHz channels used to produce this image were very noisy and, as can be seen, the resultant image is the same (Fig. 13). The only area easily identifiable as having precipitation is centered on 32N 77W with some north-south extension. This area is analyzed as having only light precipitation, 1-3 mm/h, (Table 6). This small precipitation area is centered over the incipient cyclone and is in agreement with the other channels. There are no other precipitation areas identified for this time period by the PCT image.

The $T_b(19H)$ and 37H) thresholds provide a reasonable precipitation analysis for this period. The HAC analysis is difficult to interpret as important regions in the

image are classified out-of-limits. All four analyses have an area of precipitation analyzed off the South Carolina and Georgia coasts. However, the area on the HAC image is extremely small compared to the same area on the other images. Curiously, the HAC image has no rain analyzed between this small center of mostly 1-3 mm/h rain and the large area of out of limit values stretching west to east across 30N. This analysis indicates most of the incipient cyclone circulation as a no rain area. The $T_b(19H)$ and $T_b(37H)$ GHz images provide a consistent analysis of the precipitation around the incipient cyclonic center itself and also show rain along the old frontal zone located to the east of the low center extending southwest to Cuba. The $T_b(37V-37H)$ GHz image isolates the precipitation around the cyclonic low but shows little to no rain along the old frontal boundary. Noticeable in all images, but especially in the $T_b(19H)$ GHz is the large swath of missing data centered around 28N covering the pass from one edge to the other.

b. Ship and Radar Reports for 12/2303 December 1988

To further aid in analyzing the observed precipitation Table 10 lists all 13,000 ship observations within the SSM/I pass window that were reporting some type of WMO weather code (Appendix D) for this observation period. Also included are brightness temperatures that are a numeric average over a the resolution of each individual channel. The SSM/I rain rate was read off the HAC image itself. The PCT rain rate value was read directly off the PCT brightness temperature image.

Table 10. COMPARISON OF BRIGHTNESS TEMPERATURES AND RAIN RATES AT 13/0000 UTC 15 SEPTEMBER 1988 for selected ship observations. STID is the station identity of the reporting ship. Ship weather code is from the WMO standard weather code. The values for the brightness temperatures and the rain rates are the numeric average over the resolution of each individual channel. Out of limits (OOL) values are those that have passed through the screening logic of the algorithm but the value returned from the equation is unrealizable. N/A for brightness temperatures is where the pass was too narrow to cover the area over that ship observation. MD stands for missing or bad data from the pass.

STID	POSITION		BRIGHTNESS TEMPERATURE				SSM/I RAIN RATE (mm/h)	PCT RAIN RATE (mm/h)	SHIP WX CODE
	LAT (N)	LON (W)	19H	22V	37V	37H			
KRPD	34.30	74.40	118	245	206.5	141	0	0	2
KRJP	27.60	74.40	MD	MD	MD	MD	MD	MD	0
KSYP	28.30	70.08	167	257	237.5	200.5	OOL	0	80
NJPX	34.80	75.30	128	229	217.5	165	0	0	2
NYWL	33.50	76.90	174	N/A	241.5	218	N/A	0	11
PEBO	38.50	64.0	118	198	209.5	154	0	0	70
VDBG	30.70	80.40	153	N/A	227.5	185	N/A	0	25
WDBU	31.80	74.90	157	252	235	201	OOL	0	0
WGWC	34.09	74.00	124	250	210	148	0	0	1
WPHZ	30.20	77.60	179	N/A	252.5	235	N/A	0	52
YEK2	38.85	67.00	109	205	205	143	0	0	70

Figure 14, a weather rain map, is a plot of all ship observations (Table 10) and dropwindsonde soundings, if any, for the period closest to the actual pass time. There is a one hour time difference between the ship weather observations and the SSM/I data. Included with these ship positions are the WMO standard weather code symbols reported. The outline of the precipitation and out-of-limit areas from the SSM/I HAC algorithm image are also presented on the figure. The cyclone low center position with the central pressure is marked for the observation time.

The ship data provides some confirming evidence of the satellite precipitation analyses for this time. The only ships reporting any precipitation are located along 30N. Ship VDBG, reporting rain showers in the past hour, is along the western edge of precipitation area as indicated by 19 and 37 GHz channels. Note latitude and longitude of each report are available in Table 10. The HAC algorithm is out-of-limits for this location. Moving eastward, ship WPHZ is reporting drizzle at 30N 77W. This ship is on the southern edge of the 19 and 37 GHz rain area. Coastal National Weather Service radar data also confirms the large precipitation area with the new low. The United States radar summary for 12/2135 (not shown) depicts rain along the East Coast of the U.S. from the border of South and North Carolina southward to 28N in agreement with Figs. 10, 11, and 12. In the old frontal zone, ship KSYP is reporting showers. Although the HAC algorithm indicates an out-of-limits, the 19 and 37 GHz brightness temperatures indicate precipitation in this area. Further north along 40N are two ships reporting light snow, however, the SSM/I HAC or other brightness temperature images do not indicate any precipitation in this area. Possible reasons for no microwave signatures of these reports of snow showers, include the showers not filling the entire field of view, and the SSM/I is less sensitive to snow versus liquid water. The remaining ships, all of which are reporting no precipitation, are correctly analyzed by the HAC image.

The $T_b(19H)$ image correctly indicates precipitation over two of the ships reporting rain for this time period, KSYP, and WPHZ but misses the reports of VDBG, YEK2, and PEBO. Rain is analyzed over NYWL, and it is located on the northeastern edge of the light precipitation. The remaining non-precipitation ship observations verify with the $T_b(19H)$ analysis. The $T_b(37H)$ image compares well with the ship observations depicted on the weather rain map (Fig. 14), showing precipitation over KSYP and WPHZ. It incorrectly shows precipitation over NYWL and WDBU who are not reporting rain, but are both located on the edge of the suggested rain area. This image correctly analyzes no rain over the area around 34N 74W where three ships are reporting no precipitation. The $T_b(37V-37H)$ GHz image only analyzes one rain reporting ship correctly, WPHZ, while missing the rain reported by KSYP, PEBO, VDBG, and YEK2. Like the other images it too shows precipitation over NYWL and WDBU, while analyzing no precipitation over NJPX, KRPD and WGWC. The PCT image is difficult to use in this case due to the noise. It does not appear to analyze any type of precipitation over any of the ships reporting for this period.

2. 13/2257 DECEMBER 1988

During the next 24h subjective surface analyses from Chalfant (1989) show that the initial surface cyclone has moved rapidly eastward and now has a 997 mb central pressure at 32N 66W. A new cloud mass developed off the mid-Atlantic coast associated with the second short wave and is located at 37N 70W with a central pressure of 998 mb. A coastal trough, associated with this low center, extends from the 998 mb low to Long Island (Chalfant 1989). A GOES infrared image from 13/2301, Fig. 15, shows cold cloud tops are associated with the eastern frontal zone that is connected with the early cyclone center. They extend southwestward from 35N 55W to east of Cuba. Warmer (lower) cloud tops west of the front cover the center of the new low. The new cyclone has a large solid mass of growing cold clouds from Long Island extending south-south-east to 32N, 70W. A trailing frontal cloud band of warmer cloud tops is visible to the southwest. Some convective clouds are present to the west of this low.

a. *SSM/I Data for 13/2257 December 1988*

SSM/I data is available every 12h from the F8 DMSP satellite. Unfortunately, the morning pass for the 13th was not available, so the next SSM/I data for this study was for 13/2257. The SSM/I HAC rain algorithm image for this pass, Fig. 16, shows one large band classified as out of limits extending from 35N 61W to 25N 70W, where it changes to rain rate of 1-3 mm/h and continues southwestward to Cuba. 25N is the division between the mid-latitude and tropical zone in the HAC algorithm. The change from out-of-limits to light precipitation at 25N is due to the change to different coefficients in the rain algorithm. In addition, a scattered to broken area of out-of-limits precipitation is analyzed in the cloud shield between the two systems. A large band of moderate values of precipitation, 4-8 mm/h, starts at Long Island and extends southeast to 38N then turns and continues south-southwest to 33N. This precipitation region agrees well with the cold cloud region present in the GOES data.

The individual channel brightness temperature images clarify the interpretation of HAC rain rates. Figures 17, 18, and 19, corresponding to the, $T_b(19H)$, $T_b(37H)$, and the $T_b(37V-37H)$ images respectively, all analyze an extensive precipitation area from Long Island south-southeast to 32N 70W. The $T_b(19H)$ image is the only analysis where the precipitation band is not continuous all the way to the coast. The 19II channel has two large areas of heavy precipitation, the northern one located at 38N 70W and a second larger one centered just south of the new cyclone center. The $T_b(37II)$ image has two large areas of heavy precipitation of the comparable size located in the same position as the 19II image. All channels also analyze a broad area of precipitation

east of the new low extending from 70W to the eastern edge of the pass. The $T_b(37H)$ image indicates the largest area of precipitation while the $T_b(37V-37H)$ image has the least amount of precipitation. This precipitation is associated with the circulation of the first cyclone which is now centered at 32N 66W. Precipitation is indicated along the frontal band extending from 31N, 62W to Cuba by both the $T_b(19H)$ image and the $T_b(37H)$ image. The $T_b(37V-37H)$ image only depicts scattered precipitation in the front. Only the $T_b(37H)$ image analyzes any precipitation along the trailing front extending southwest from the new low and shower activity in the cold air west of the new cyclone center. Recall the resolution of the 37H channel is 37 km and is better than that of the 19 GHz channel.

The PCT image (Fig. 20) for this time shows a large band of light precipitation with a few small heavy precipitation cells embedded centered along 70W running from 40N to 33N. This area corresponds well with the cold cloud mass of the new cyclone center. The Spencer equation does not analyze any significant area of heavy rain. The PCT image shows no rain along the old frontal boundary or in the warm clouds between the two cyclone centers. The data remains quite noisy in this channel.

The SSM/I HAC algorithm compares extremely well with the other three images in analyzing the precipitation from Long Island south southeast to 31N 70W. All four images analyze rain rates to 15 mm/h along the front extending northward. The large broken area of HAC out-of-limit values analyzed east of the new cyclone center to the eastern edge of the pass appears to be light precipitation. The three brightness temperature images show from 50% to 80-85% rain coverage over this area. The HAC image analysis of out-of-limit values for the old frontal band extending from 31N 63W southwestward to Cuba, appears to be light precipitation. At 25N, where the HAC regression coefficients change due to a change in the climate code, the out-of-limit values on the SSM/I HAC image abruptly change to light precipitation. Rain rates calculated slightly north (25.4N) of 25N along this frontal band using coefficients for mid-latitude winter turn out to be small negative numbers. While rain rates calculated slightly south (24.8N) of 25N using coefficients for lower latitude transition zone, with similar brightness temperatures for the four channels, yield positive rain rates of 1-3 mm/h. The out-of-limit values in the area north of 25N occurs when the screening logic shows rain yet the calculated rain rate using the mid-latitude winter coefficients is a negative value. The disagreement occurs over a significant area. The $T_b(19H)$ and $T_b(37H)$ images both show some type of light to moderate precipitation along the entire length of this frontal

band, while the $T_b(37V-37H)$ image only shows a small band of rain along part of the length.

b. Ship and Radar Reports for 14/0000 December 1988

Ship weather reports for 14/0000, one hour after the pass, are plotted on Fig. 21 and listed in Table 11. Looking at Fig. 21, the probable precipitation area along 70W has nine ships located within it, and all are reporting precipitation. Five ships, GUQT, OYEK, VCWX, PJYG, and C6BB are reporting moderate to heavy rain around 35N 70W which confirms the moderate rain analyzed by the HAC image as well as the three brightness temperature images. KSYP is located in the shower activity (west of the new cyclone) within a small cell of precipitation analyzed as 1-3 mm/h, and she is reporting slight to moderate thunderstorms with hail. Microwave precipitation estimates with the 20-30 km horizontal resolution can not resolve shower activity properly. Note the 19H channel (69 km resolution) does not capture this convective area. KRPD is reporting light drizzle and is located within a small cell of light precipitation east of the main precipitation area. The U. S. radar summary for 13/2135 (not shown) shows a large area of rain extending from southern New England southward to 39N, and from the coast of New Jersey eastward to 70W. East of North Carolina a solitary cell of precipitation is shown centered at 35.5N 72.5W. The first area confirms the analysis of the HAC, $T_b(37H)$, and the $T_b(37V-37H)$ images, which all show precipitation in this area. The $T_b(19H)$ image shows some precipitation south of Long Island but it is not extensive enough to match the radar area. The second area on the radar summary indicates the showery precipitation indicated by the SSM/I HAC image and the 37H image west of the new low.

To the northeast KRHX is reporting drizzle and is located just to the north of a cell of light precipitation. Only two ships reporting rain, DHRG and C6WS are not within the microwave analysis areas. However, C6WS is right on the edge of the SSM/I pass while DHRG is reporting intermittent rain. There is the 63 minute difference between the SSM/I pass and the DHRG report. The large area of out-of-limit values around the old cyclone center (32N 66W) has no ship observations available within it. However, looking at Figs. 17, 18, and 19, it is likely that there is precipitation between the two low centers and along the front extending from the old low southwest to Cuba. The HAC algorithm agrees with most of the observation of intermittent type precipitation, Table 11, and, for the most part it indicates higher rain rates for the continuous precipitation reports.

Table 11. COMPARISON OF BRIGHTNESS TEMPERATURES AND RAIN RATES AT 14/0000 DECEMBER 1988 for selected ship observations. STID is the station identity of the reporting ship. Ship weather code is from the WMO standard weather code. The values for the brightness temperatures and the rain rates are the numeric average over the resolution of each individual channel. N/A for brightness temperatures is where the pass was too narrow to cover the area over that ship observation. For dropwindsondes an A for the first digit means it was dropped by and Air Weather service (AWS) aircraft, an N means it was NOAA/NCAR/Navy aircraft drop. S775 for a dropwindsonde WX code means the sounding was saturated to 775 mb.

STID	POSITION		BRIGHTNESS TEMPERATURE				SSM/I RAIN RATE (mm h)	PCT RAIN RATE (mm h)	SHIP WX CODE
	LAT (N)	LON (W)	19H	22V	37V	37H			
C6BB	34.70	70.69	228	216	251.5	245	7	1-3	63
C6A7	33.59	75.60	138	N/A	216.5	174	1	0	2
C6WS	35.5	60.02	N/A	N/A	N/A	N/A	N/A	0	63
DHRG	35.80	62.20	164	234	247	224	0	0	60
EHT9	37.80	73.80	116	224.5	205	142	0	0	0
GUQI	40.70	72.60	172.5	212	238	218	6	1-3	63
KAFO	34.80	75.50	122.5	N/A	210	150	N/A	0	0
KGTI	34.20	71.30	223	211	252	244	6	1-3	92
KK01	39.90	65.00	127	242	209	153	0	0	3
KLHC	34.20	75.30	133	N/A	222	173.5	N/A	0	1
KRHX	40.40	63.20	143	238.5	223	179	0	0	20
KRPB	33.30	71.19	184	210	232	185	0	0	29
KRPD	36.90	66.10	179.5	257	243	219	1	0	20
KSYP	33.00	73.69	136	206	222.5	177	1	0	96
OYEK	36.09	70.69	204	219	248	236	4.5	1-3	81
PJYG	36.20	69.60	184	210	233	203	2	1-3	81

SIPU	37.90	71.50	156	201	220	171	0	0	64
UEYP	37.50	70.80	178	206	235	206	2	1-3	62
VCWX	34.00	69.60	170	213	234	203	0	1-3	63
WTEZ	37.80	73.00	126	N/A	204	139.5	N/A	0	2
WZJC	37.80	73.00	126	211.5	210	150.5	0	0	1
A230	32.10	72.10	146	206	219.5	172	0	0	S775
A235	31.00	74.90	131	203	216	162	0	0	--
N002	39.14	67.19	125	246	207.5	148	0	0	--

All three brightness temperature images, Figs. 17, 18, and 19, strongly agree with the ship observations. The ship observations clustered around the center of the new cyclone located off the Virginia coast are all under an area of analyzed precipitation with a maximum intensity of 15 mm/h. The 19H and 37H T_b 's also correctly indicate precipitation within the warmer cloud tops between the two cyclone centers, thereby showing rain over DHRG, which the HAC algorithm missed. However, only the T_b (37H) image correctly analyzed precipitation over KRHX and KSYF. The reason the T_b (19H) image missed these areas is most of the ships are reporting intermittent rain or drizzle so the precipitation did not fill the wider field of view of the 19 GHz channel. It was detected by the better resolution of the 37 GHz channel. There were no discrepancies between any of the images reporting rain over observations not reporting rain.

The PCT image does depict heavy precipitation around 33N 71W in the vicinity of the thunderstorms reported by KGTI and KRPB. Table 11 shows that the PCT rain rate image verified with all ships reporting continuous precipitation at the reporting time except for KSYF. In that respect it compares well to the HAC algorithm image. However, the PCT image is showing the same intensity rain rate, 1-3 mm/h for all ships which reported rain, which considering the diversity in intensity of reported rain, seems suspect.

3. 16/2220 December 1988

The next three SSM/I passes occurred during the following ERICA observing period, IOP 3. The IOP 3 cyclone developed east of the mid Atlantic coast on the

morning of 17 December. This cyclone rapidly deepened moving northeastward to western Newfoundland. Central pressure of the system dropped from 1011 mb (17/0600) to 978 (18/1200). Multiple centers were analyzed during the rapid development similar to IOP 2.

a. SSM/I Data for 16/2220 December 1988

The first IOP 3 SSM/I pass investigated occurred at 16/2220. At this synoptic time the incipient low center had not formed. GOES imagery (Fig. 22) for 16/2231 shows a large area of mid and high clouds along the US East Coast. These clouds are associated with a cold front preceding the IOP 3 cyclone. The disturbance which will initiate the development is now producing a solid overcast cloud area over the Great Lakes.

The SSM/I pass at this time covered the frontal zone along the coast. The HAC SSM/I image, Fig. 23, shows a large broken area of out-of-limits rain rates oriented from 45°N 48°W to 30°N 64°W. Smaller areas of light precipitation are evident centered at 37°N latitude between 62°W and 67°W associated with the frontal clouds. These areas of precipitation correlate well with the center of the large cloud mass shown in the infrared image (Fig. 22). However, some of the out-of-limit area is probably additional precipitation along the front.

The $T_b(19H)$ image, Fig. 24, and the $T_b(37V-37H)$ image, Fig. 25, both show a band of probable rain with similar extent and intensity along a line running from 35°N, at the western edge of the pass, northeast to 42°N 50°W. This line follows the center of cold clouds depicted in the GOES imagery. On the other hand the $T_b(37H)$ image, Fig. 26, analyzes a somewhat broader band of rain along the same area but extends it northward to 48°N 47°W. The brightness temperature enhancements include the HAC rain pixels plus part of the out-of-limits area. The $T_b(19H)$ and the $T_b(37V-37H)$ data suggest higher rain rates toward the western side of the pass (35°N 67°W to 37.5°N 62°W). The $T_b(19H)$, $T_b(37H)$, and the $T_b(37V-37H)$ images all analyze precipitation areas centered on 27°N 63°W corresponding to a thunderstorm area located in this same area as shown on the GOES infrared image.

Again, the SSM/I HAC image does not compare well with the three images constructed solely from brightness temperatures. The small areas of light precipitation analyzed by the HAC image around 37°N 62°W are also analyzed by all three other images. However, the three brightness temperature images locate these areas within the elongated area of frontal precipitation. The SSM/I HAC image shows primarily out-of-limit values in this area. The SSM/I HAC image would be in much greater agreement

with the other images if the areas evaluated as out- of-limits were changed to some light precipitation.

Table 12. COMPARISON OF BRIGHTNESS TEMPERATURES AND RAIN RATES AT 17/0000 DECEMBER 1988 for selected ship observations. STID is the station identity of the reporting ship. Ship weather code is from the WMO standard weather code. The values for the brightness temperatures and the rain rates are the numeric average over the resolution of each individual channel. Out of limits (OOL) values are those that have passed through the screening logic of the algorithm but the value returned from the equation is unrealizable. N/A for brightness temperatures is where the pass was too narrow to cover the area over that ship observation. For dropwinsondes an A for the first digit means it was dropped by an Air Weather service (AWS) aircraft. S600 for a dropwinsonde WX code means the sounding was saturated to 600 mb.

STID	POSITION		BRIGHTNESS TEMPERATURE				SSM/I RAIN RATE (mm·h)	SHIP WX CODE
	LAT (N)	Lon (W)	19H	22V	37V	37H		
9VAP	32.59	72.50	N/A	N/A	N/A	N/A	N/A	2
BBXX	32.20	58.90	130	218	210	150	0	3
KK01	40.59	53.80	134	223	232.5	154.5	0	2
C959	42.50	51.40	163	234	233	197	0	61
GCCC	40.09	55.40	145	227	219	176	OOL	54
GYOQ	33.09	58.90	130	219.5	215	153.5	0	16
KRGJ	30.90	56.30	124.5	217.5	210	146	0	1
LAHD	33.20	59.90	131	220	211	151	0	0
S6BS	33.00	52.80	122	211	207	143	0	0
SQDR	31.70	55.50	122	213.5	209	143.5	0	2
UPAR	47.30	59.40	129.5	195	213	164	9	71
VYQJ	46.60	55.10	124	193	207.5	155.5	0	27

WMLH	38.40	52.50	135.5	221	211.5	156	0	2
WYBI	35.59	72.19	N/A	N/A	N/A	N/A	N/A	2
XCSG	36.70	66.60	158	229	233	197	0	63
Y5OV	30.70	72.19	N/A	N/A	N/A	N/A	N/A	25
A220	32.66	68.50	N/A	N/A	N/A	N/A	N/A	S600
A224	30.20	69.20	N/A	N/A	N/A	N/A	N/A	--

b. Ship Reports for 17/0000 December 1988

Ship weather reports are presented in Table 12 and plotted on Fig. 27. Only three ships reporting rain, C959, GCCC, and UPAR, are located within areas analyzed with measurable or out-of-limits precipitation and, therefore, can definitely confirm the rain analysis of the SSM/I HAC image. GYOQ, located just south of the out-of-limits area at 59W, reported precipitation was within sight but not at the time of observation. This ship report is also considered as verifying the rain analysis. The saturated dropwindsonde A220, located slightly west of the pass edge at 32.6N, is the only sounding that confirms rain for this observation period. No non-precipitation reporting ships are located in areas of suggested rain. There is only one ship, XCSG (36.7N 66.6W), that is reporting rain but is not located within a suggested rain area. However, it is on the western edge of the pass next to a raining area. Of the remaining eight ship observations within the pass borders, seven of them report no rain and are located in areas of no precipitation. The only exception is VYQJ, located at 46N 55W, which is so close to the Newfoundland coast it can not be properly distinguished from the land by the algorithm, so it is not used in the verification.

A study of the $T_b(19H)$ and $T_b(37V-37H)$ images indicate only one rain reporting ship is within an area analyzed as precipitation, C959. The $T_b(37H)$ channel rain enhancement covers both ship C959 and XCSG as well. Of the remaining four ships reporting rain two (UPAR and VYQJ) are located just south of Newfoundland and are too close to land to interpret. Of the last two rain reporting ships, GCCC is close to, but not in, an area of suggested precipitation. However, due to the 100 minute time difference between the orbit and ship reporting time and the intermittent nature of the precipitation, this report is not consistent with the analyses. The last rain reporting ship, GYOQ (33N 59W) is too far to the southeast of the rain areas to be valid. For all three

brightness temperature images the no precipitation ship reports were located in areas of analyzed no precipitation.

4. 17/2208 December 1988

Rapid cyclogenesis during IOP 3 started after 17/1200. The initial cyclone formed off the Delaware coast and moved eastward. By the time of the next SSM/I pass two distinct surface circulation systems were present, one located at 39N 68W (990 mb central pressure) and a second located at 40.5N 63.5W (central pressure of 991 mb), east of the first center. Both cyclonic centers are located under a comma-shaped large mass of cold clouds off the New England coast (Fig. 28). Also visible at the eastern edge of the GOES image is the old frontal cloud band trailing from the remnants of the IOP 2 cyclone. A distinct bulge is evident along the front at approximately 45N 45-50W and is associated with a frontal wave. The evening SSM/I pass at 17/2208 primarily covers this eastern frontal zone. Unfortunately, the western edge of the pass is along the edge of the developing IOP 3 storms. The SSM/I passes are not contiguous at this latitude and the next orbit provides coverage west of the cyclone over the East Coast. The frontal rain reports as well as the precipitation ahead of the IOP 3 storm will be investigated for this period.

a. SSM/I Data for 17/2208 December 1988

The HAC SSM/I image, dominated by out-of-limit classifications (Fig. 29), shows a large broken area of out-of-limit values extending southwestward from 45N 45W to 30N 55W corresponding to the old frontal boundary remaining from an earlier cyclone. Two small areas of light precipitation are outlined in the pass. One is embedded in the front and located southeast of Newfoundland at 45N 48W, while the other is at the western edge of the pass located at 42N 62W corresponding to the eastern edge of the deepening cyclone south of Nova Scotia.

The $T_b(19H)$ image from this pass, Fig. 30, analyzes one nearly continuous area of precipitation from 48N 55W extending to the southwest to 27N 65W along the frontal cloud band. It has four moderate to heavy rain regions embedded within its band with only a small break at 38N. The largest area of heavy precipitation is located at the northern end of the frontal band near the developing surface wave off the western edge of the pass. The $T_b(19H)$ channel image analyzes no precipitation, along the western edge of the pass, centered at 41N as did the HAC image, but shows rain at 39N.

The $T_b(37H)$ image, Fig. 31, analyzes similar precipitation areas along the frontal zone with the same break in the pattern at 38N. It also shows a large area of heavy rain in the northern end of the precipitation area. Also indicated is some precip-

itation at the western edge of the pass at 41N, corresponding to the eastern edge of the large cold cloud mass off the New England coast. Some scattered areas of light precipitation are also indicated east of the IOP 3 cyclone along 40N. If the out-of-limit values for the SSM/I HAC image were considered as rain areas, the $T_b(37H)$ and HAC images would be very similar.

The $T_b(37V-37H)$ image, Fig. 32, gives the same general pattern of precipitation as the two previous images; however, the analyzed precipitation along the old frontal band is discontinuous and narrow. At 45N 48W there is a large area of moderate precipitation with three embedded cells of heavy intensity rain. This agrees with the enhancements from the other channels.

The one significant area of HAC analyzed precipitation is a light to moderate area located at 44N 48W. This area compares well with the three brightness temperature images which all indicate moderate to heavy precipitation in this area. One other small area light precipitation analyzed by the HAC image is located just above 40N at the western edge of the pass. Only the $T_b(37H)$ image analyzed precipitation here, while the other two images show precipitation just to the south of 40N. The large area of out-of-limit values evaluated in the HAC image corresponds to the frontal rain bands that all three brightness temperature enhancements suggest as rain.

b. Ship Reports for 18/0000 December 1988

The ship reports for 18/0000 are listed in Table 13 and plotted on Fig. 39. Three rain reporting ships, KRGJ, S6BS, and 4XID, were located within the large area of suggested precipitation by the SSM/I HAC image. While FNRW and GUQI, both located on the western edge of the pass, are reporting rain, they are close enough to the light precipitation analyzed by the HAC image to verify that portion of the analysis. Two other reports, XCSG and the dropwinsonde A222, located to the east of FNRW and GUQI, are also in proximity to a small analyzed rain area (44N 58W) to validate that area. Only one ship LAHE (36.7N 55.2W) is reporting no rain yet it is located within an area analyzed as rain, although positioned on the far western edge of the rain area. The remaining seven ship observations of no rain are positioned in areas analyzed as no rain by the HAC algorithm.

Table 13. COMPARISON OF BRIGHTNESS TEMPERATURES AND RAIN RATES AT 18/0000 DECEMBER 1988 for selected ship observations. STID is the station identity of the reporting ship. Ship weather code is from the WMO standard weather code. The values for the brightness temperatures and the rain rates are the numeric average over the resolution of each individual channel. Out of limits (OOL) values are those that have passed through the screening logic of the algorithm but the value returned from the equation is unrealizable. N/A for brightness temperatures is where the pass was too narrow to cover the area over that ship observation. For dropwindsondes an A for the first digit means it was dropped by an Air Weather service (AWS) aircraft, an N means it was a NOAA/NAVY/NCAR aircraft drop.

STID	POSITION		BRIGHTNESS TEMPERATURE				SSM/I RAIN RATE (mm h)	SHIP WX CODE
	LAT (N)	LON (W)	19H	22V	37V	37H		
4XID	37.90	51.70	154	240.5	222	185	OOL	60
C6DS	35.80	68.60	N/A	N/A	N/A	N/A	N/A	25
DDQS	36.40	69.90	N/A	N/A	N/A	N/A	N/A	96
FNRW	41.50	63.20	N/A	N/A	N/A	N/A	N/A	63
GHZK	40.40	69.90	N/A	N/A	N/A	N/A	N/A	75
GUQI	39.09	63.50	162	231	235	206	0	71
J8QX	46.70	59.50	103	186	204	134	0	2
KRGJ	30.80	62.40	160	245.5	224.5	178	OOL	80
KRHG	36.09	67.80	N/A	N/A	N/A	N/A	N/A	0
LAHD	33.59	52.90	141	231	215	158	0	0
LAHE	36.70	55.30	149	234	217	166	OOL	0
PJYG	36.59	69.19	N/A	N/A	N/A	N/A	N/A	81
S6BS	31.00	61.40	145	238	217.5	163	OOL	81
SQDR	30.00	60.80	141	235	216	159	0	2
VOGT	46.40	55.40	107	191	205	136	0	2
WIEE	32.40	52.60	137	230	213	155	0	0

WPKD	39.00	53.90	141	227	212	158	0	1
WWPI	37.09	67.80	N/A	N/A	N/A	N/A	N/A	0
XCSG	40.59	59.50	142	219	227	186	0	81
Y4IO	42.60	50.90	174	241.5	248	230	0	46
Y5OV	32.80	65.50	N/A	N/A	N/A	N/A	N/A	50
N214	39.80	65.80	N/A	N/A	N/A	N/A	N/A	S500
N220	39.21	66.88	N/A	N/A	N/A	N/A	N/A	S500
A222	40.99	60.10	139	217	220	173.5	0	S720
N223	38.13	68.66	N/A	N/A	N/A	N/A	N/A	S850

For the $T_b(19H)$ channel enhancement image only two rain reporting ships, GUQI and KRGH, are located in areas of analyzed precipitation. The $T_b(37H)$ and $T_b(37V-37H)$ images indicate a smaller precipitation area and only GUQI is covered by these channels. Another ship, Y4IO is positioned in an area of possible precipitation, yet the ship is only reporting fog. All three brightness temperature images show no rain areas over three ships that are reporting rain, 4XID, S6BS, and XCSG, and one dropwinsonde, A222, that is saturated. However, precipitation is analyzed in the proximity of 4XID. Since there is a two hour time difference between the SSM/I pass and the ship observations time, this ship is considered as consistent with the analysis. The $T_b(37H)$ image shows a suggested precipitation area close to the rain report of XCSG and the saturated sounding A222. Ship S6BS, reporting moderate or heavy rain showers, is located in a non-rain area according to the SSM/I; however, the frontal precipitation is analyzed 100 km to the northeast. Given this observation is two hours after the pass, the ship may be reporting frontal precipitation. The remaining seven ships reporting no rain are positioned in non-precipitation areas.

5. 18/0941 December 1988

At the time of this pass, the IOP 3 cyclone reached its lowest central pressure, 978 mb. The low center has almost reached the Nova Scotia coast and is depicted on the GOES infrared data (Fig. 37) as a large comma cloud covering the Canadian maritime provinces. Most of the higher clouds are located north of the low with a front ex-

tending southwest from the eastern tip of Newfoundland all the way to Cuba. A large outbreak of convective cloudiness is present west of the frontal band associated with the movement of cold air over the warmer ocean waters. This SSM/I pass covers an area from Newfoundland southeast over the Atlantic ocean to 20N. A subscene from 69W to 50W and 30N to 50N is used to analyze the cyclone and frontal precipitation.

a. SSM/I Data for 18/0941 December 1988

The SSM/I HAC image, Fig. 35, contains a large broken area of out-of-limit values extending northeast from 30N 63W to 39N 52W, with a narrow northward extension along 55W stopping at 45N. There are four areas of precipitation outlined in the SSM/I HAC image. Two are collocated within a large mass of out of limit values at 37N 54W. The largest area is centered at 37N 67W under some convective clouds. The fourth area is a scattered area of 1-3 mm/h precipitation extending from 42N 67W to 42N 59W.

The main area of analyzed precipitation for the T_b (19H) image, Fig. 36, extends northeast from 30N 65W to 38N 53W. Three heavy precipitation cells are embedded within its length, the two eastern-most correspond to the light to moderate precipitation areas outlined in the SSM/I HAC image. This main area of precipitation is also similar to the areas analyzed by the T_b (37H) image, Fig. 37, and the T_b (37V-37H) image, Fig. 38. However the T_b (37H) image indicates a broader coverage of this area, while the T_b (37V-37H) image is narrower and not as continuous. The T_b (37H) image is the only one of the three that shows a continuous band of precipitation extending northward along 55W. This image also shows a large mass of light precipitation at 37N, 67W, corresponding to some developing convective cloudiness.

b. Ship Reports for 18/1200 December 1988

The precipitation areas of the SSM/I HAC image correlate well with six precipitating reporting ships, LAHE, ZBWF, DDQS, GYOQ, VCLM, and WPVF (Table 14). Three rain reporting ships Y4IO, PJYG, and WIEE, are very close to the edge of suggested rain areas and, because of the more than two hour difference between the SSM/I orbit time and ship observation time, they are counted as consistent reports. Finally, C6DS (35.6N 68.3W) is slightly off the western edge of the pass and adjacent to an area analyzed as light precipitation, so this observation is also considered as verifying correctly. No non-precipitation reporting ships are in areas of suggested rain, nor are any precipitation reporting ships in any analyzed areas of no rain. Unfortunately, all of the reports near the northern edge of the pass near Nova Scotia and

Newfoundland coasts are either within a 3° wide swath of missing data or are too close to land to be used with any confidence.

The $T_b(19H)$, $T_b(37H)$, and the $T_b(37V-37H)$ enhanced brightness temperature images show LAHE and ZBWF, who are reporting rain, located within areas of suggested rain. GYOQ, reporting intermittent showers is within rain areas for the 19H and 37H channels only. VCLM and WPVF are either in reasonable proximity to rain areas to verify as a consistent report or are actually analyzed within an area of suggested rain. PJYG (37N 67W) and Y4IO (42.4N 52.1W) are only analyzed correctly by the $T_b(37H)$ image. The three remaining rain reporting ships, DDQS, WIEE, and VCTG, are located in non-rain areas for all three brightness temperature images. DDQS is located to the north of a shower region for the $T_b(37H)$ image, so it is consistent with the analyses. However, neither the $T_b(19H)$ nor the $T_b(37V-37H)$ images analyze showers in the area. WIEE is located southeast of the frontal rain band for all three brightness temperature images. Allowing for the time difference of two hours between the SSM/I orbit time and ship observation reporting time this is not a strong disagreement. The last missed rain report is that of VCTG, but this ship is located just east of Nova Scotia and is affected by the land/sea discrimination table within the SSM/I channels. None of the images show rain areas analyzed over non-precipitating ship reports. The remaining six non-precipitating ship reports are within areas of no precipitation in all three brightness temperature images.

Table 14. COMPARISON OF BRIGHTNESS TEMPERATURES AND RAIN RATES AT 18/1200 UTC DECEMBER 88 for selected ship observations. STID is the station identity of the reporting ship. Ship weather code is from the WMO standard weather code. The values for the brightness temperatures and the rain rates are the numeric average over the resolution of each individual channel. MD stands for missing or bad data from the pass. N/A for brightness temperatures is where the pass was too narrow to cover the area over that ship observation. MD stands for missing or bad data from the pass. For dropwindsondes an A for the first digit means it was dropped by an Air Weather service (AWS) aircraft, an N means it was NOAA/NAVY/NCAR aircraft drop.

STID	POSITION		BRIGHTNESS TEMPERATURE				SSM/I RAIN RATE (mm/h)	SHIP WX CODE
	LAT (N)	LON (W)	19H	22V	37V	37H		
C6DS	35.59	68.30	N/A	N/A	N/A	N/A	N/A	88
C389	45.10	61.70	MD	MD	MD	MD	MD	70
CGCQ	45.80	60.70	211	238	N/A	N/A	N/A	69
CYML	45.50	60.20	MD	MD	MD	MD	MD	10
DDQS	37.80	66.80	123	203	215	164	2	16
FNRW	42.20	65.80	MD	MD	MD	MD	MD	83
GYOQ	30.40	65.69	156	241	235	199	OOL	60
J8QX	45.30	57.00	MD	MD	MD	MD	MD	1
KRGJ	31.30	65.30	146.5	231	218	166	0	2
KRNJ	46.30	54.90	MD	MD	MD	MD	MD	60
LAHE	36.20	58.30	160	240	230.5	192	OOL	25
PJYG	34.70	67.10	144	220	228	190	0	80
VCLM	33.30	54.30	152	242.5	225	177	OOL	65
VCTG	46.50	59.90	149	218	223	183	IND	23
VCWJ	43.10	65.90	MD	MD	MD	MD	MD	15
VRKB	39.20	59.80	136	215	214	159	0	3

VYSV	44.80	66.69	MD	MD	MD	MD	MD	22
WIEE	32.09	56.80	145	234	218	163	0	20
WPKD	39.20	58.10	139	222	215	163	0	1
WPVF	36.80	53.90	140.5	220	221	172.5	OOL	60
WWPI	35.90	63.40	139	222	220	175.5	0	0
XCSG	42.30	55.80	152	227	227.5	193	0	1
Y4IO	42.40	54.10	135.5	225	213	156	0	62
YWD6	40.50	68.10	115	191.5	205	145	0	2
ZBWF	37.59	53.50	197	254.5	252	238	1	82
N081	42.21	63.07	MD	MD	MD	MD	MD	--
N082	41.26	62.15	133.5	205	211	157	0	--
N085	39.69	60.65	135	211	213	163	0	--

V. SUMMARY AND CONCLUSIONS

SSM/I rain rate estimates have been investigated for two periods of cyclogenesis observed by the ERICA project. Four precipitation analysis methods were studied, (1) the current SSM/I HAC algorithm, (2) the Spencer et al (1989) 85 GHz polarization difference (PCT), (3) enhancements to the $T_b(19H)$ and $T_b(37H)$ brightness temperature images and, (4) the $T_b(37)$ GHz polarization difference. Ship, coastal radar data and dropwinsonde soundings for the closest reporting period to each orbit were used to validate the images in each IOP.

There is considerable uncertainty in the interpretation of the HAC rain rate algorithm. Specifically, large out-of-limits rain rate areas occur in the vicinity of winter cyclones. This was a common occurrence for mid-latitude winter data examined in this study. The study of the SSM/I HAC rain rate has indicated the out-of-limits areas occur where the rain flags indicate rain (i.e. when $T_b(19H)$ greater than 160 K, or when $T_b(37V-37H)$ is less than 30 K) yet the rain rate calculated from the regression equations is less than zero. One approach for the display of the HAC data would be to treat the out-of-limit classification as no rain. The data analyzed in this thesis suggests this approach would eliminate significant areas of light precipitation. A second approach would be to reclassify the out-of-limit values as light precipitation and this approach would be the preferred short range solution.

The areas of light-moderate precipitation, 1-8 mm/h, analyzed by the HAC data do compare well with ship, radar data and the dropwinsonde soundings. Although the overall areas designated as light and moderate precipitation by the HAC data is small, relative to the large out-of-limits area, they accurately depict regions of rain. The SSM/I HAC data also does well in analyzing shower activity and isolated cells of moderate to heavy precipitation. The PCT images, studied in IOP 2, were extremely noisy and, therefore, difficult to interpret. However, the areas of suggested precipitation were located in close vicinity to convective and heavy precipitation areas. The amount of noise in the 85 GHz image prevented a more detailed analysis.

The enhanced $T_b(19H)$ and $T_b(37H)$ GHz provided alternative, useful rain-no rain analyses. The $T_b(37H)$ is found to be better at mapping total rain areas. In particular, the $T_b(37H)$ with its higher resolution resolves post-frontal shower activity which is not resolved by $T_b(19H)$ channel. Also, the $T_b(37H)$ channel has better sensitivity to light

rain areas than the $T_b(19H)$. The $T_b(37H)$'s warmer temperature enhancements appear to overestimate the extent of moderate and heavy precipitation areas. The threshold temperature of 220 K for the heaviest rain should be increased to 245 K. For improved heavy precipitation analysis, the $T_b(19H)$ channel should be used. The $T_b(37V-37H)$ indicates the smallest regions of precipitation areas. The rain/no rain flag of 30 K appears too low and should be revised upward.

The rain/no rain comparisons between the ship observations and the four different brightness temperature channels from the five SSM/I orbits studied in IOP 2 and 3 have been summed and are presented in Tables 15, 16, 17, 18, and 19. Tables 15 and 16 summarize the SSM/I HAC results. The out-of-limits areas are handled two different ways in the tables. In Table 15, the out-of-limit area is assumed to be no rain, while Table 16 uses these areas as rain. Comparing these two tables it is evident that over twice as many ship rain reports are correctly identified when the out-of-limit areas are considered as precipitation regions. Although the no rain ship reports classification is slightly less successful, the overall percentage of correct reports increases by 16%, from 61% to 77%. The out-of-limit areas appear to be reliable estimates of rain, but a major problem is the regression estimates of negative rain rates. New regression equations are urgently needed to eliminate this out-of-limits category. For now, labeling of the out-of-limit values as light rain, 1-3 mm/h, would be a reasonable approach, which is supported by the results in Table 16.

Table 15. RAIN/NO RAIN STATISTICS FOR THE SSM/I HAC IMAGE when OOL values are considered to be no rain.

SSM/I VS SHIP OBSERVATIONS		SHIP AND DROPWINDSONDE OBSERVATIONS	
		RAIN	NO RAIN
SSM/I HAC IMAGE	RAIN	11	1
	NO RAIN	26	32

Table 16. RAIN/NO RAIN STATISTICS FOR THE SSM/I HAC IMAGE when OOL values are considered to be rain values.

SSM/I VS SHIP OBSERVATIONS		SHIP AND DROPWINDSONDE OBSERVATIONS	
		RAIN	NO RAIN
SSM/I HAC IMAGE	RAIN	24	3
	NO RAIN	13	30

Tables 17, 18, and 19 describe the comparison between ship and dropwindsonde reports and the $T_b(19H)$, $T_b(37H)$, and $T_b(37V-37H)$ channel enhanced brightness temperature images. From Tables 17 and 18, it can be seen that they both have a better percentage of correct reports, 74% and 71%, respectively, than the SSM/I HAC image excluding the out-of-limits areas. The $T_b(37V-37H)$ brightness temperature image does the poorest of the three enhanced brightness images, with only 64% of the ship and dropwindsondes correctly analyzed. However, even with this lower percentage it is still slightly better than the basic SSM/I HAC image. This channel does better than all the others in analyzing areas of no precipitation over ships reporting no rain, but did not successfully analyze the rain reporting ships, missing two-thirds of them.

When the out-of-limits areas are classified as rain, the statistics from the HAC (Table 16), $T_b(19H)$ and $T_b(37H)$ are comparable. The classification of no rain ships is quite successful. The major difficulty appears to be the classification of rain reporting ships as no rain. Most of this is attributable to two causes: (1) the time difference between the SSM/I pass and the ship reporting times (over 2h for the worst case), and (2) the intermittent or shower type weather reported by the ships. Approximately 50% of the rain reporting ships classified as no rain by all the methods is due to the intermittent or shower type weather reported, while only 15% of the missed rain reporting ships is due to the time difference between the SSM/I pass and the ship reporting time.

There were a total of 12 moderate to heavy rain reports for this data period. The $T_b(37H)$ analyzed nine correctly, the $T_b(19H)$ correctly analyzed eight, while the $T_b(37V-37H)$ images only interpreted seven correctly. The SSM/I HAC images were able to correctly analyze seven, with two analyzed in out-of-limits areas. Therefore, all the enhanced brightness temperature images were as successful as the basic HAC image at analyzing the moderate to heavy rain reports.

Table 17. RAIN/NO RAIN STATISTICS FOR THE T_b (19H) IMAGE

SSM/I VS SHIP OBSERVATIONS		SHIP AND DROPWINDSONDE OBSERVATIONS	
		RAIN	NO RAIN
T_b (19H) IMAGE	RAIN	21	2
	NO RAIN	18	35

Table 18. RAIN/NO RAIN STATISTICS FOR THE T_b (37H) IMAGE

SSM/I VS SHIP OBSERVATIONS		SHIP AND DROPWINDSONDE OBSERVATIONS	
		RAIN	NO RAIN
T_b (37H) IMAGE	RAIN	20	4
	NO RAIN	18	33

Table 19. RAIN/NO RAIN STATISTICS FOR THE T_b (37V-37H) IMAGE

SSM/I VS SHIP OBSERVATIONS		SHIP AND DROPWINDSONDE OBSERVATIONS	
		RAIN	NO RAIN
T_b (37H) IMAGE	RAIN	12	1
	NO RAIN	26	36

From this study it is obvious that the four channel SSM/I HAC regression algorithm, in its current form can not satisfactorily analyze the operational precipitation. Using a single or dual channel measurement appears to give similar results. Until a better precipitation algorithm is devised, enhancements of the basic channel images would provide valuable information for the operational meteorologist.

Recommendations for future study include studying more SSM/I passes within the remaining ERICA IOP's. Hopefully, SSM/I data over fully mature cyclone centers can be obtained to more accurately determine how the SSM/I HAC regression algorithm resolves heavy rainfall. Further study is needed to determine if the regression approach can be used to estimate precipitation areas, particularly in light precipitation areas. The best method of SSM/I verification would be with aircraft radar data at the same time as the satellite pass. Numerous flights by the NOAA P-3 radar-equipped aircraft were

made during ERICA. The intercomparison of radar and SSM/I data would provide an exciting data base to develop new SSM/I rain rate algorithms.

APPENDIX A. SATELLITE PRECIPITATION ESTIMATION FIGURES

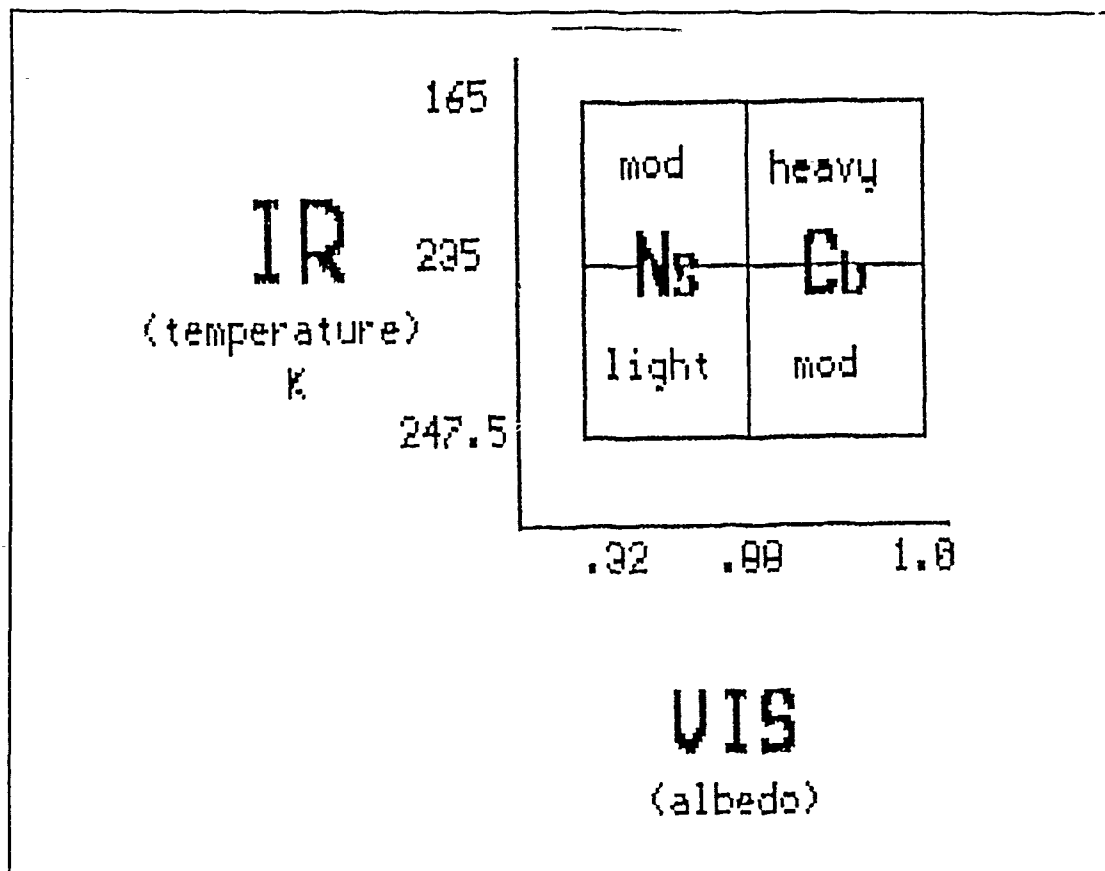


Fig. 1. Two dimensional precipitation histogram using GOES IR and VIS digital satellite data. [After Sheridan (1988).]

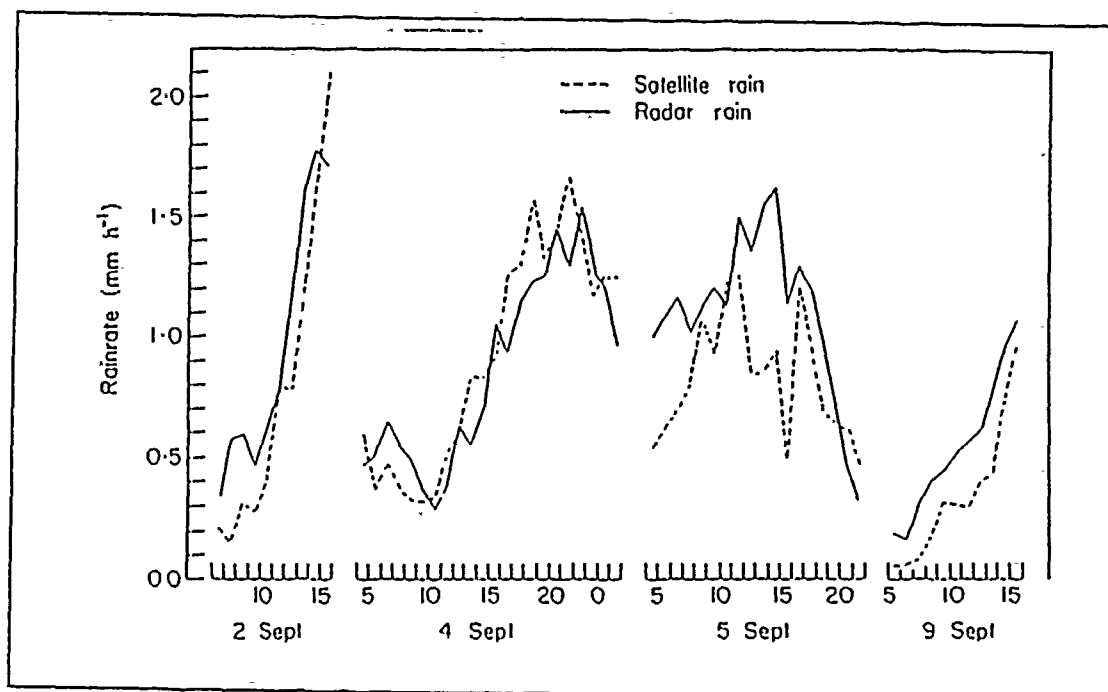


Fig. 2. Satellite rain rate versus radar rain rate. [After Stout et al (1979).]

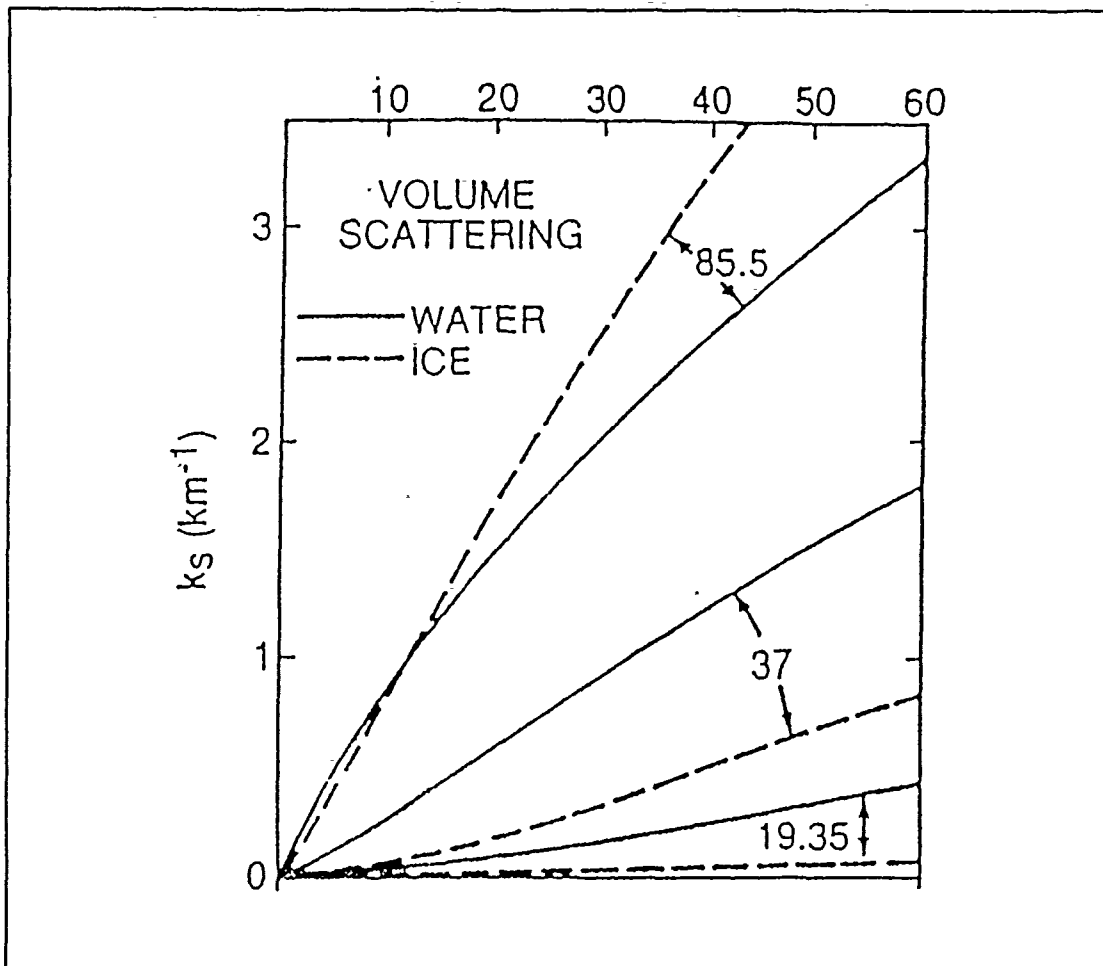


Fig. 3. Mie volume scattering coefficients for a Marshall-Palmer precipitation size distribution of water and ice spheres at three frequencies (GHz). [After Kidder and Vonder Harr (1990).]

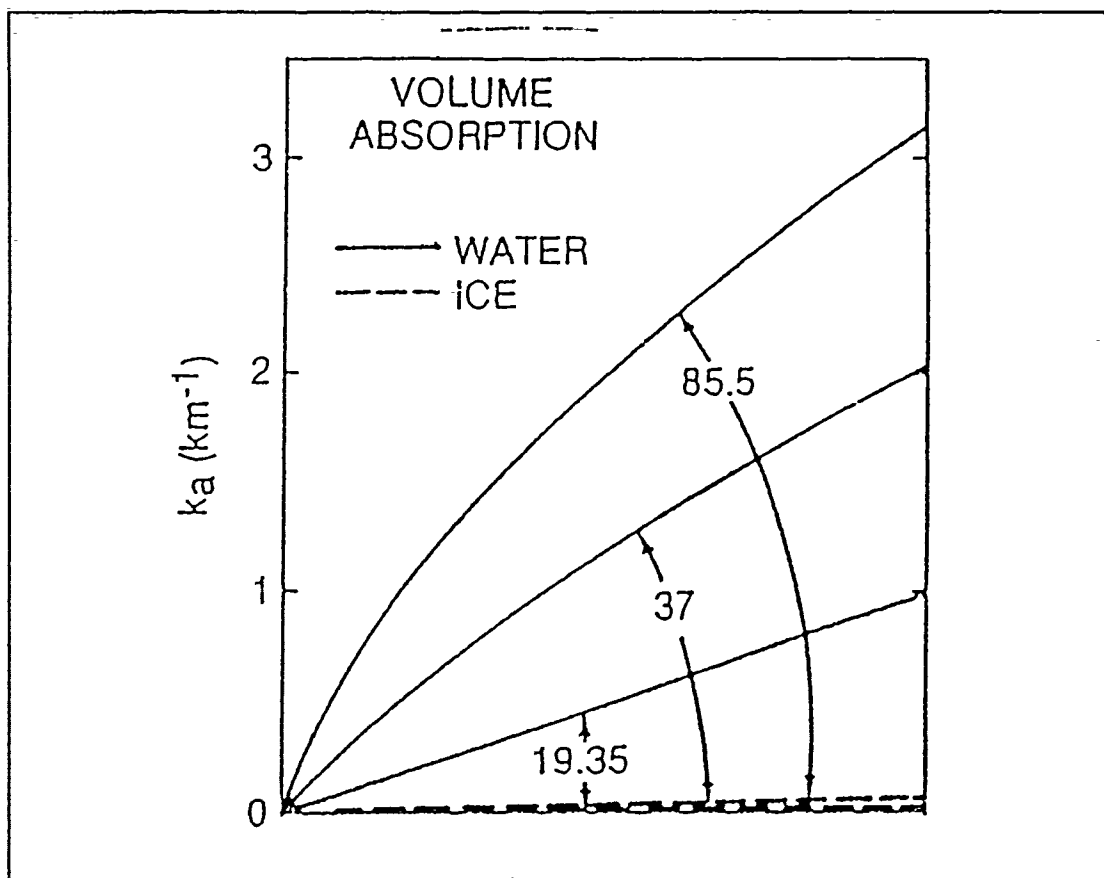


Fig. 4. Volume absorption coefficients for a Marshall-Palmer precipitation size distribution of water and ice spheres at three frequencies (GHz). [After Kidder and Vonder Harr (1990).]

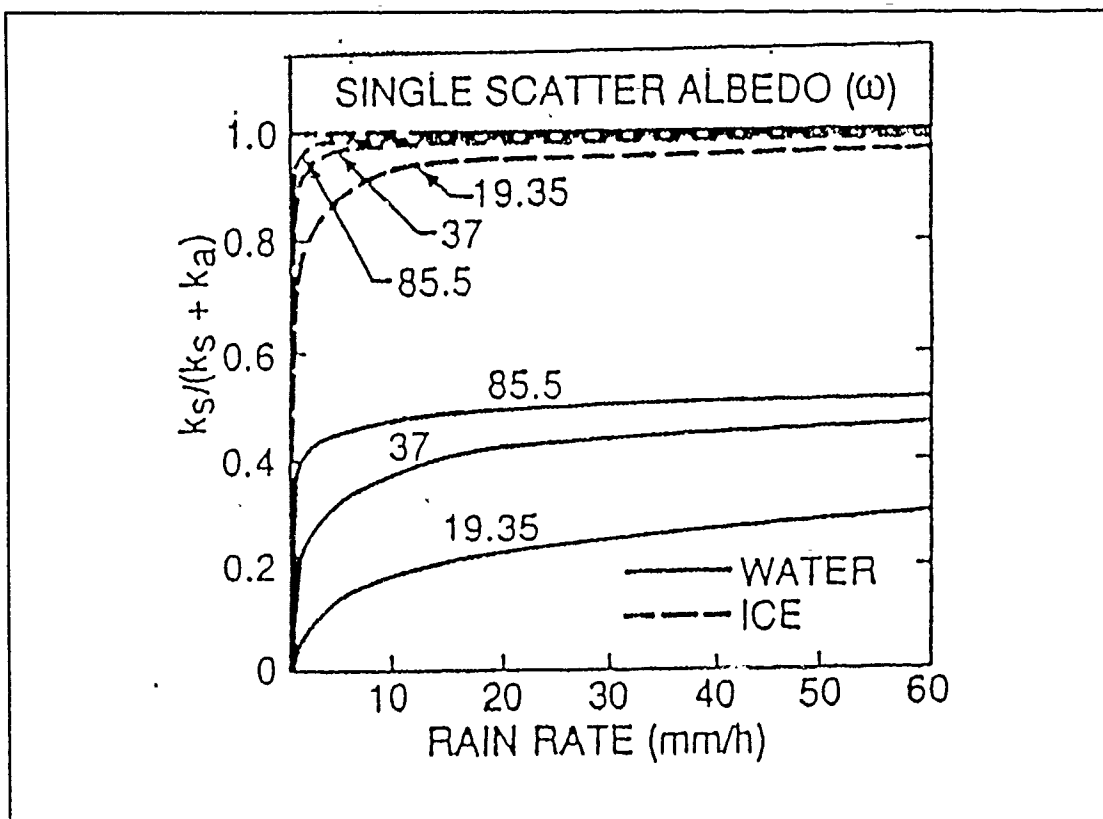


Fig. 5. Single scattering albedos for a Marshall-Palmer precipitation size distribution of water and ice spheres at three frequencies (GHz). [After Kidder and Vonder Harr (1990).]

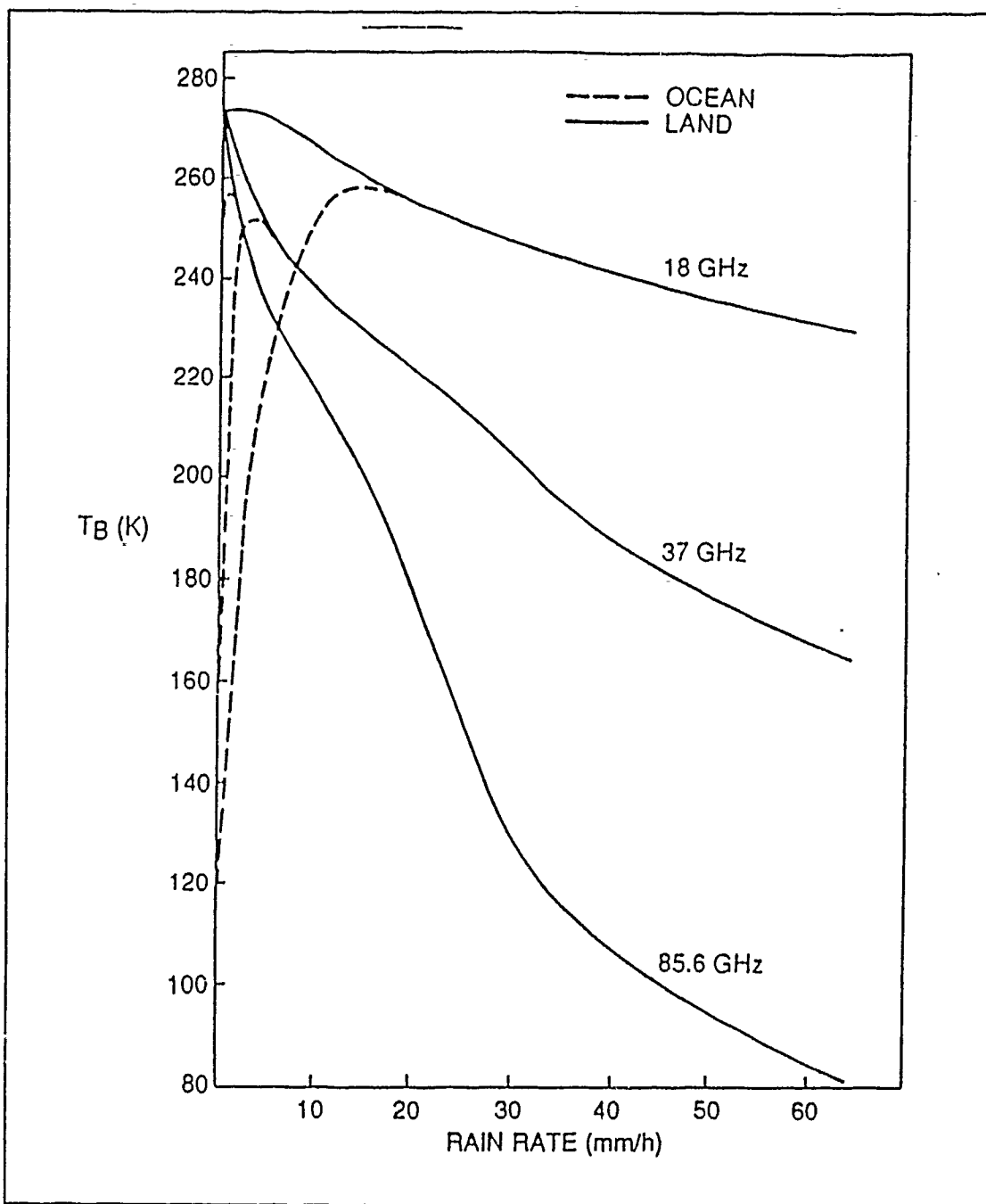


Fig. 6. Brightness temperature versus rain rate. [After Kidder and Vonder Harr (1990).]

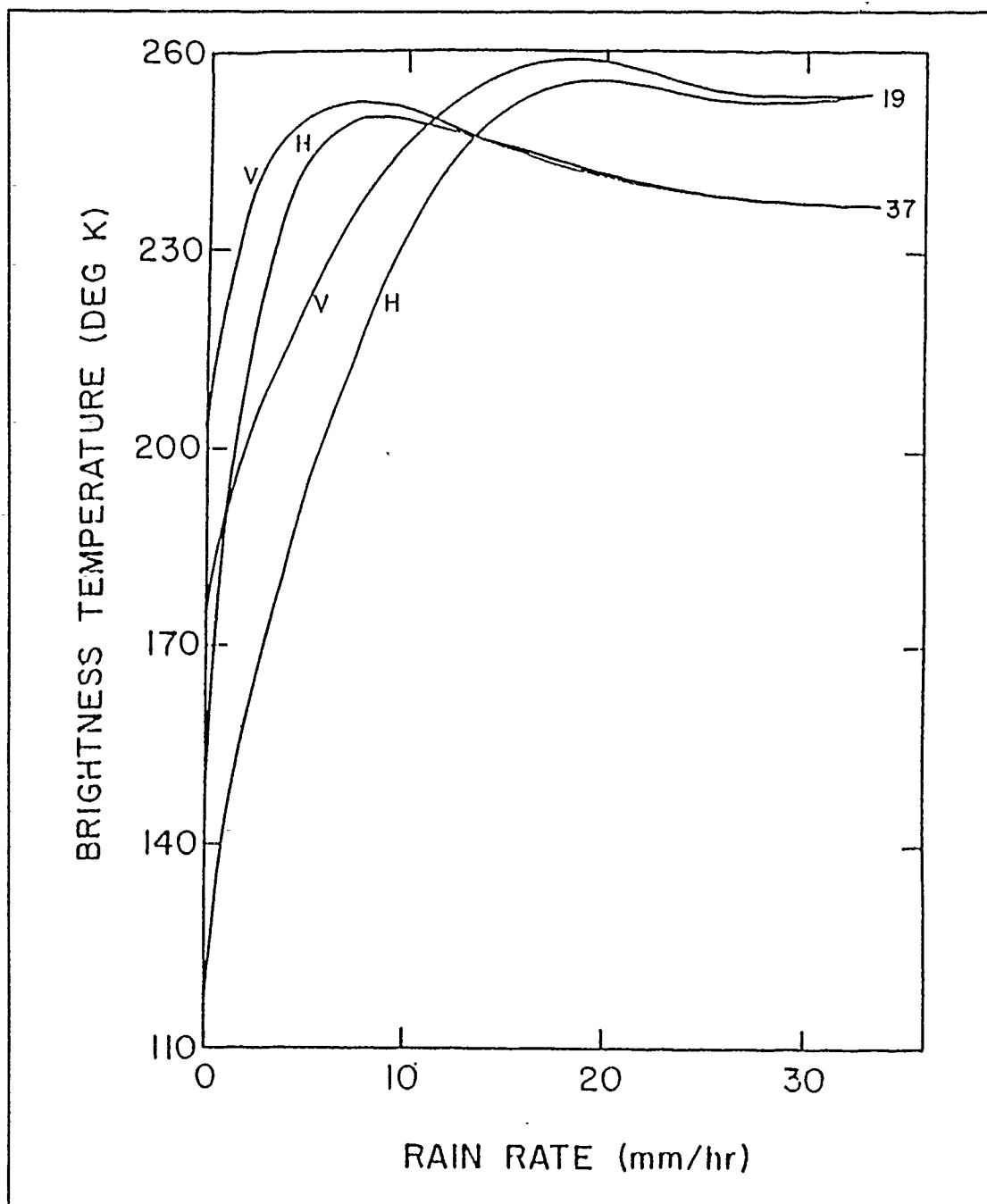


Fig. 7. Mid-latitude ocean brightness temperature versus rain rate at 19 and 37 GHz. [After Hollinger et al (1987).]

APPENDIX B. CASE STUDY OF IOP 2

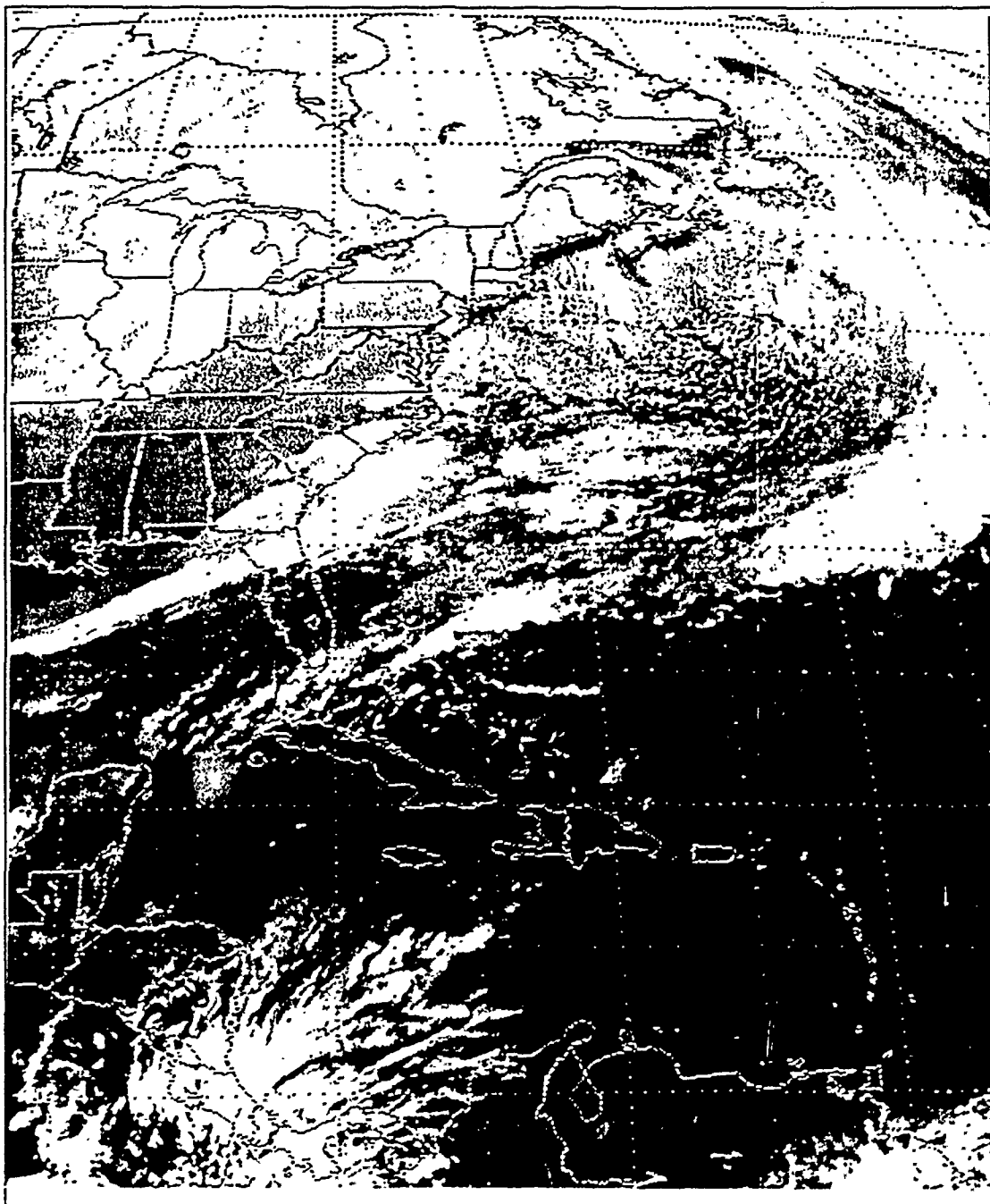


Fig. 8. GOES infrared east coast U.S. sector imagery for 12/2301 December 1988.

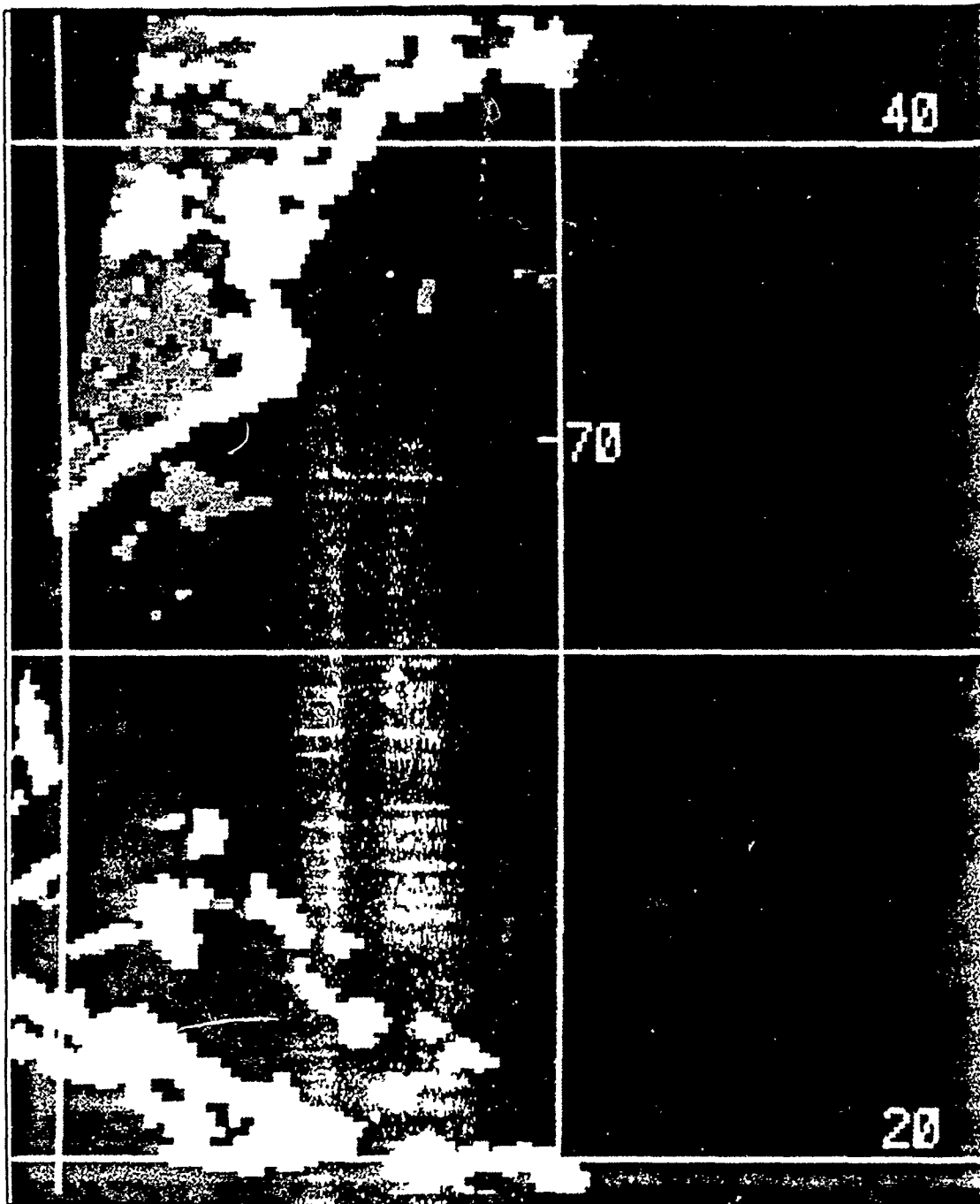


Fig. 9. SSM/I HAC precipitation image at 12:2303 December 1988. For color code values see table 5.

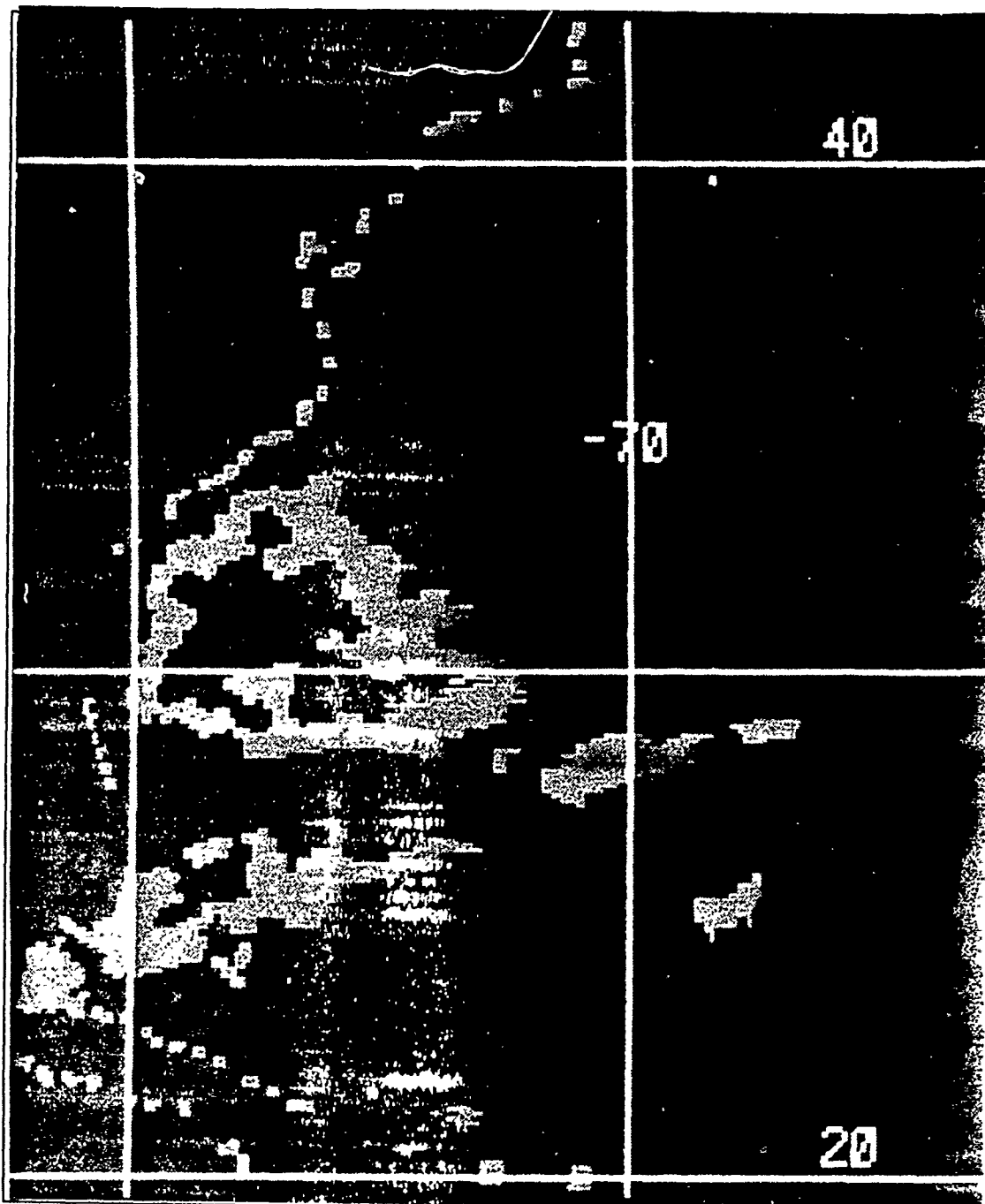


Fig. 10. SSM I 19H GHz brightness temperature image at 12:2303 December 1988. For color code values see table 9.

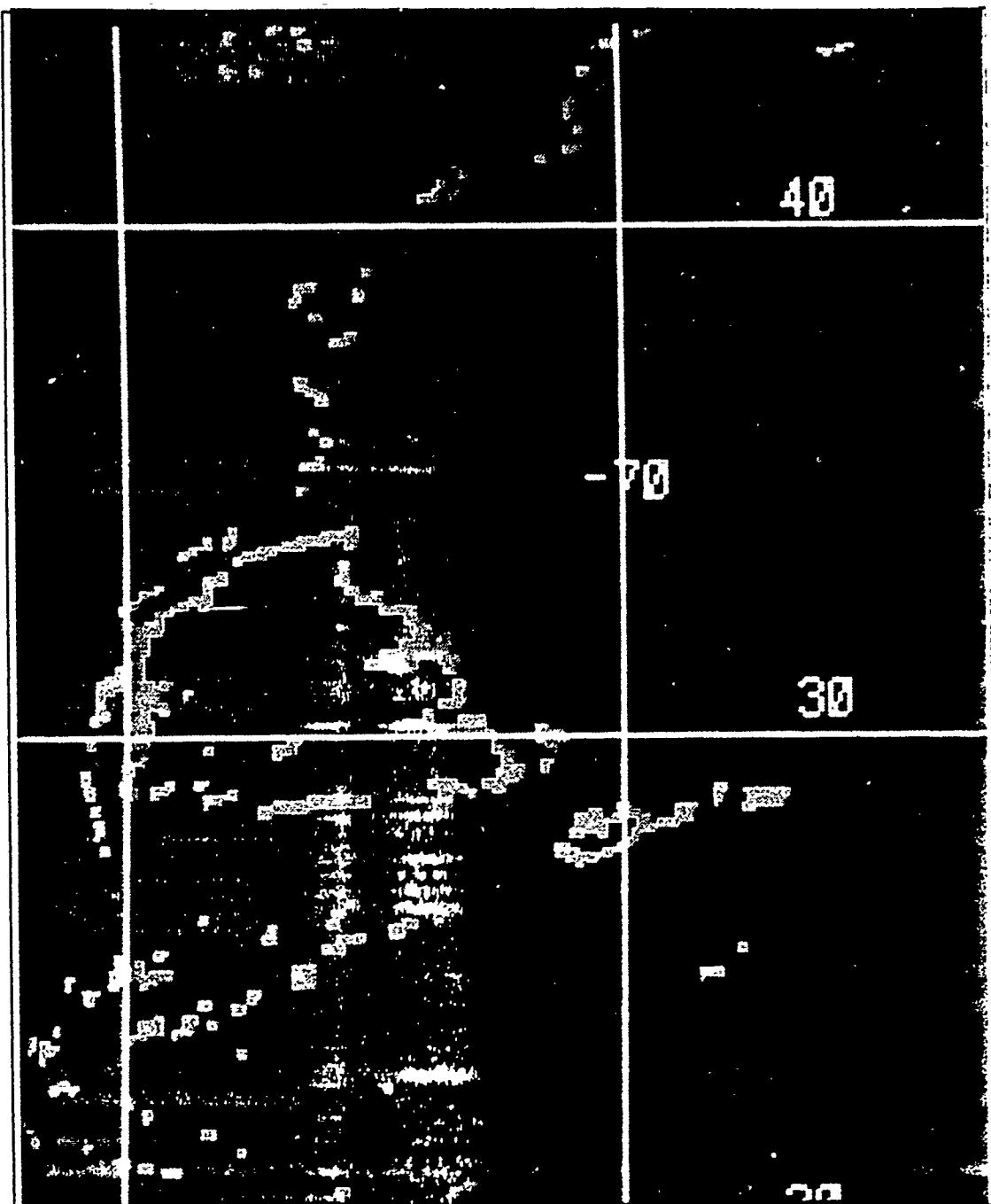


Fig. 11. SSM/I 37H GHz brightness temperature image at 12/2303 December 1988. For color code values see table 7.

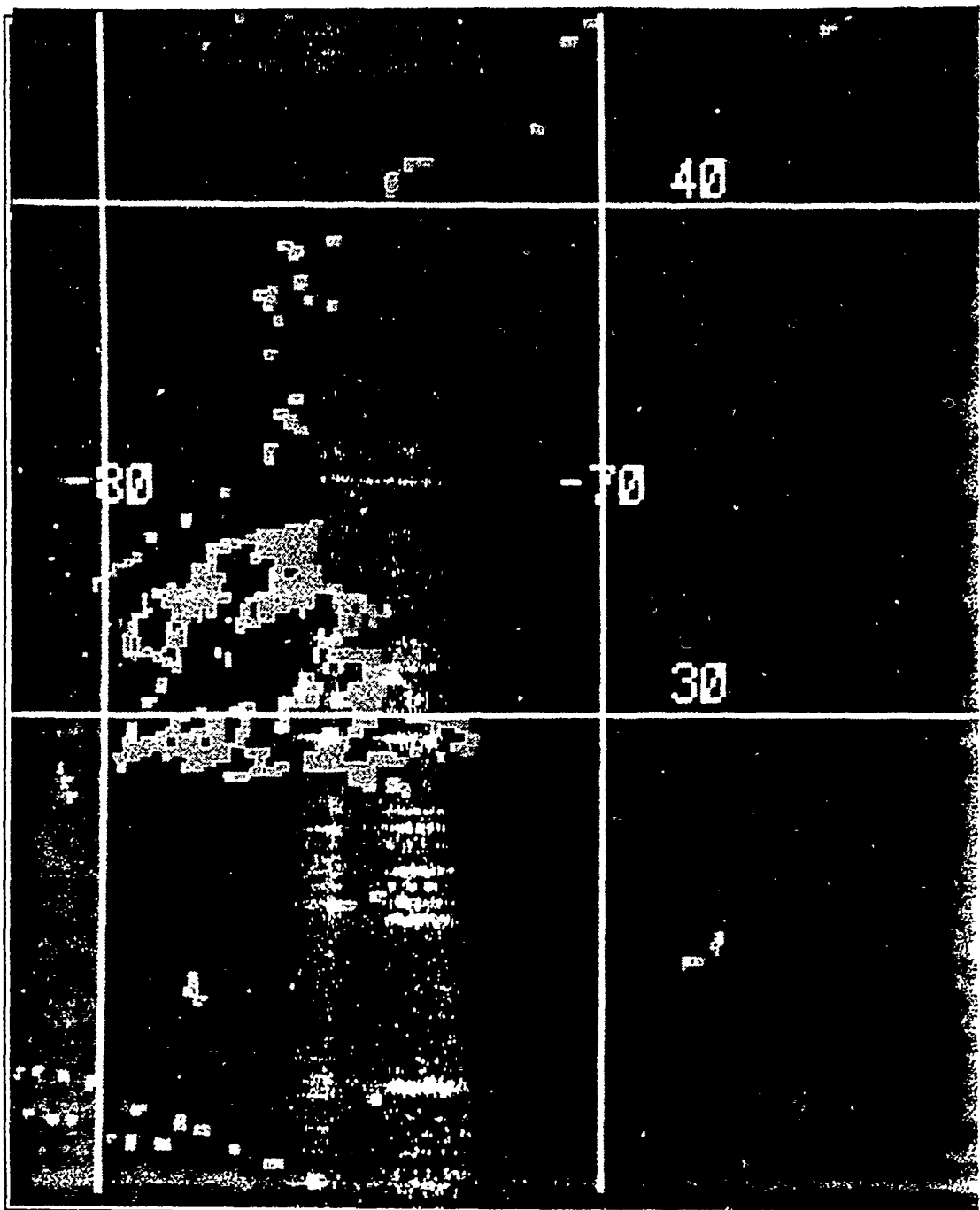


Fig. 12. SSM I 37V - 37H GHz brightness temperature image at 12:2303 December 1988. For color code values see table 8.

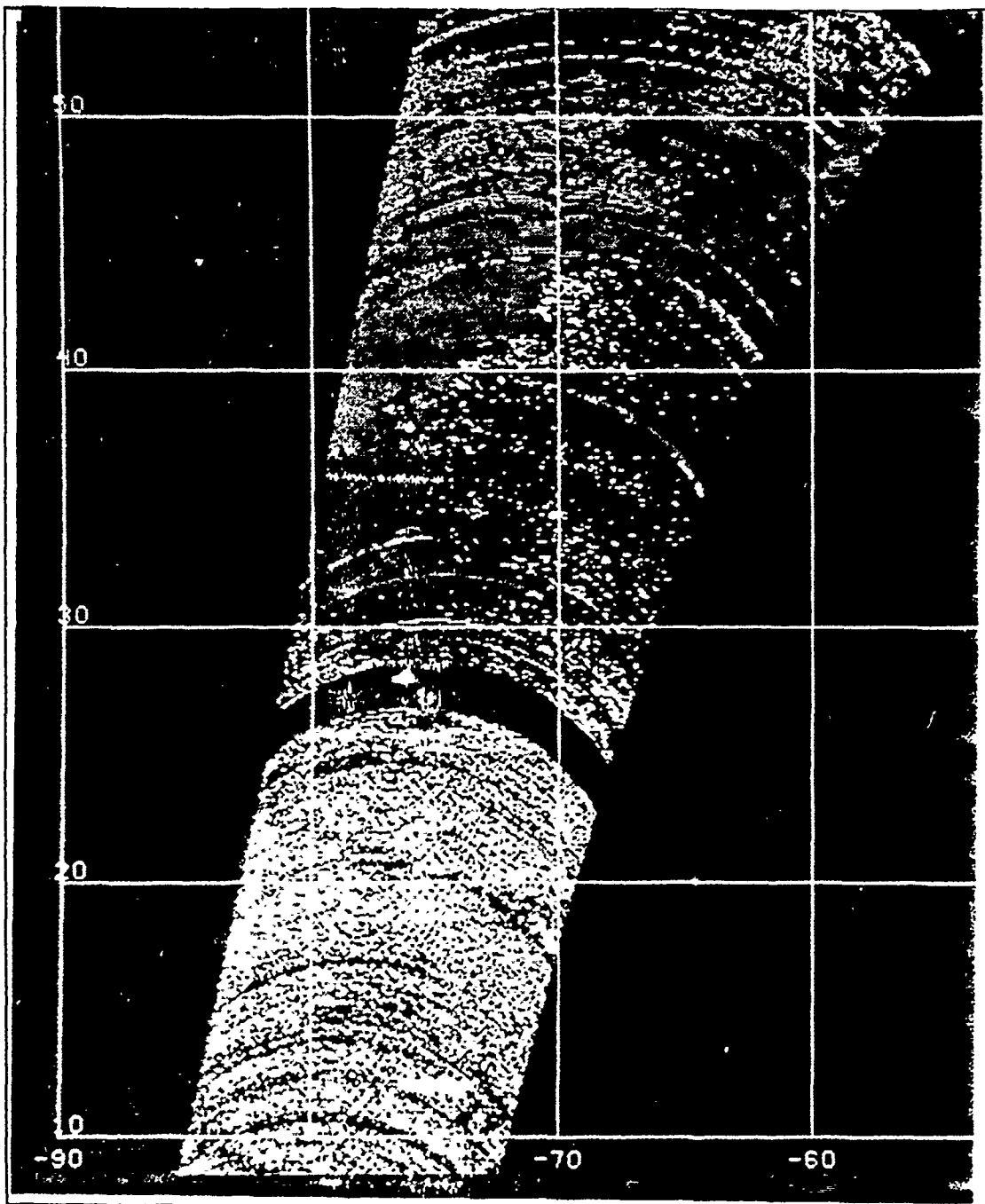


Fig. 13. PCT brightness temperature image at 12/2303 December 1988. For color code values see table 6.

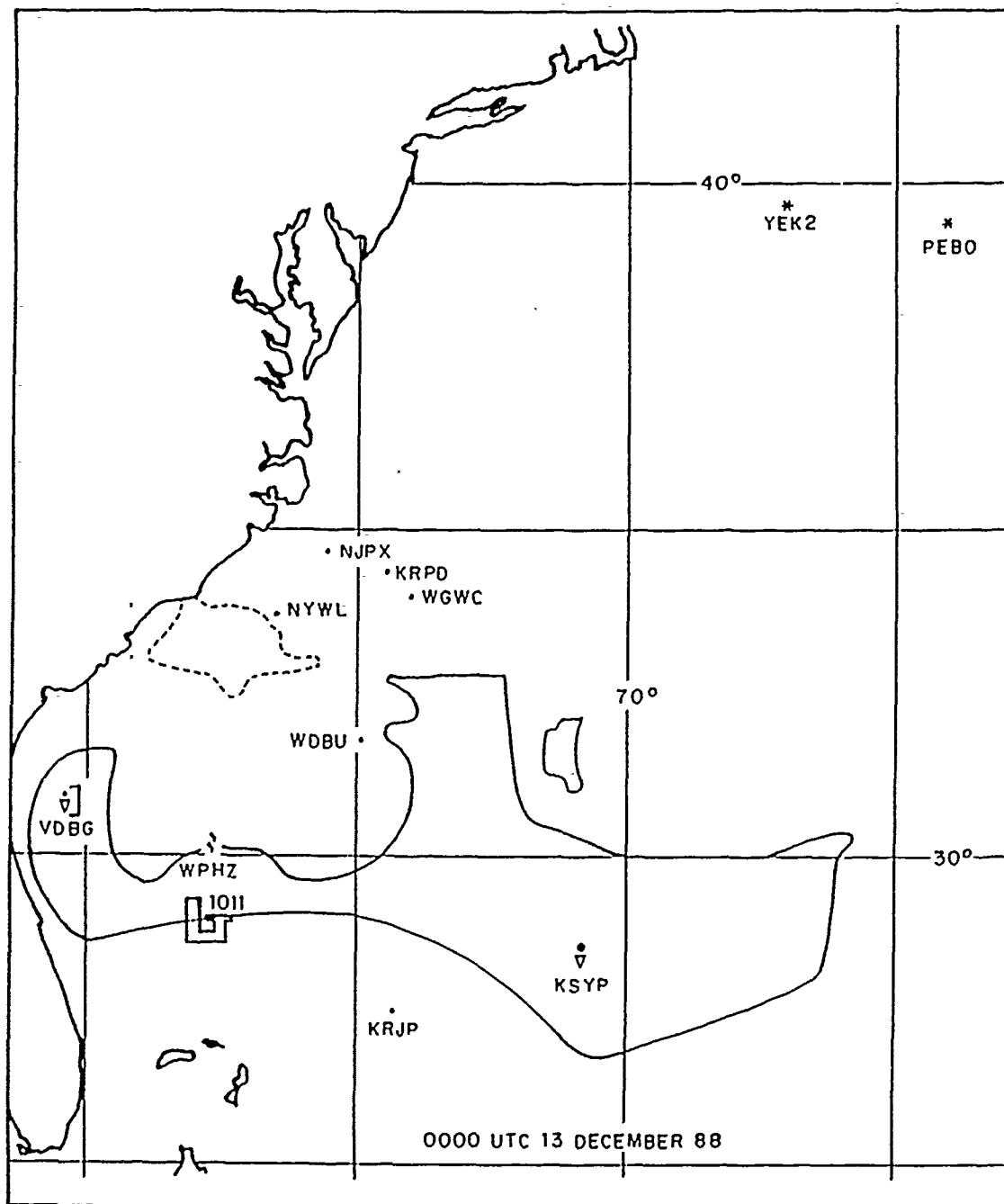


Fig. 14. Weather rain map for 13/0000 December 1988. Weather symbols are from the WMO standard weather code table. The solid line outlines the area of OOL values, while the dashed line outlines the area of rain less than 15 mm/hr.

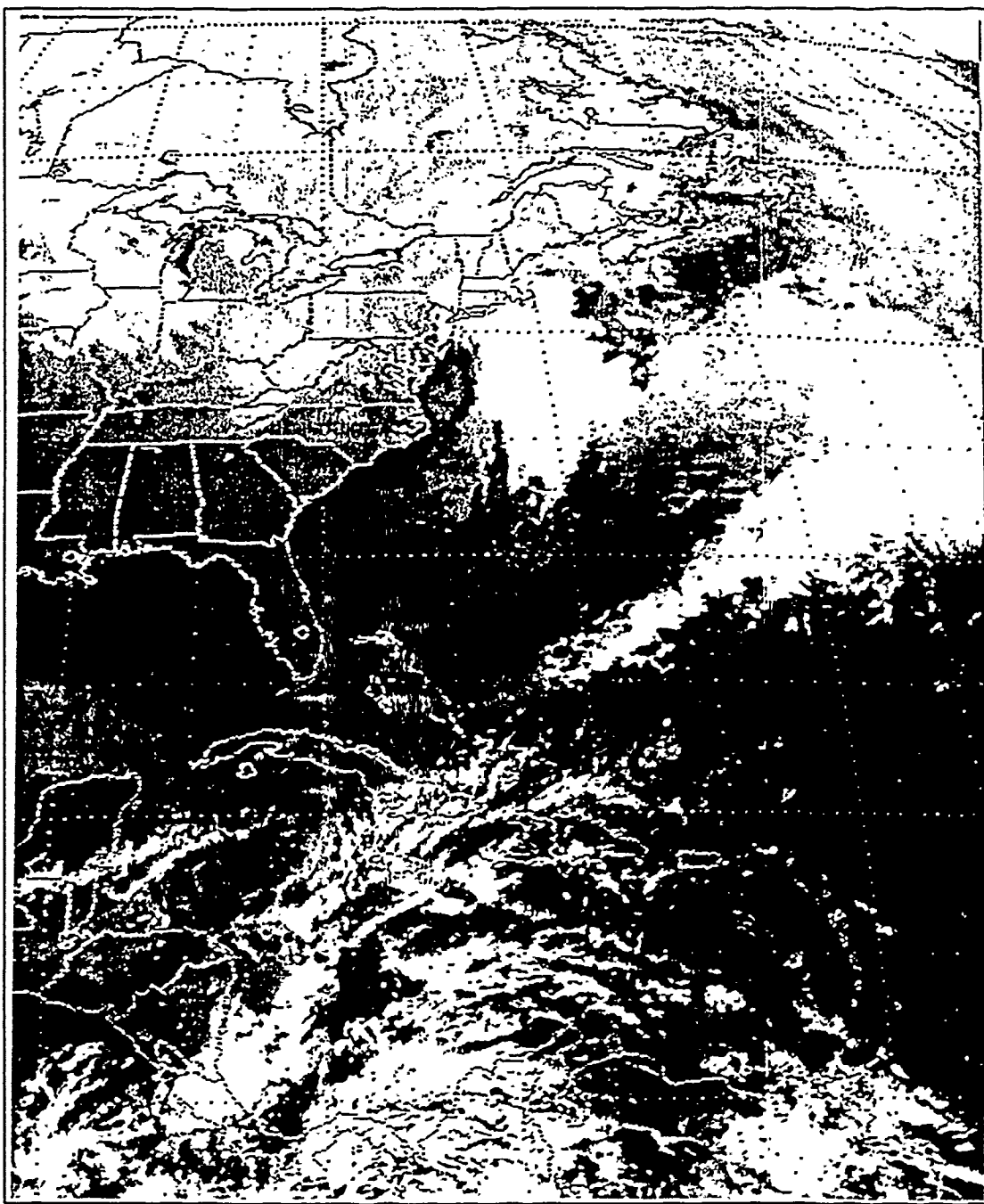


Fig. 15. GOES infrared east coast U.S. sector imagery for 13/2301 UTC December 1988.

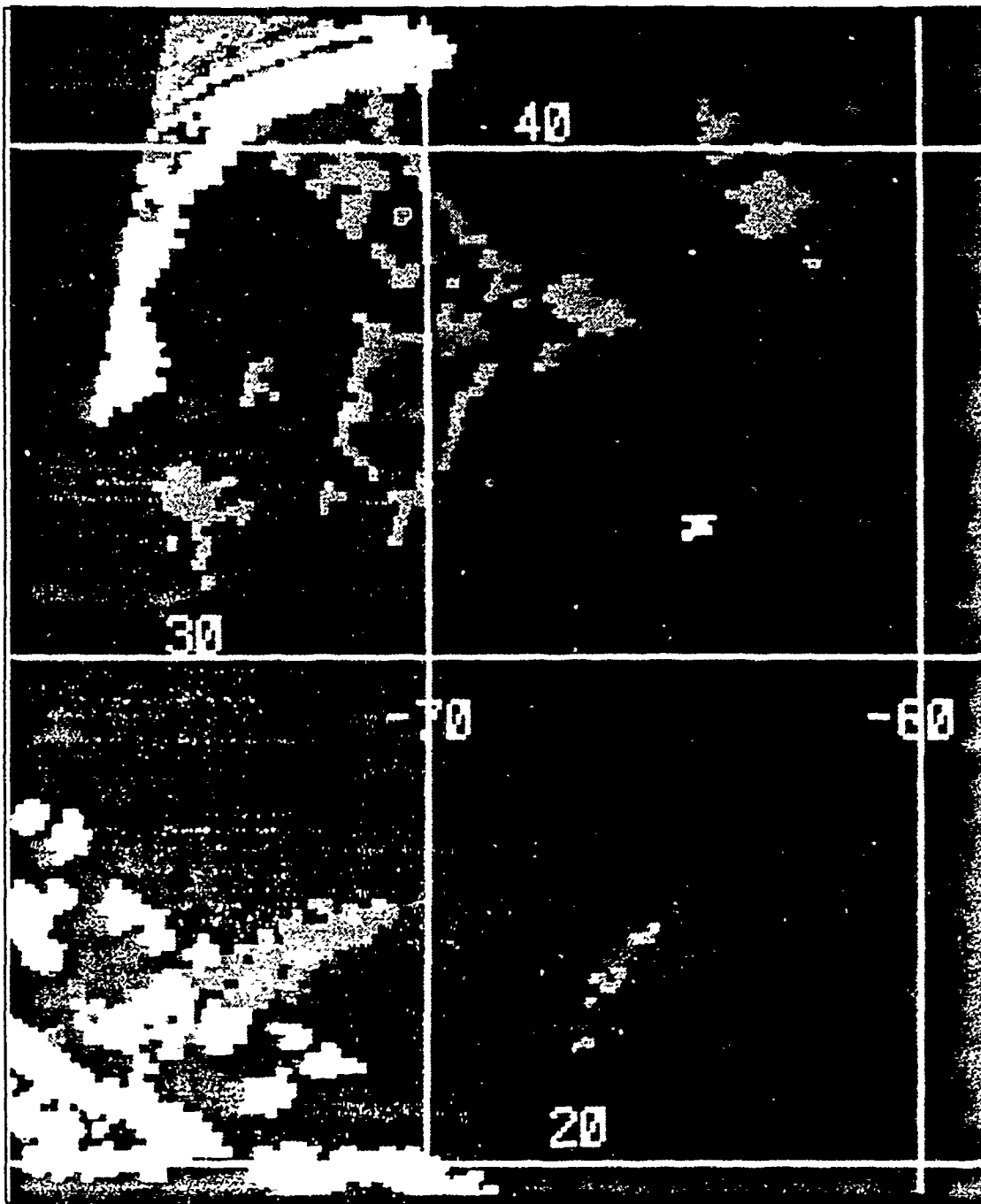


Fig. 16. SSM I HAC precipitation image at 13:2257 December 1988. For color code values see table 5.

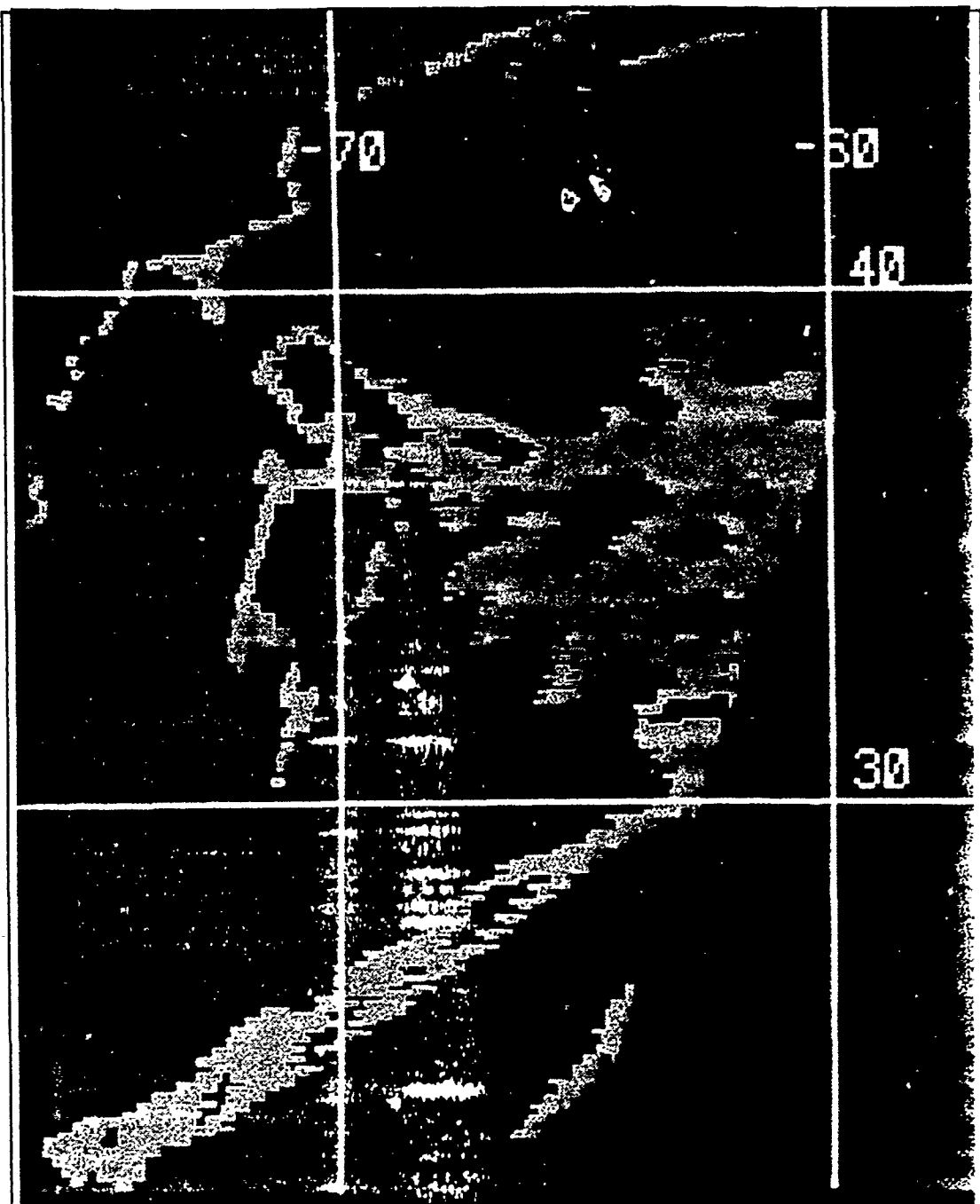


Fig. 17. SSM/I 19H GHz brightness temperature image at 13:2257 December 1988. For color code values see table 9.

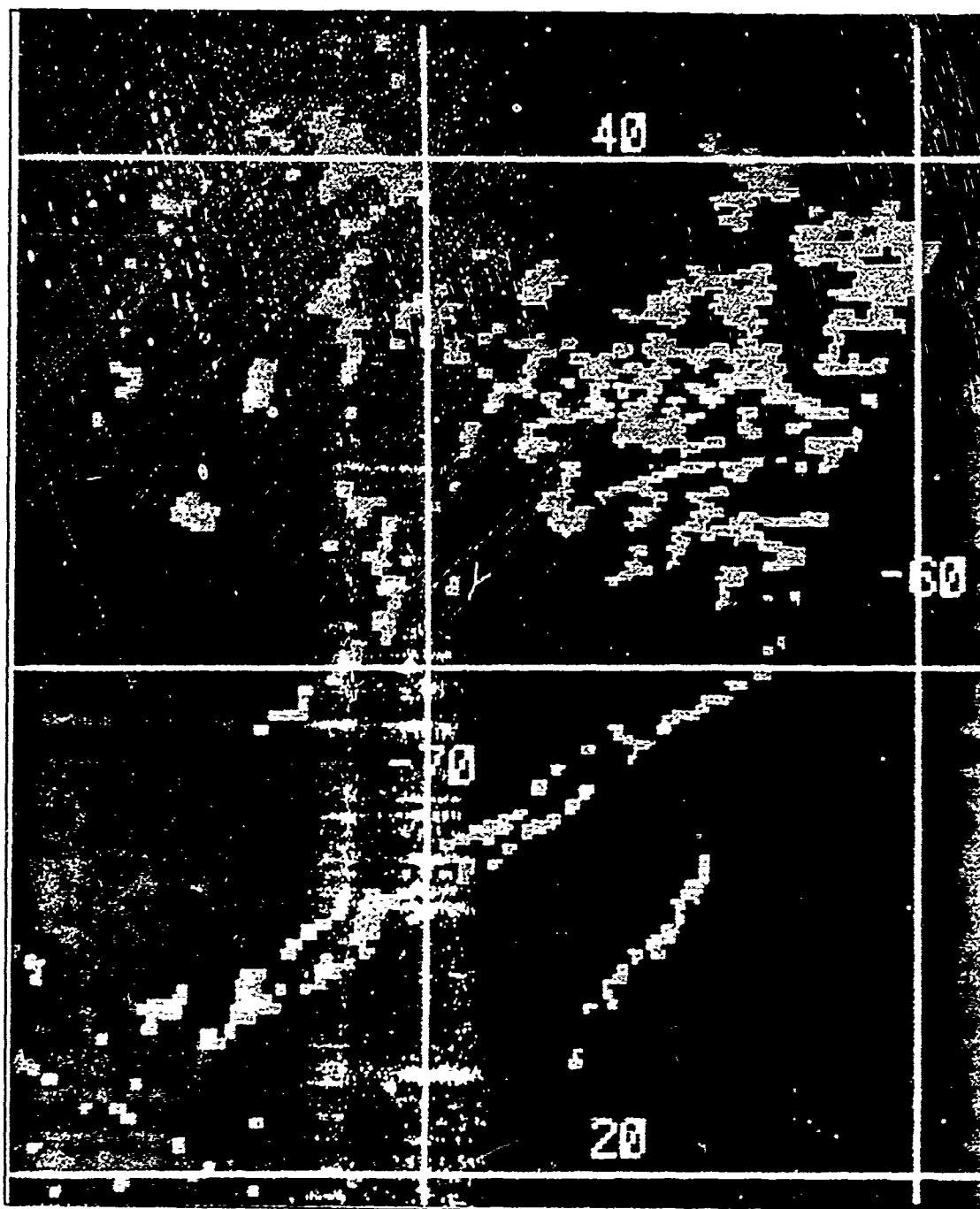


Fig. 18. SSM I 37H GHz brightness temperature image at 13.2257 December 1988. For color code values see table 7.

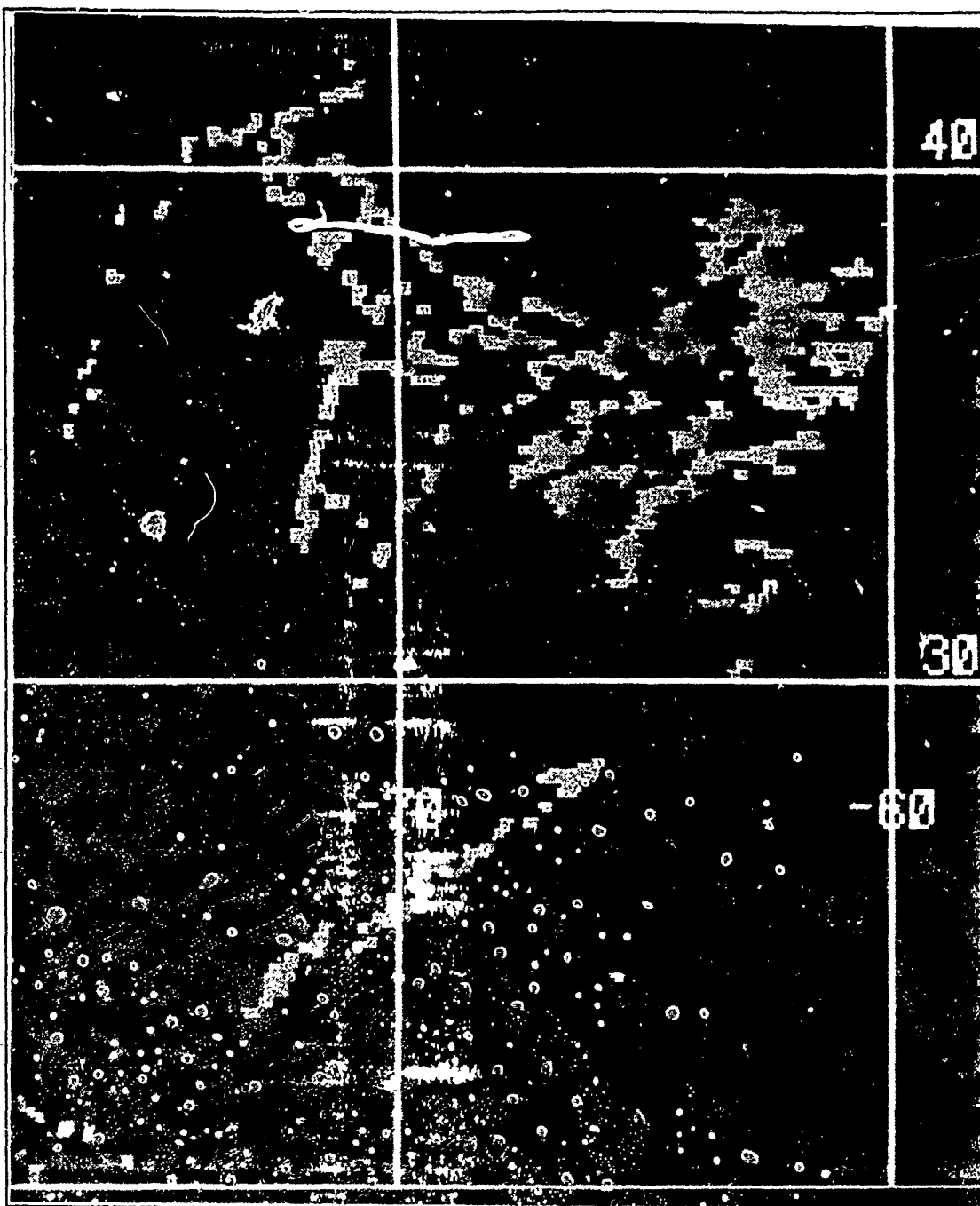


Fig. 19. SSM/I 37V - 37H GHz brightness temperature image at 13/2257 December 1988. For color code values see table 8.

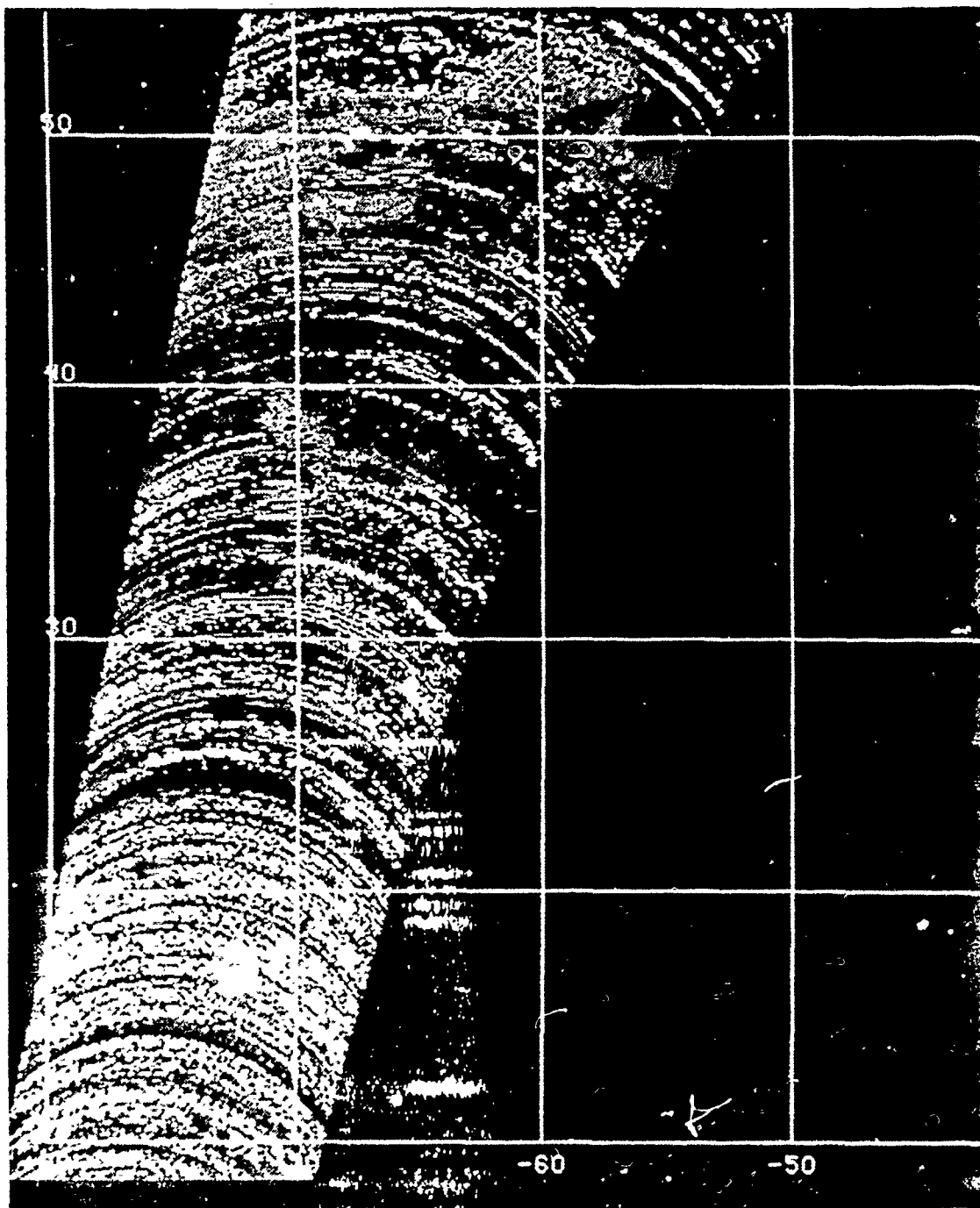


Fig. 20. PCT brightness temperature image at 13/2257 December 1988. For color code values see table 6.

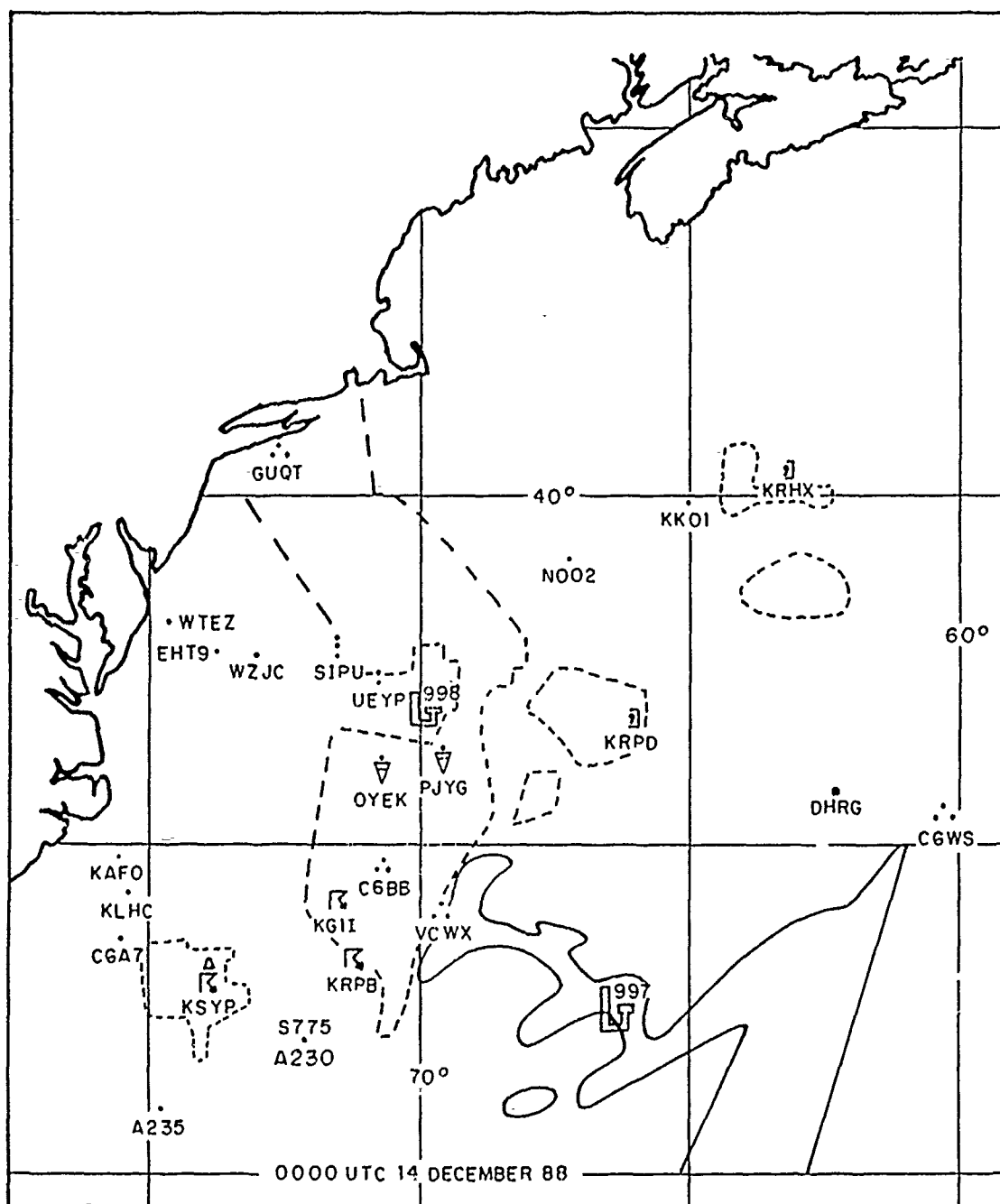


Fig. 21. Weather rain map for 14/0000 December 1988. Weather symbols are from the WMO standard weather code table. The solid line outlines the area of OOL values, while the dashed line outlines the area of rain less than 15 mm/hr.

APPENDIX C. CASE STUDY OF IOP 3

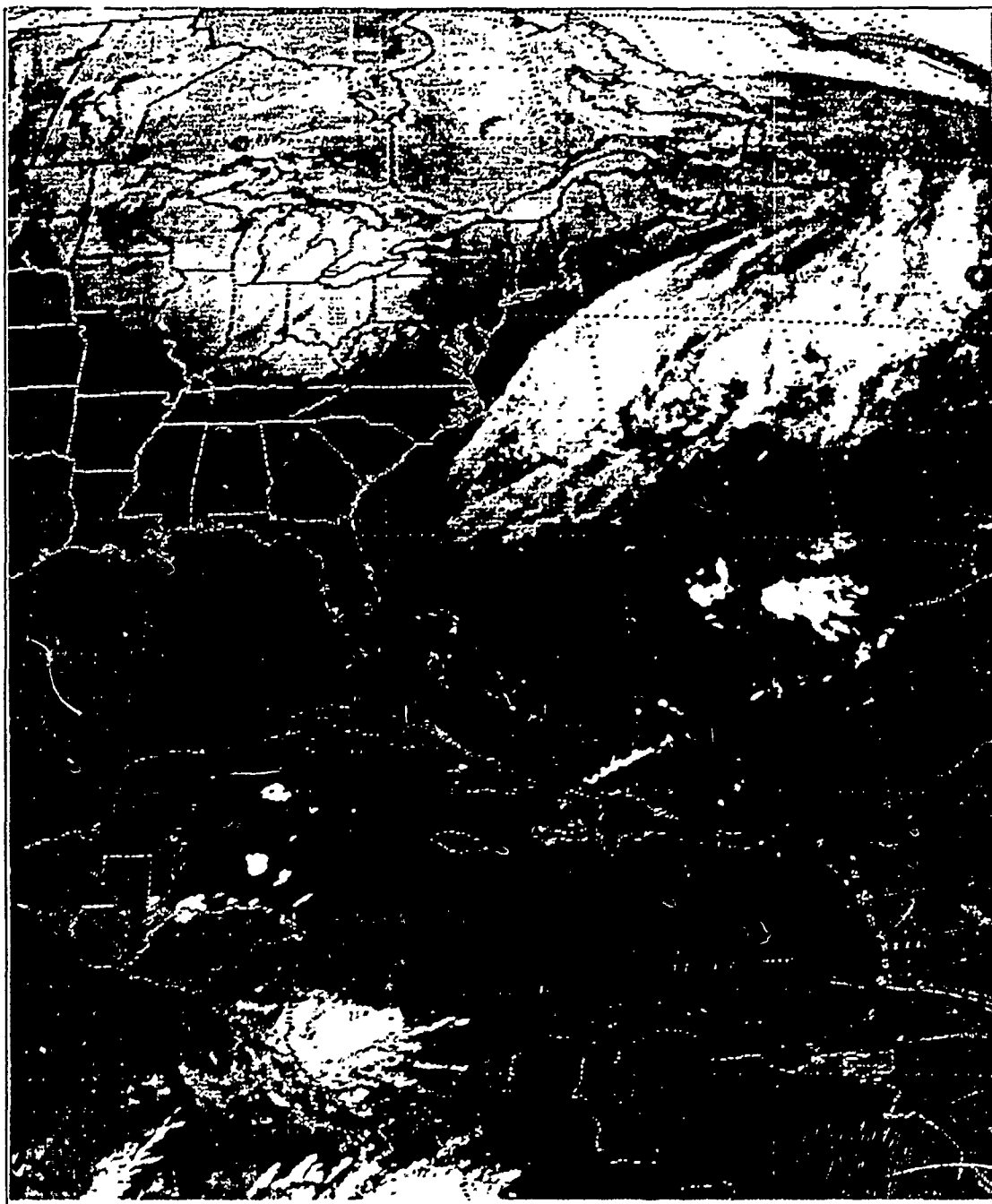


Fig. 22. GOES infrared east coast U.S. sector imagery for 16/2231 December 1988.

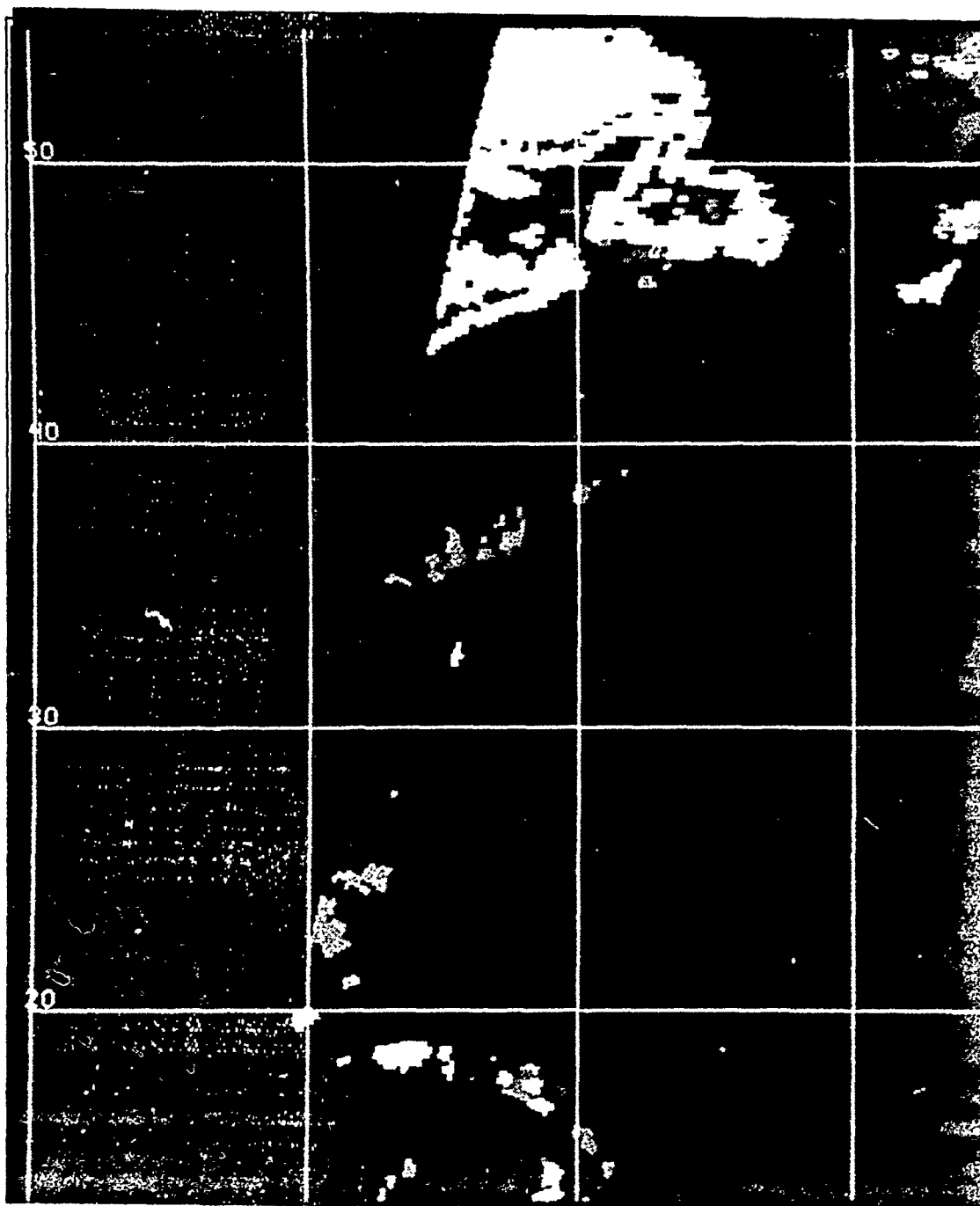


Fig. 23. SSM/I HAC precipitation image at 16,2220 December 1988. For color code values see table 5. Latitude and longitude lines are 10° apart with the south latitude of 20°N and the western longitude of 70°W .

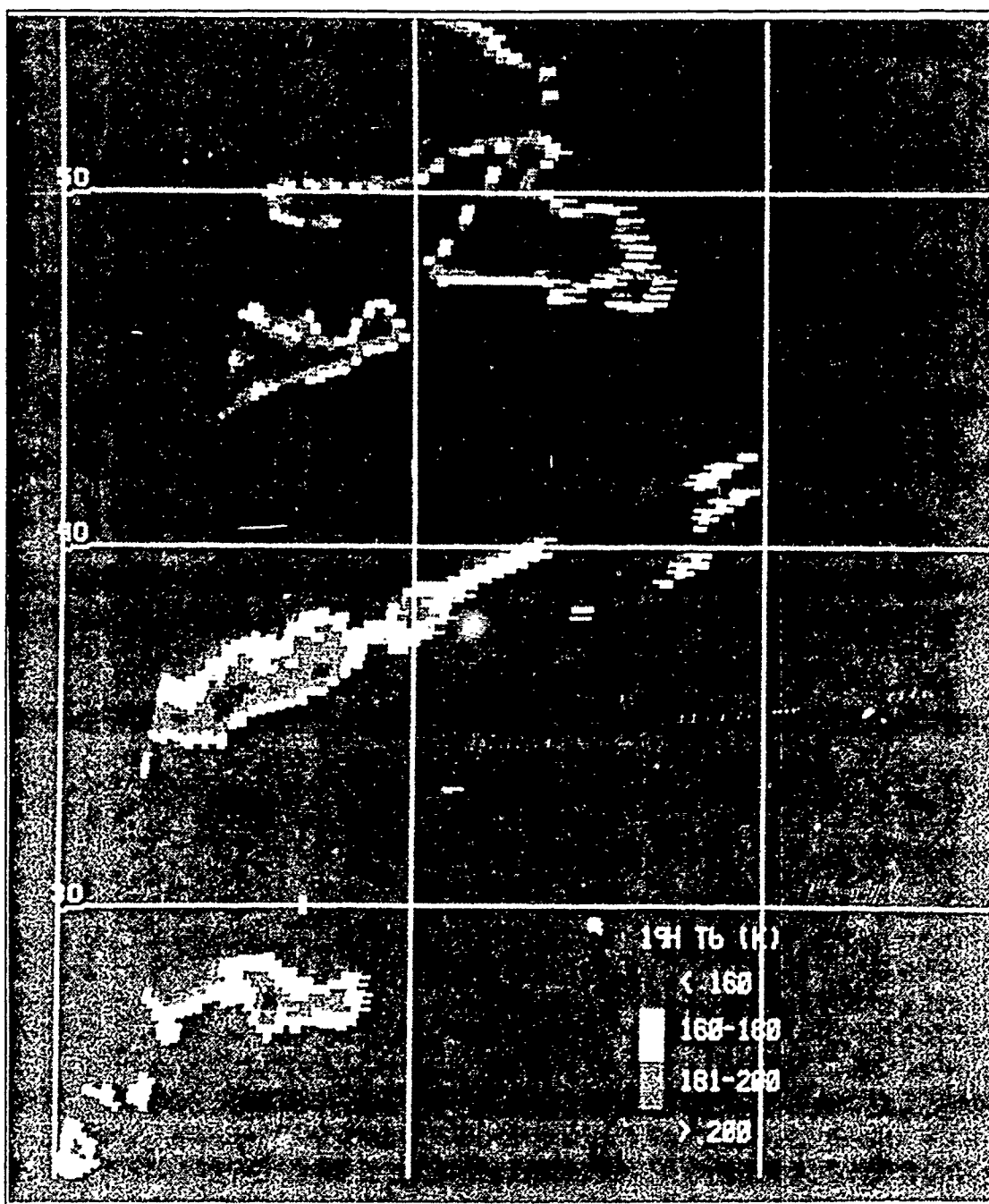


Fig. 24. SSM/I 19H GHz brightness temperature image at 16:22:20 December 1988.

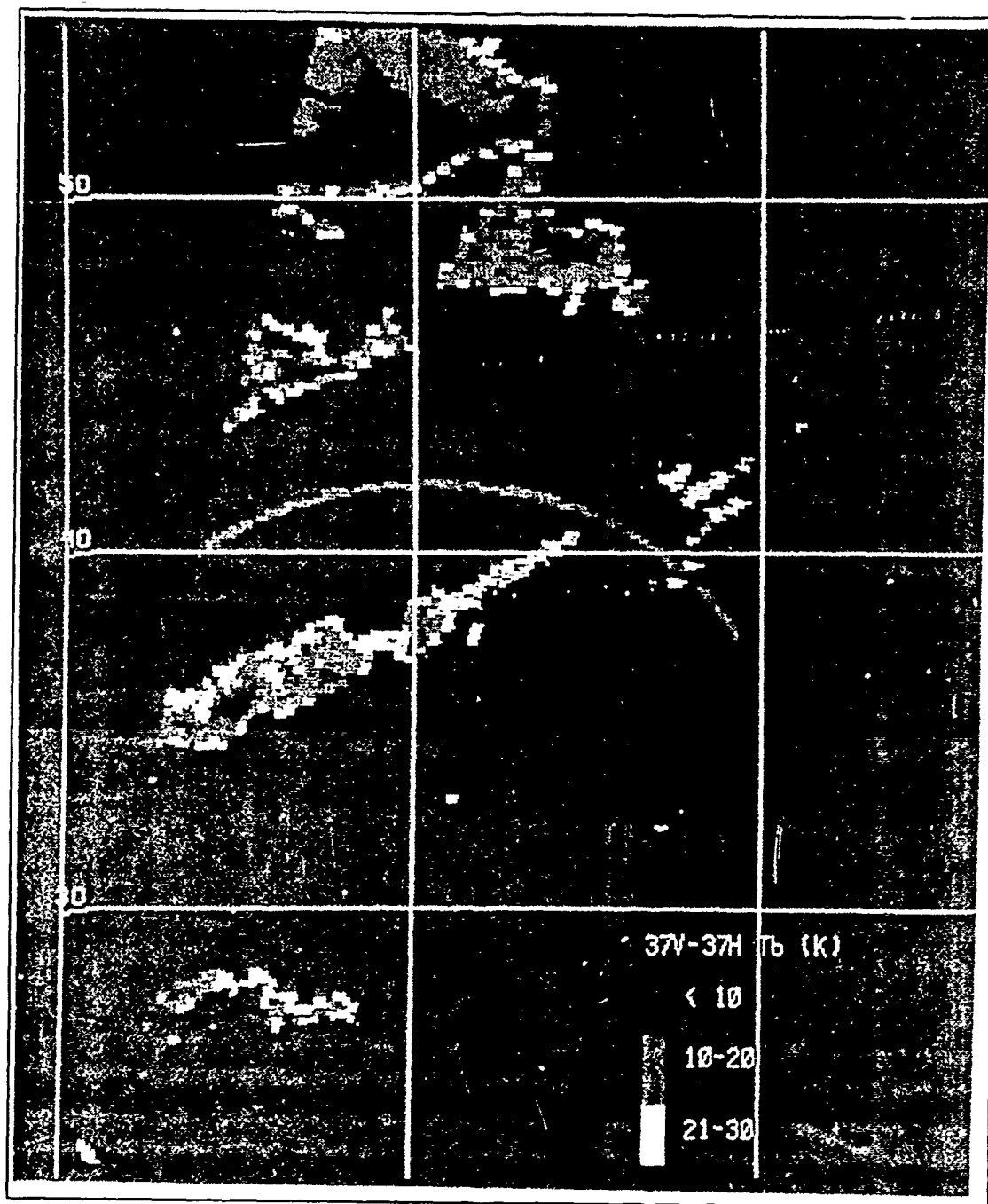


Fig. 25. SSM/I 37V - 37H GHz brightness temperature image at 16/2220 December 1988.

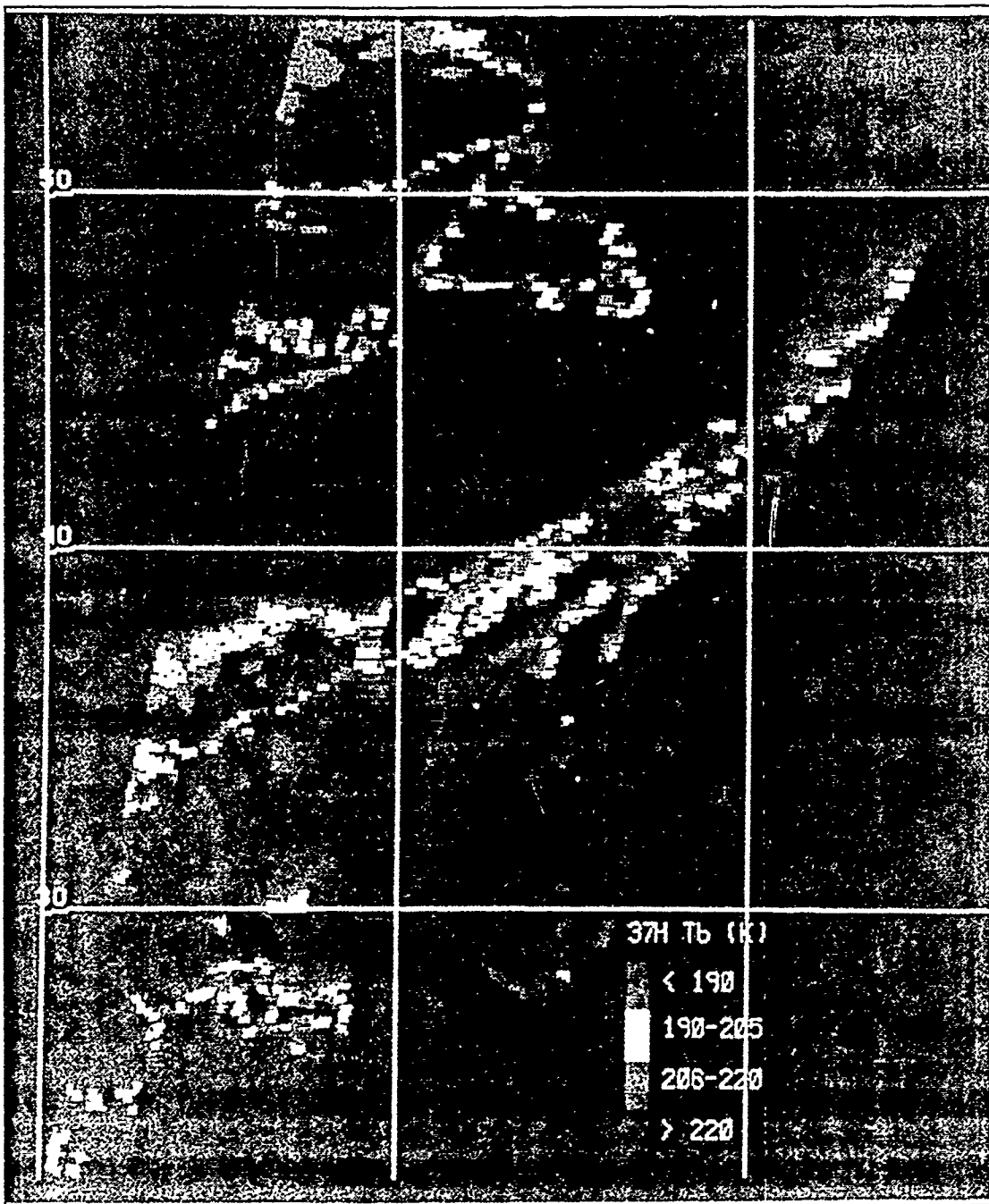


Fig. 26. SSM/I 37H GHz brightness temperature image at 16:22:00 December 1988.

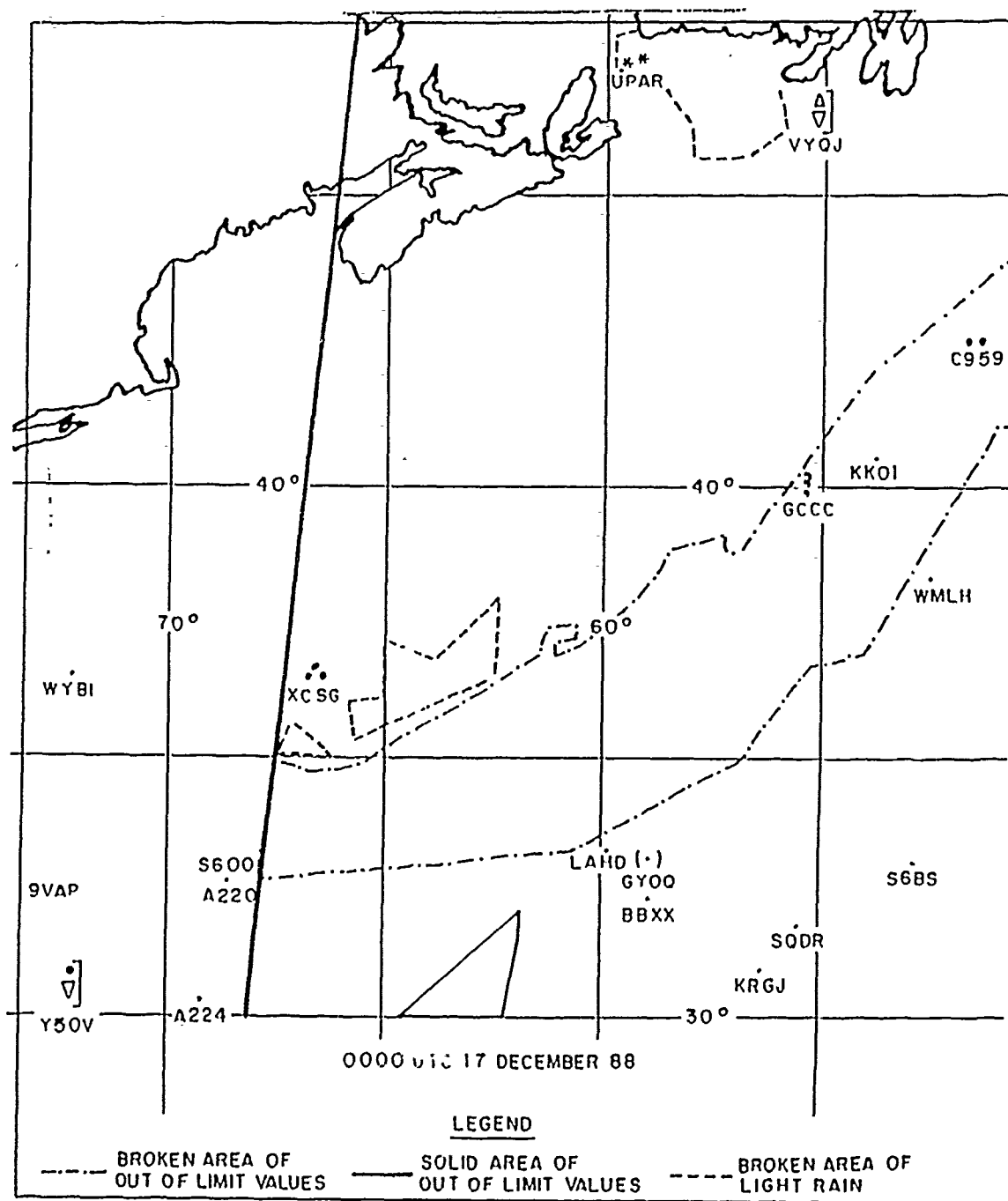


Fig. 27. Weather rain map for 17/0000 December 1988. Weather symbols are from the WMO standard weather code table.

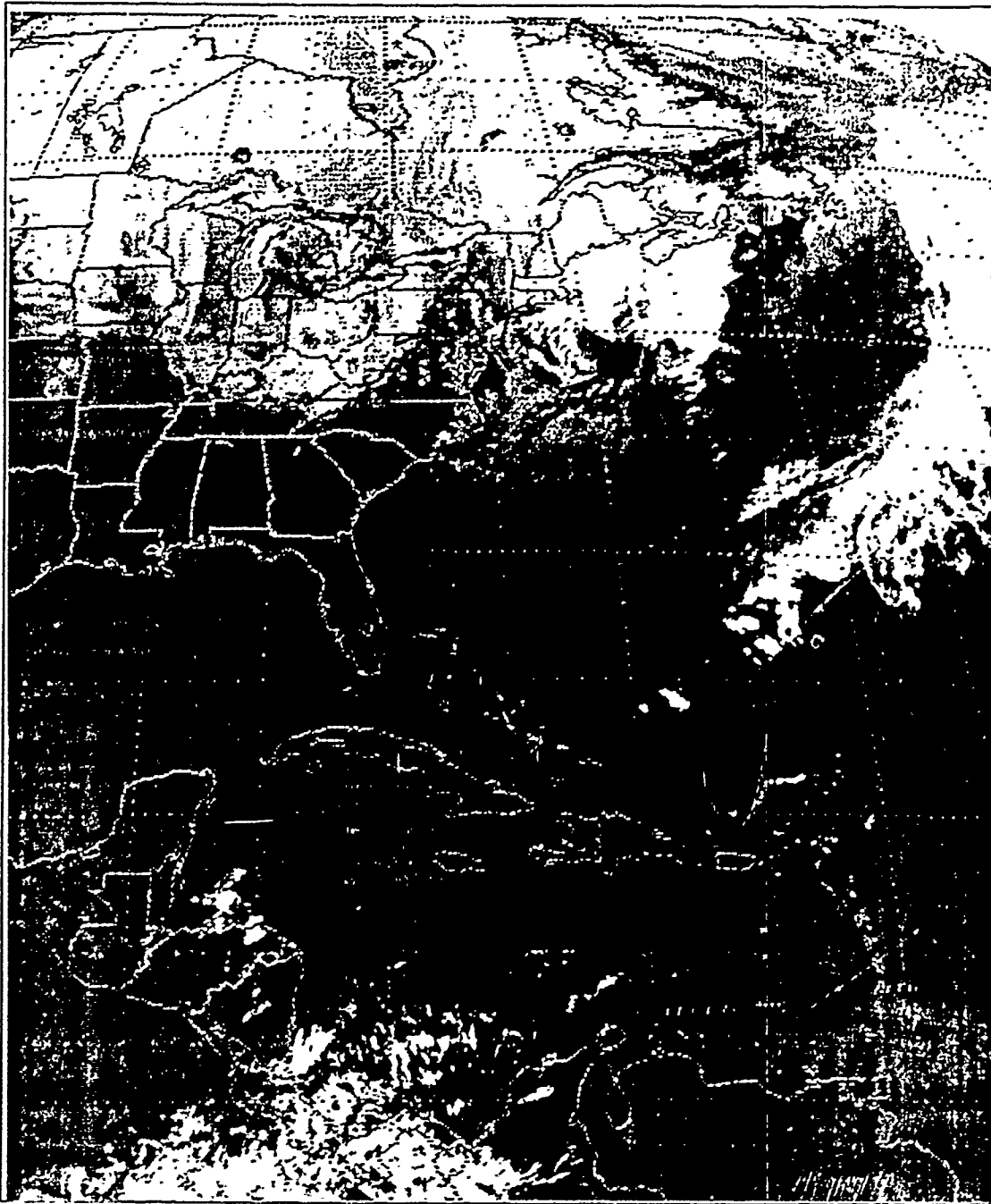


Fig. 28. GOES infrared east coast U.S. sector imagery for 17/2231 UTC December 1988.

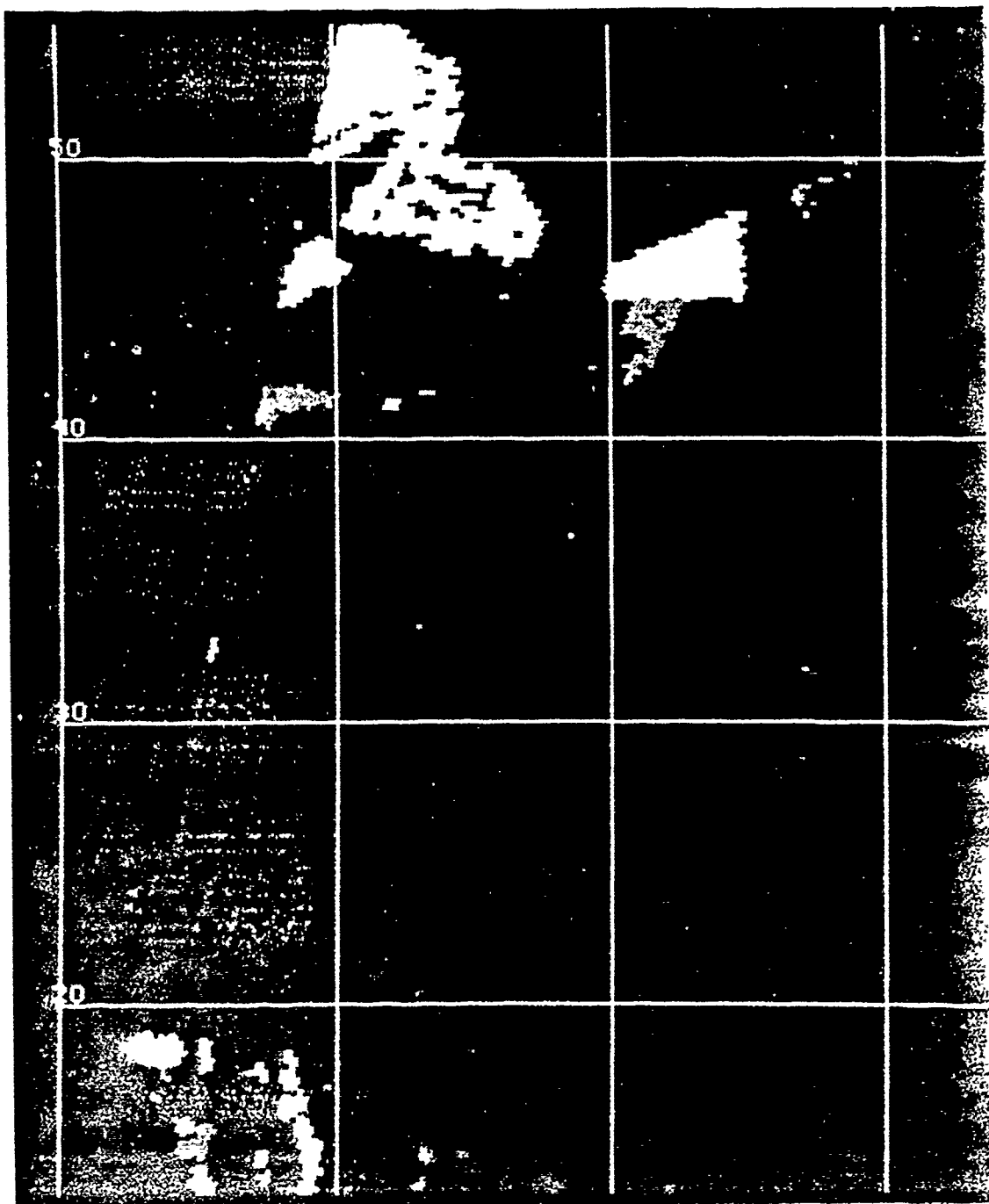


Fig. 29. SSM I HAC precipitation image at 17.2208 December 1988. Longitude lines are 10° apart, with the western most longitude 70°W . For color code values see table 5.

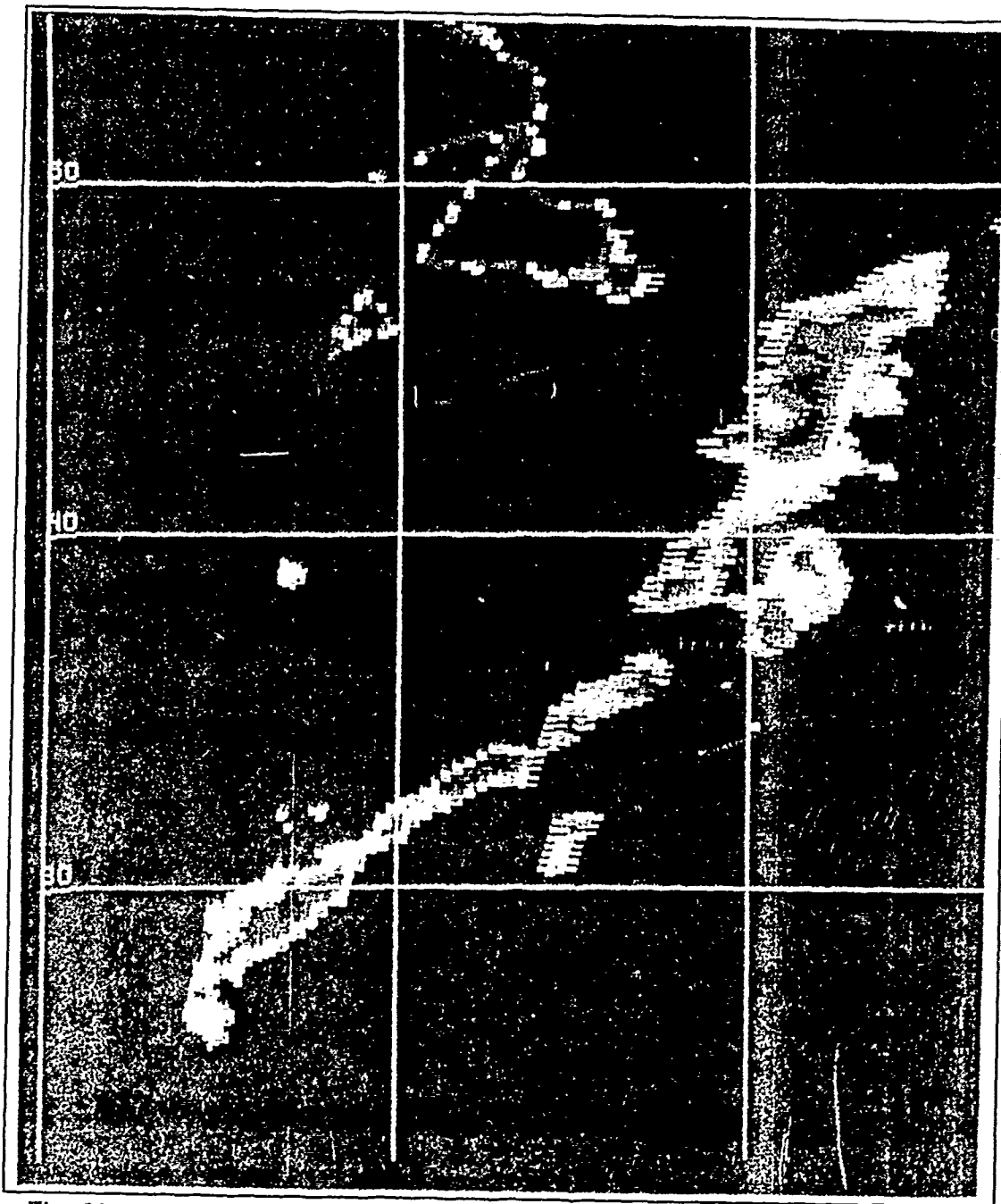


Fig. 30. SSM/I 1911 GHz brightness temperature image at 17/2208 December 1988. Grey scale is same as that of figure 26.

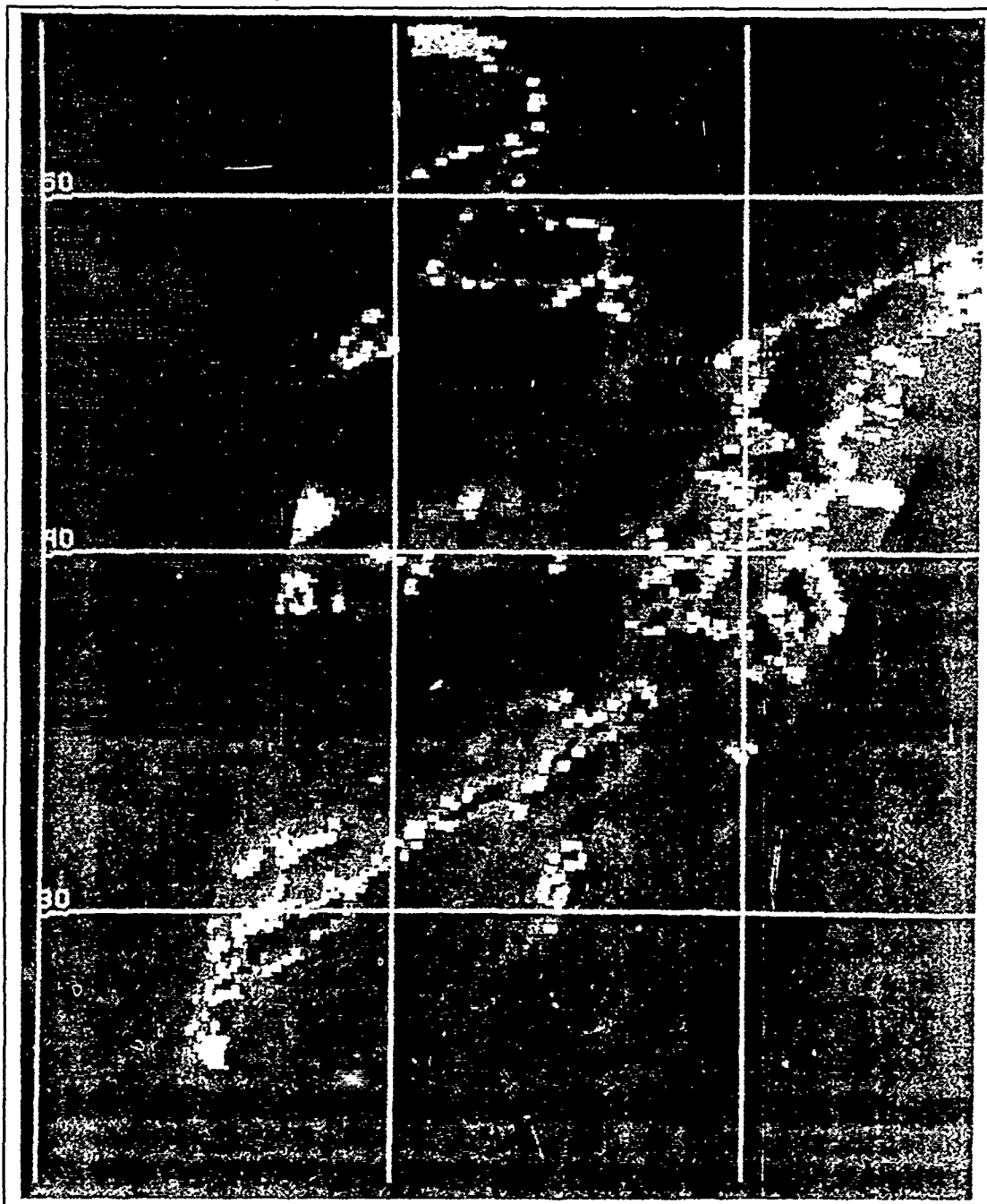


Fig. 31. SSM/I 37H GHz brightness temperature image at 17/2208 December 1988. Grey scale is same as that of figure 24.

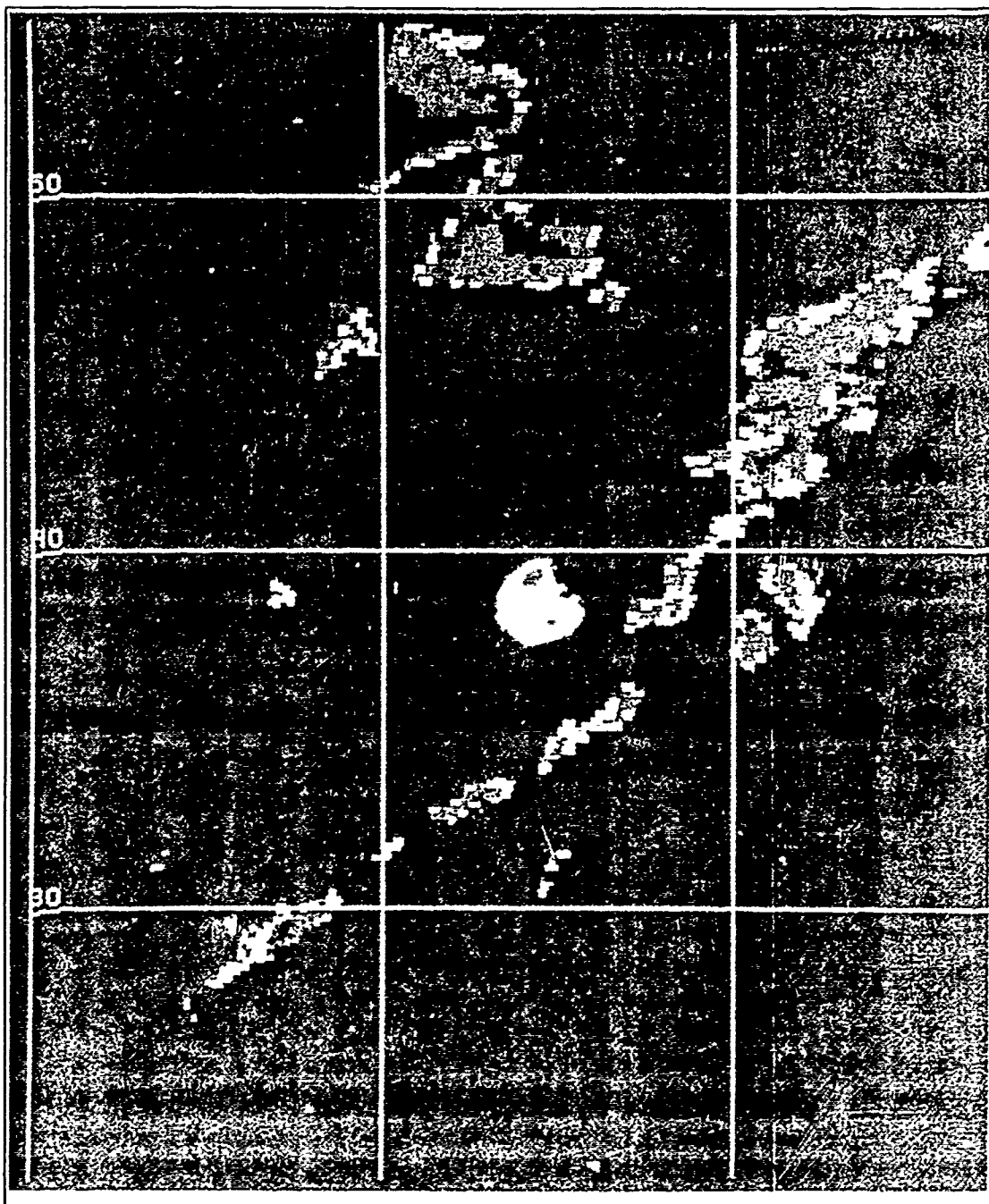


Fig. 32. SSM/I 37V - 37H GHz brightness temperature image at 17/2208 December 1988. Grey scale is same as that of figure 25.

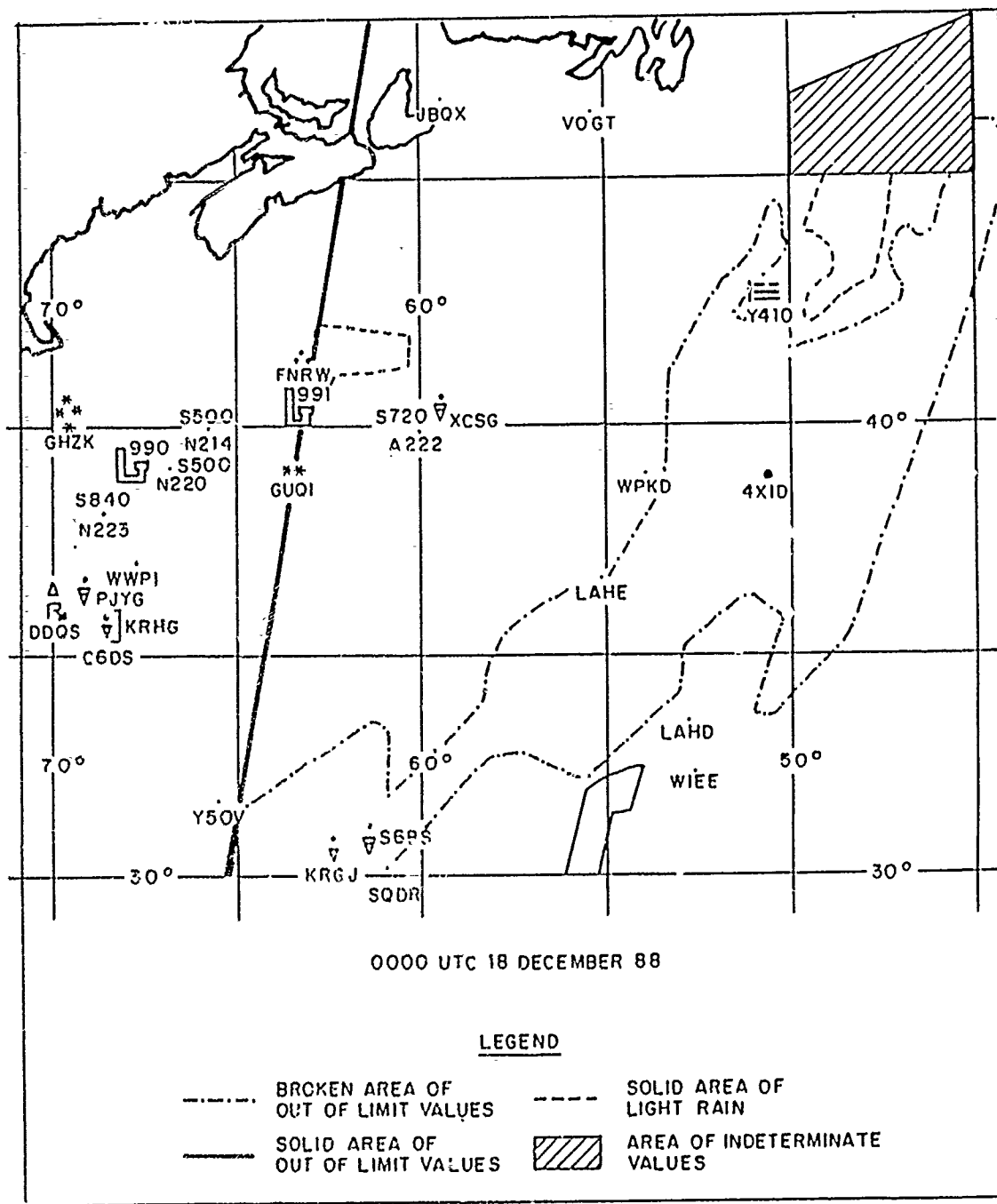


Fig. 33. Weather rain map for 18/0000 December 1988. Weather symbols are from the WMO standard weather code table.

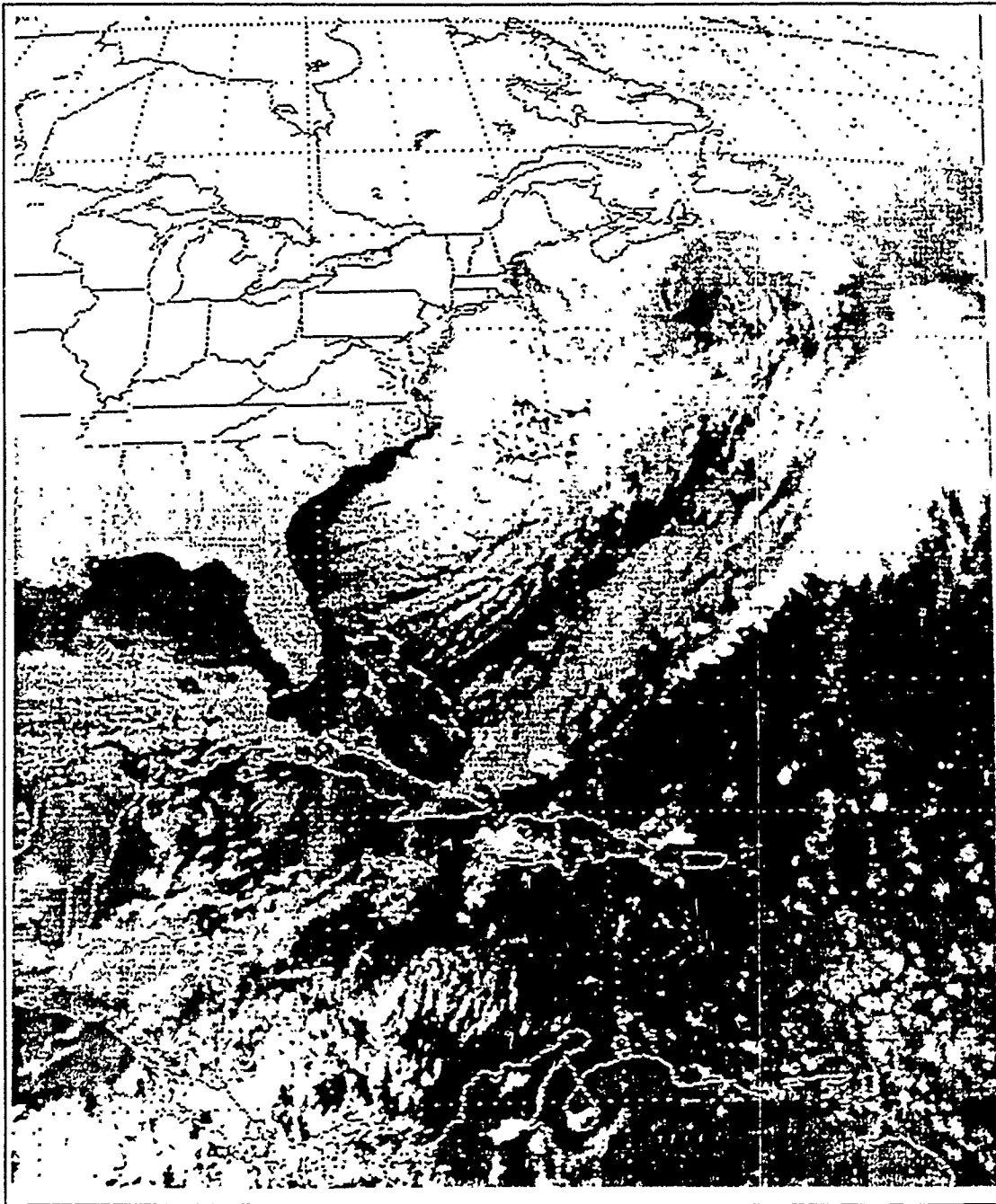


Fig. 34. GOES infrared east coast U.S. sector imagery for 18/0901 UTC December 1988.

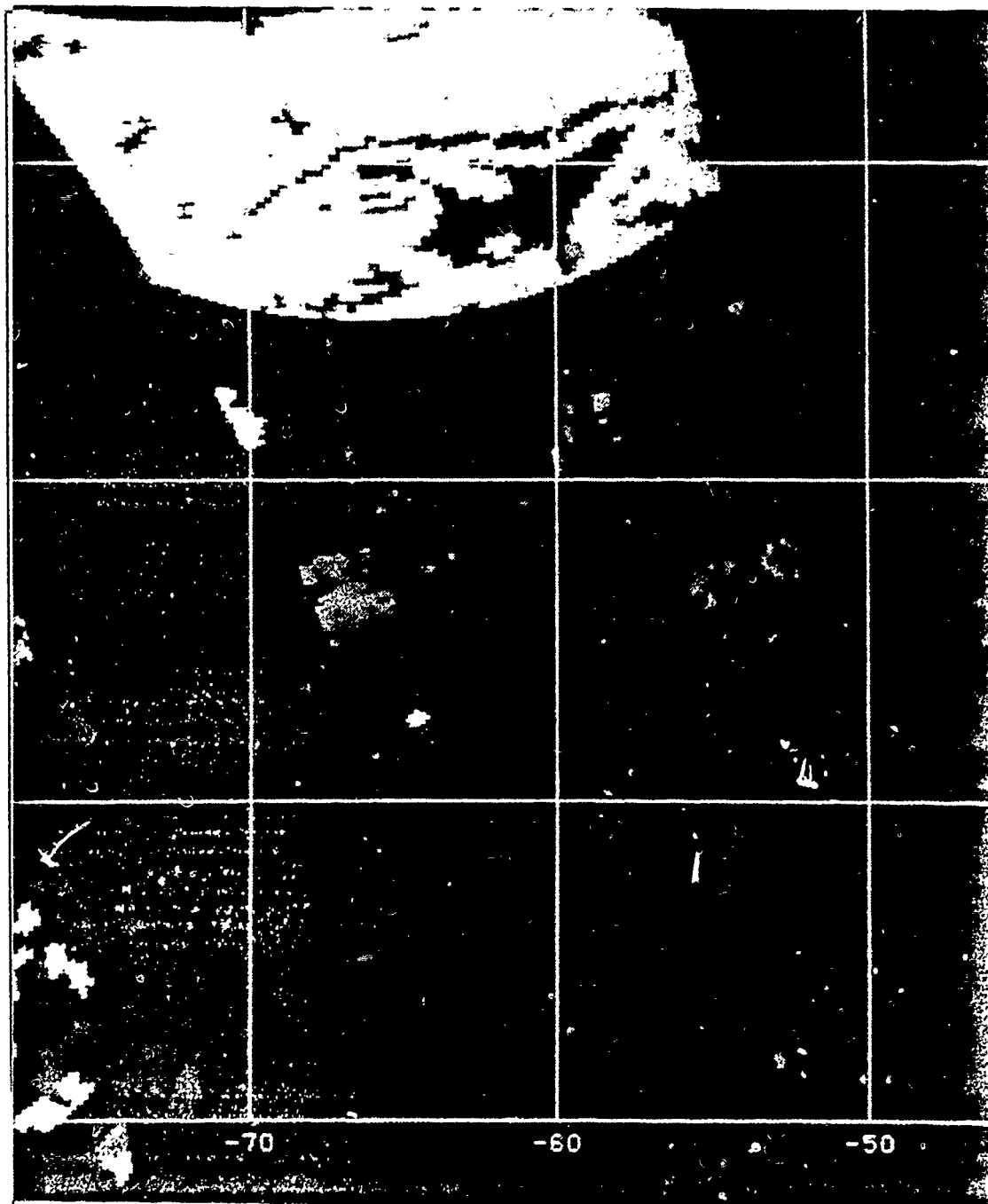


Fig. 35. SSM/I HAC precipitation image at 18:0941 December 1988. For color code values see table 5. Latitude lines are 10° apart with the southern most latitude 20°N .

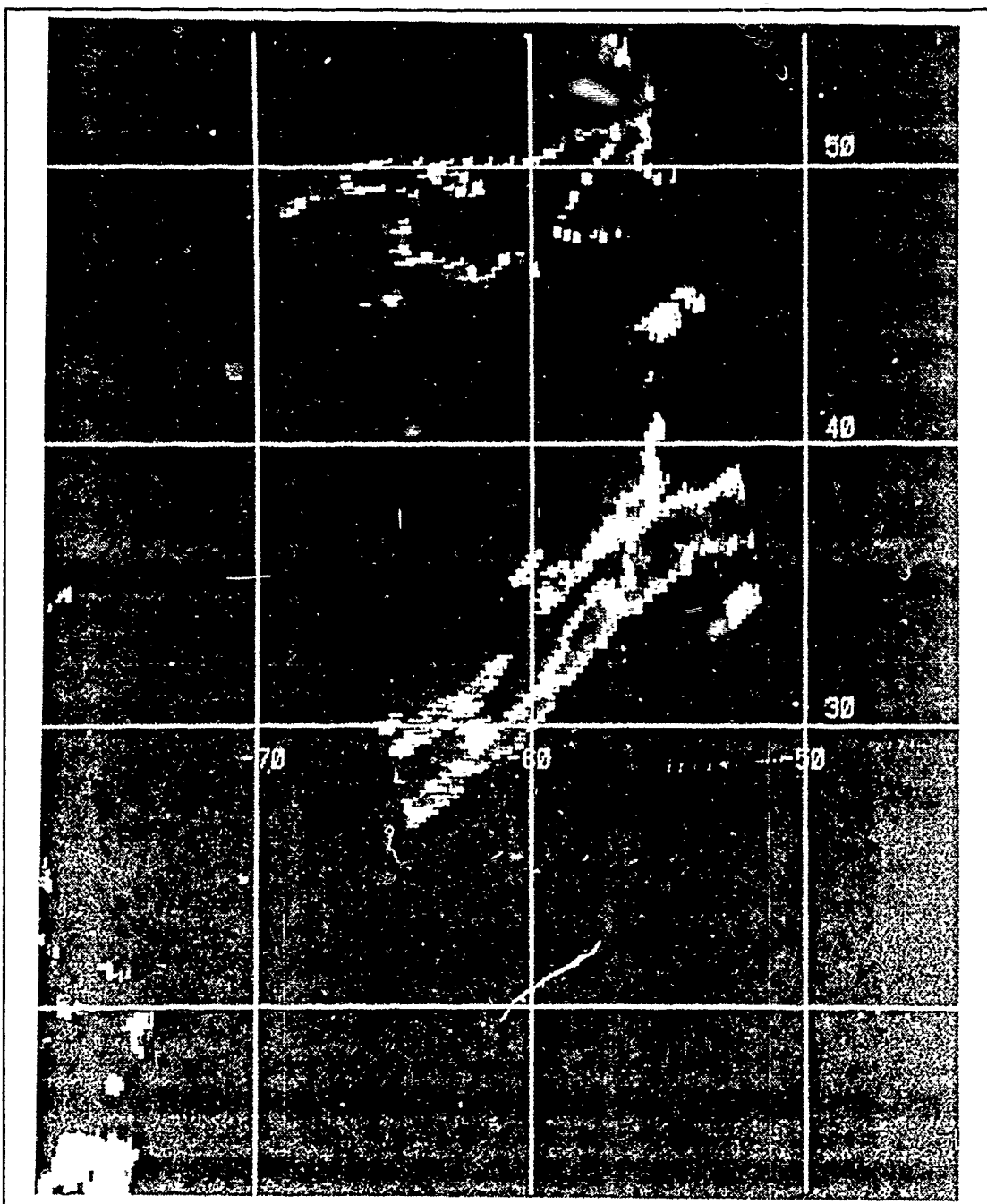


Fig. 36. SSM/I 1911 GHz brightness temperature image at 18/0941 December 1988. Grey scale is the same as that of figure 26.

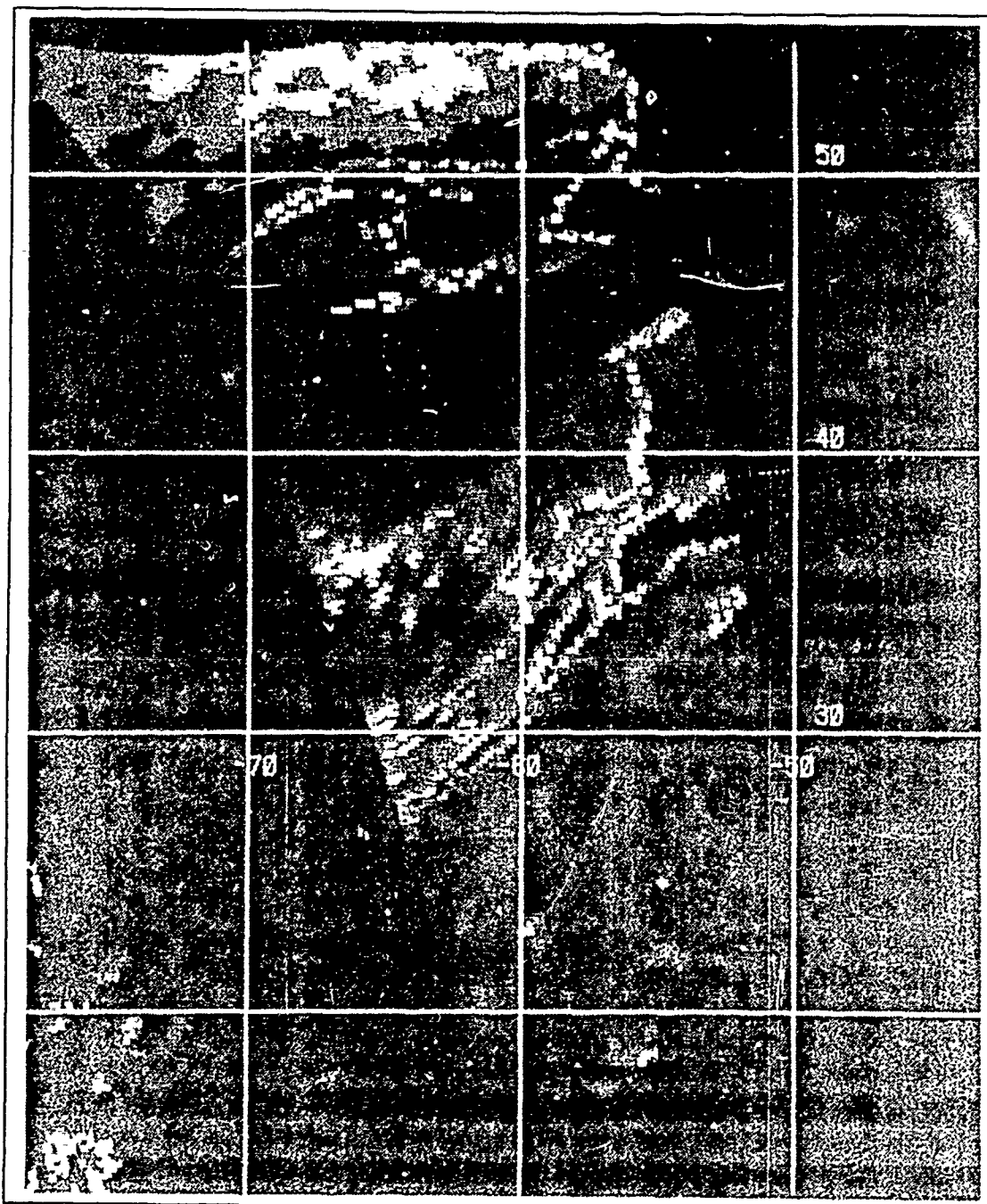


Fig. 37. SSM/I 37H GHz brightness temperature image at 18/0941 December 1988. Grey scale is the same as that of figure 24.

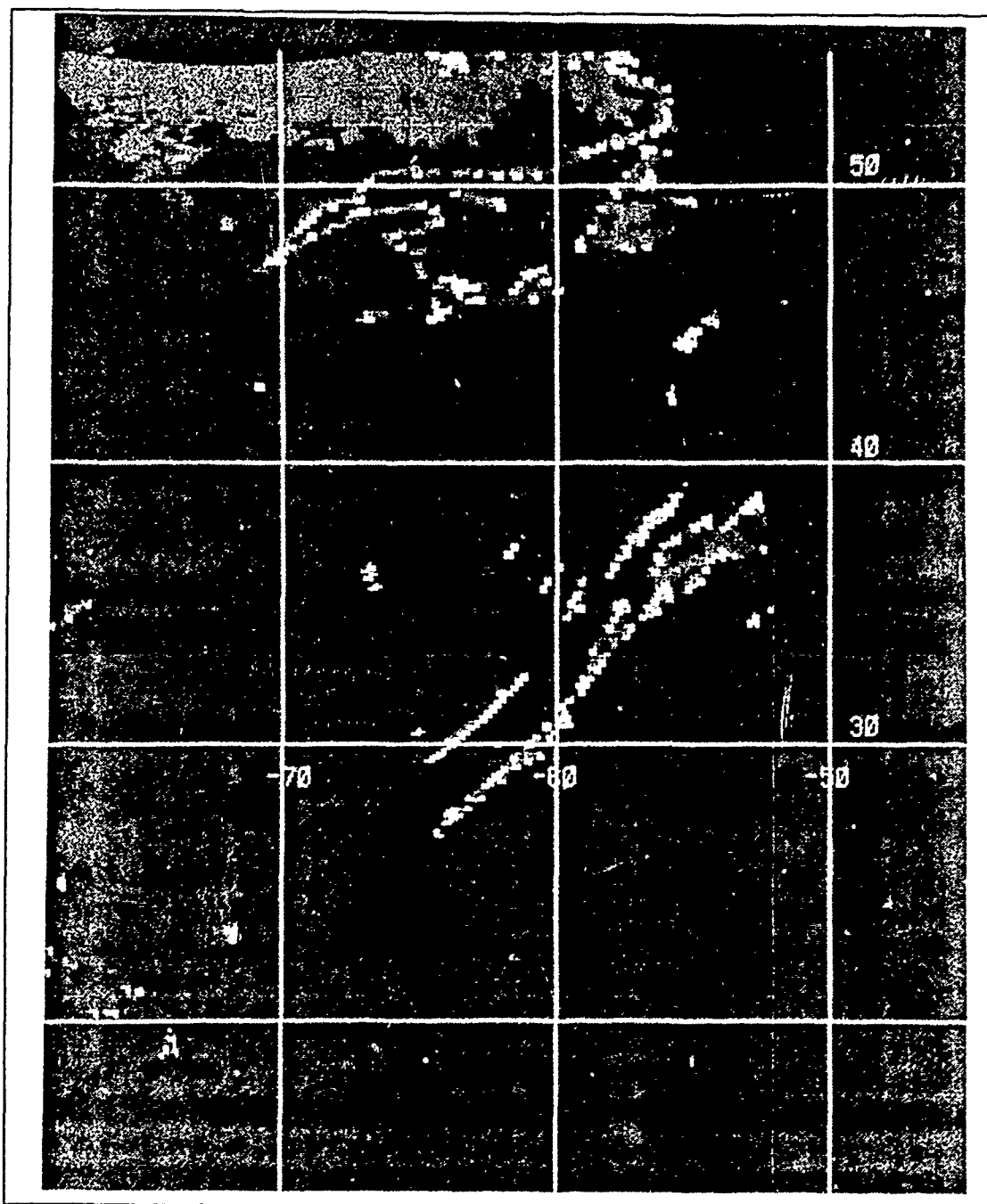


Fig. 38. SSM/I 37V - 37H GHz brightness temperature image at 18/0941 December 1988. Grey scale is the same as that of figure 25.

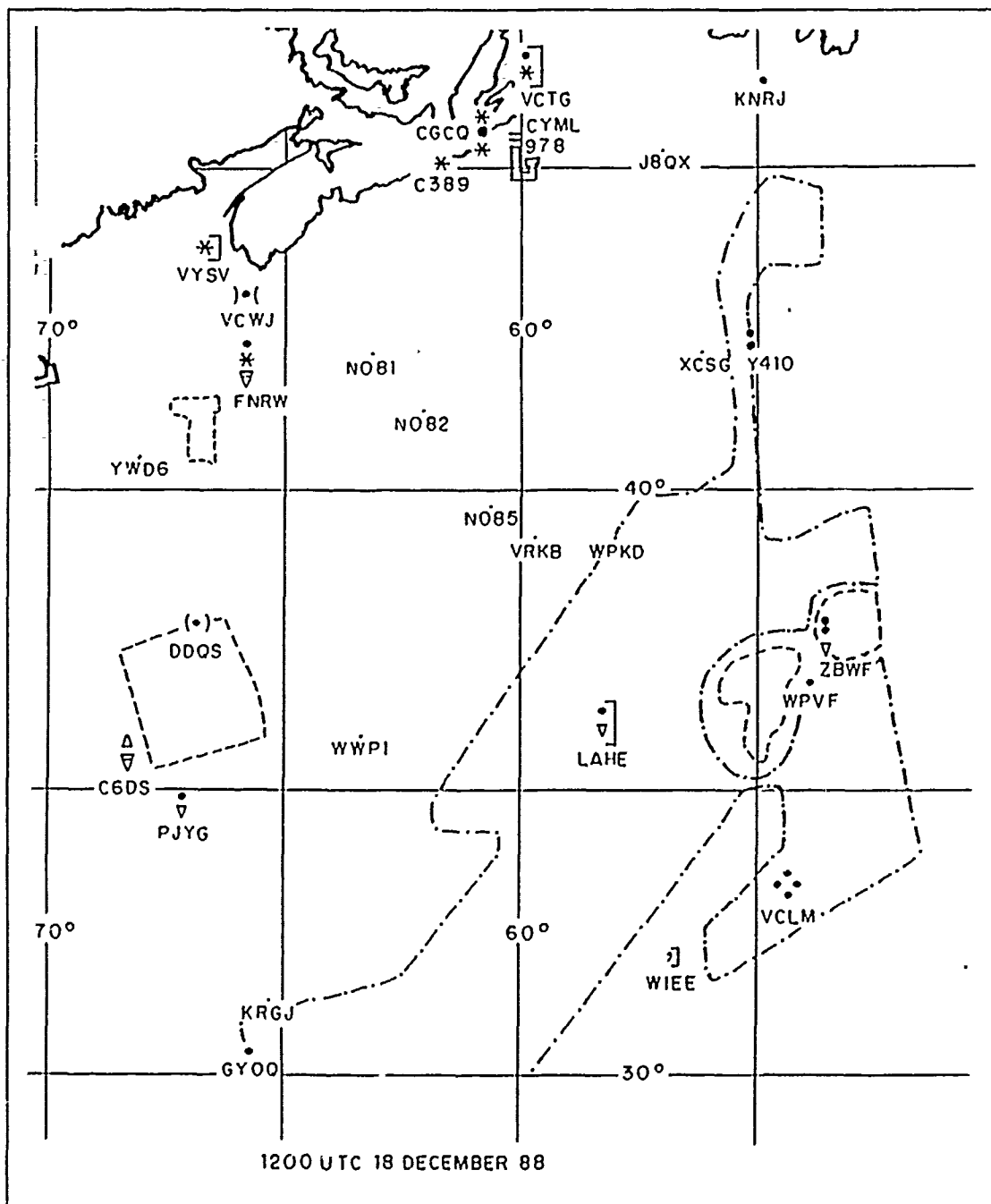


Fig. 39. Weather rain map for 18/1200 December 1988. Weather symbols are from the WMO standard weather code table. The dash/dot line outlines broken areas of OOL values, while the dashed line outlines solid areas of rain less than 15 mm/hr.

LIST OF REFERENCES

- Barrett, E.C., and D.W. Martin, 1981: The use of satellite data in rainfall monitoring. Academic Press, London, UK, 340 pp.
- Chalfant, A.E., 1989: Dynamics of an ERICA cyclone. M.S. Thesis, Naval Postgraduate School, Monterey, CA, 56 pp.
- Griffith, C.G., W.L. Woodley, S. Browner, J. Teijeiro, M. Maier, D.W. Martin, J. Stout and D.N. Sikdar, 1976: Rainfall estimation from Geosynchronous satellite imagery during daylight hours. NOAA Tech. Rep. ERL 356-WMPO 7, Boulder, CO, 106 pp.
- , W.L. Woodley, P.G. Grube, P.W. Martin, J. Stout, and D.N. Skidar, 1978: Rain estimation from geosynchronous satellite imagery-visible and infrared studies. *Mon. Wea. Rev.*, 106, 1153-1171.
- Hadley, R., and C.W. Kreitzberg, 1988: The experiment on rapidly intensifying cyclones over the Atlantic (ERICA) field study: objectives and plans. *Bull. Amer. Meteor. Soc.*, 69, 1309-1326.
- Harnett, E., G. Forbes, and R. Hadlock, 1989: Experiment on rapid intensification of cyclones over the Atlantic (ERICA) field phase summary. Department of Physics and Atmospheric Science, Drexel University, Philadelphia, PA, 300 pp.
- Hollinger, J., R. Lo, G. Poe, R. Savage, and J. Peirce, 1987: Special sensor microwave/imager user's guide, Naval Research Laboratory. 120 pp.
- Katsaros, K.B., I. Bhatti, L.A. McMurdie, and G.W. Petty, 1989: Identification of atmospheric fronts over the ocean with microwave measurements of water vapor and rain. *Wea. and Forecasting*, 4, 449-460.
- Kidder, S., and T. Vonder Harr, 1990: Principles of satellite meteorology. Academic Press, New York, NY, in printing.
- Liljas, E., 1984: Processed satellite images for operational forecasting. Swedish Meteorological and Hydrological Institute, Morrkoping, Sweden, 43 pp.
- Scofield, R.A. and V.J. Oliver, 1977: A scheme for estimating convective rainfall from satellite imagery. NOAA Technical Memorandum NESS 86, Washington, DC, 47 pp.
- Sheridan, T.F., 1988: Satellite precipitation analysis for a developing North Pacific Ocean cyclone. M.S. Thesis, Naval Postgraduate School, Monterey, CA, 72 pp.
- Spencer, R.W., H.M. Goodman, and R.E. Hood, 1989: Precipitation retrieval over land and ocean with the SSM/I: Identification and characteristics of the scattering signal. *J. Atmos. Ocean Tech.* 6, 254-273.

- Stout, J.E., D.W. Martin, and D.N. Skidar, 1979: Estimating GATE rainfall with geosynchronous satellite images. *Mon. Wea. Rev.* 107, 585-598.
- Wash, C.H., L.A. Spray and L.C. Chou, 1985: Satellite cloud and precipitation analysis using a minicomputer. NPS-63-85-003, 90 pp.
- Wilheit, T.T., J.S. Theon, W.E. Shenk, L. Allison and E.B. Rodger 1976: Meteorological interpretations of the images from the Nimbus 5 electrically scanned microwave radiometer. *J. Appl. Meteor.*, 15, 166-172.
- , A.T.C. Chang, 1980: An algorithm for retrieval of ocean surface and atmospheric parameters from the observations of the Scanning Multichannel Microwave Radiometer (SMMR). *Radio Science.*, 15, 525-544.
- Woodley, W., C.G. Griffith, J.S. Griffith, and S.C. Stromatt, 1980: The inference of GATE convective rainfall from SMS-1 imagery. *J. Appl. Meteor.*, 19, 338-408.